Critical Reviews in Solid State and Materials Sciences Volume 47, Issue 5, Pages 772 – 805, 2022

https://doi.org/10.1080/10408436.2021.1989663

Recent progress in the electrochemical deposition of ZnO nanowires: Synthesis approaches and applications

Cristina V. Manzano [a]*, Laetitia Philippe[b], and Albert Serrà [b,c,d]*

[a]*Instituto de Micro y Nanotecnología, IMN-CNM, CSIC (CEI UAM+CSIC) Isaac Newton, 8, E-28760, Tres Cantos, Madrid, Spain;* [b] *Empa, Swiss Federal Laboratories for Materials Science and Technology, Laboratory for Mechanics of Materials and Nanostructures, Feuerwerkerstrasse 39, CH-3602 Thun, Switzerland.* [c] *Grup d'Electrodeposició de Capes Primes i Nanoestructures (GE-CPN), Departament de Ciència de Materials i Química Física, Universitat de Barcelona, Martí i Franquès, 1, E-08028, Barcelona, Catalonia, Spain;* [d] *Institute of Nanoscience and Nanotechnology (IN2UB), Universitat de Barcelona, Barcelona, Catalonia, Spain.*

E-mail: cristina.vicente@csic.es (C.V.M.); a.serra@ub.edu (A.S.)

Critical Reviews in Solid State and Materials Sciences Volume 47, Issue 5, Pages 772 – 805, 2022

https://doi.org/10.1080/10408436.2021.1989663

Recent progress in the electrochemical deposition of ZnO nanowires: Synthesis approaches and applications

In the last decade, nanostructuration is a demanding research topic due to the observation of interesting properties and, in consequence, applications on these nanostructures. This review collects the synthesis and possible applications of ZnO nanowires grown by electrodeposition and electroless methods. Respect to the synthesis of ZnO nanowires, growth mechanism and parameters are analysed depending on the technique used, electrodeposition or electroless. The mechanism growth of the nanowires using templateless and hard-templates is analysed resulting in different architecture of the ZnO nanowires. Moreover, ZnO nanowires and hybrid materials based on ZnO are also considered. Depending on the architecture of ZnO nanowires, the properties and applications are different. This review also studies the properties and applications in which ZnO nanowires can be used and how these applications are different depending on the architecture of the nanostructure. This review gives a complete perspective referent to the synthesis, properties and application of ZnO nanowires grown by electrosynthesis techniques.

Keywords: ZnO; electrodeposition; electroless deposition; nanowires; nanorods; synthesis; growth mechanism; properties; applications

Introduction

Zinc oxide (ZnO) materials, especially nanostructured materials, have been extensively investigated, as seen from a surge of relevant number of publications, due to their burgeoning performance in electronics, optics, photonics, energy, photocatalysis, among other applications [1–7]. The first reports go back to 1935 or earlier, but the reliance of future technologies based on ZnO materials has significantly spurred intense and rapid progress during the last two decades. The potential applicability of ZnO-based technologies lies on its optoelectronic and structural properties at room temperature. ZnO has a direct and wide band gap (E_g = approx. 3.36 eV) in the near-UV spectral region and poses a relatively large exciton binding energy (approx. 60

Critical Reviews in Solid State and Materials Sciences Volume 47, Issue 5, Pages 772 – 805, 2022

https://doi.org/10.1080/10408436.2021.1989663

meV) at room temperature [8–11]. The crystal structures of ZnO are wurtzite, zinc blende, or rock salt, but at ambient pressure and temperature, the thermodynamically stable phase is wurtzite structure. That is composed of two interpenetrating hexagonal close-packed (hcp) sublattices, in which each zinc ion is surrounded by a tetrahedral of oxygen ions, and vice versa, providing a polar symmetry along the hexagonal axis. That polarity determines a number of properties of ZnO as well as is a pivotal factor in crystal growth [8–10].

Despite the intrinsic optoelectronic and structural properties of ZnO materials, their architecture, including their shape, dimensions, and morphology, especially at the nanometer scale, manifest other physical and chemical properties. [12–15]. For that reason, widespread efforts have been devoted to developing and understanding the synthesis and properties of ZnO nanomaterials. Most ZnO nanomaterials studied during the past two decades have been in the form of nanoparticles, although other nanostructures (e.g., nanowires, nanorods, and nanotubes) have attracted increased attention during the same period [12,14,16,17]. Owing to quantum confinement, the nanostructured architecture, especially of one-dimensional ZnO nanomaterials, facilitates the movement of electrons and holes as well as enhances the transport properties related to phonons and photons The small size of nanostructured materials also increases the specific surface area and the surface-to-volume ratio, which benefits the interaction of nanostructures and external agents (e.g., light and chemicals) or environments [12,14,17,18].

Among the most reported ZnO nanostructures, including zero-dimensional (e.g., nanoparticles), two-dimensional (2D; e.g., nanobelts and thin films), and three-dimensional (3D) complex morphologies (e.g., nanorings, nanocages, and nanoflowers, particularly ones fabricated by learning from nature with devices possessing extraordinary optical properties), ZnO nanowires and nanorods are ideal candidates not only for understanding fundamental nanoscale phenomena but also as fundamental building blocks for fabricating more competitive, more complex ZnO-based devices. Many 3D complex morphologies are formed by nanowires

Critical Reviews in Solid State and Materials Sciences Volume 47, Issue 5, Pages 772 – 805, 2022

https://doi.org/10.1080/10408436.2021.1989663

or nanorods as their basic building blocks [19–22]. ZnO nanowires and nanorods exhibit extraordinarily high surface-to-volume ratios and an excellent capacity to be integrated into devices and interact with other micro- and nanoscopic systems [12,14,16]. The potential of ZnO nanowires and nanorods rests not only in their incredible physical and chemical properties but also in the reasonably rapid, simple, low-cost approaches to synthesizing them. At the same time, synthesizing one-dimensional nanomaterials continues to require great ingenuity in order to consolidate fabricating routes and thereby attain well-controlled dimensions, morphologies, phase purities, and chemical compositions in terms of cost, throughput, scalability, and volume of production [14,16].

The growth of ZnO nanowires and nanorods can be accomplished with a wide range of approaches, including physical vapor–liquid–solid (VLS) processes, sol–gel, and hydrothermal, solvothermal, and electrochemical deposition approaches or by using advanced nanolithographic techniques [12,23–26]. Most studies to date have focused on either VLS growth processes at relatively high temperatures with rather complex equipment or else wet chemical processes, primarily hydrothermal ones, at relatively low temperatures [24]. The crux of those processes is their ability to facilitate the control of the nanowires' architecture, including their dimensions and alignment, on relatively large surfaces such that their material properties can be fine-tuned, as well as their extensive usability as a building blocks in multiple applications [12,24,27].

Against that background, electrochemical deposition, both electrodeposition and electroless deposition, seem to be promising wet chemical approaches for synthesizing well-defined, well-aligned ZnO nanowires and nanorods. The potential of the electrochemical approaches rests in their simplicity, their possible use for large-scale depositions, and the low cost of the required equipment, precursors, and processes [4,17,28]. The simple electrochemical deposition process is based on the electrogeneration of hydroxide ions, followed by the precipitation of $Zn(OH)_2$ and its dehydration to obtain ZnO. Unlike other materials, ZnO

Critical Reviews in Solid State and Materials Sciences Volume 47, Issue 5, Pages 772 – 805, 2022

https://doi.org/10.1080/10408436.2021.1989663

nanowires and nanorods can be easily obtained by using a hard-template electrochemical deposition, which is the most extended strategy for electrosynthesizing nanowires and nanorods, or by using a simple templateless process [6,29,30]. The viability of using templateless deposition stems from the local increase of pH in the substrate's vicinity, which determines the speciation of Zn(II) that facilitates the adsorption of dominant negatively charged Zn(II) species on the positively charged Zn-terminated (0001) planes, thereby resulting in fast growth in the direction of the c-axis [12,27,28,30].

The aim of this review is to offer a global, holistic overview of the progress of the electrochemical deposition of ZnO nanowires and nanorods, with special focus on approaches of electrosynthesis and the potential applications of ZnO nanowires and nanorods. The review thus stands as the first to holistically address the full range of electrochemical deposition processes by not only considering templateless and hard-template electrodeposition but also analyzing and discussing electroless deposition. In the following sections, we discuss the mechanisms of growth and the primary parameters governing the architectural, physical, and chemical properties of the electrodeposition of ZnO nanowires and nanorods, including in terms of the concentration of Zn(II), the precursors, optimal temperatures for deposition, and the substrates involved. The sections also briefly introduce the modification of ZnO, which is vital to the development of more competitive ZnO-based nanowires and nanorods with the potential to improve the optical, electric, and electronic properties of those one-dimensional nanostructures. Last, we describe the principal properties of ZnO nanowires and nanorods as well as illustrate the major advances and potential of those nanostructures for a wide range of applications, including in photocatalysis, water oxidation, antibacterial applications, solar cells, UV photodetectors, supercapacitators, batteries, nanosensing, hydrogen evolution, and light-emitting diodes.

Critical Reviews in Solid State and Materials Sciences Volume 47, Issue 5, Pages 772 – 805, 2022

https://doi.org/10.1080/10408436.2021.1989663

Electrodeposition of ZnO nanowires

Traditionally used to grow metals or alloys on conductive surfaces, electrodeposition involves the electrochemical reduction of metal ions (M^{n+}) from aqueous, organic, fused-salt, or ionic liquid electrolytes. In that process (Eq. 1), a potential (or current) is applied between two conductive surfaces (i.e., electrodes) immersed in a conductive solution (i.e., electrolyte) containing the electroactive species to be reduced, such that an external power supply provides *n* electrons, thereby precluding the use of additional aggressive reducing agents [29,31]:

$$M^{n+}_{(aq)} + n\, e^- \rightarrow M_{(s)} \qquad \text{(Eq. 1)}$$

Despite the simplicity of the equation, electrodeposition is a complex heterogeneous process that requires understanding the metal–solution interface as the locus of deposition, as well as the kinetics, mechanisms, nucleation, and growth processes to be interpreted [29,31].

Electrodeposition entails a range of other processes, including electroforming, anodic electrodeposition, electrowinning, electroanalysis, electroplating, electro-precipitation, and electropolymerization. In the electrodeposition of metal oxides in particular, three processes can be readily distinguished: (i) electrode oxidation, in which the metal of the electrode's surface is oxidized, thereby forming an oxide or hydroxide layer on the substrate; (ii) anodic electrodeposition, in which soluble precursors are electrochemically oxidized to insoluble oxides (e.g., MnO_2, Fe_2O_3, and NiO); and (iii) electroprecipitation, in which oxides or hydroxides are precipitated from the electrochemical generation of hydroxide ions. In electroprecipitation, the oxidation state of metal ions—for example, ZrO_2, ZnO, $Ni(OH)_2$, and CeO_2—does not change [12,16,29,32].

Critical Reviews in Solid State and Materials Sciences Volume 47, Issue 5, Pages 772 – 805, 2022

https://doi.org/10.1080/10408436.2021.1989663

Mechanism of electrodeposition of ZnO nanowires

The electrodeposition of ZnO is a process of electroprecipitation that involves the electrochemical formation of hydroxide ions—that is, increasing the pH—on the surface of the working electrode. As Zn^{2+} ions react with hydroxide ions, the latter precipitate in the form of $Zn(OH)_2$. However, at temperatures greater than 40 °C, $Zn(OH)_2$ is dehydrated by a solid–solid phase transformation, and as a result, the formation of ZnO occurs. The global reaction to obtain ZnO by electrochemical deposition is as follows [28,30,33–37]:

$$Zn^{2+}{}_{(aq)} + 2\,OH^{-}{}_{(ads)} \rightarrow Zn(OH)_{2(s)} \rightarrow ZnO_{(s)} \qquad \text{(Eq. 2)}$$

In aqueous systems, the increase of the electrolyte's pH, especially on the electrode–solution interface, can be promoted by various reduction reactions, all of which are based on the consumption of hydrogen ions or the generation of hydroxide ions by water electrolysis (Eq. 3), hydrogen adsorption and absorption (Eq. 4), or the hydrogen evolution reaction (Eq. 5) [28,30,33,35]:

$$2\,H_2O_{(l)} + 2\,e^{-} \rightarrow H_{2(g)} + 2\,OH^{-}{}_{(aq)} \qquad \text{(Eq. 3)}$$

$$H^{+}{}_{(aq)} + e^{-} \rightarrow H_{ads}\ or\ H_{abs} \qquad \text{(Eq. 4)}$$

$$2\,H^{+}{}_{(aq)} + 2\,e^{-} \rightarrow H_{2(g)} \qquad \text{(Eq. 5)}$$

Those processes can dramatically influence the electrodeposition of a variety of materials and play an important role in the deposition of ZnO. However, the need to control supersaturation and electrocrystallization during ZnO's deposition, as well as due to thermodynamic considerations, typically requires the use of precursors to manage the rising pH in the electrode–solution interface. Although other precursors, albeit rarely, are used in aqueous

https://doi.org/10.1080/10408436.2021.1989663

solutions, three far more common precursors can be used to form ZnO nanowires: molecular oxygen, nitrate ions, and hydrogen peroxide [28,30,34].

(i) **Molecular oxygen**: Oxygen is possibly the most widely used precursor for the electrodeposition of ZnO. In that process, the first step is electrogenerating hydroxide ions by reducing molecular oxygen (Eq. 6), such that hydroxide ions subsequently react with Zn^{2+} ions [30,33,35]:

$$\frac{1}{2}O_{2\,(aq)} + H_2O_{(l)} + 2\,e^- \rightarrow 2\,OH^-_{(aq\ and\ ads)} \qquad \text{(Eq. 6)}$$

With a standard potential versus the standard hydrogen electrode (SHE) of 0.400 V, the strategy is green and produces no negative byproducts during electrodeposition. In the presence of Cl^-, it is also possible to form oxygen peroxide via a parallel two-electron process, as well to form hydrogen peroxide, which can benefit the formation of ZnO. At the same time, the kinetics and growth of ZnO nanowires can be easily controlled by adjusting the electrochemical parameters. For the purpose of optimization, the oxygen reduction reaction can be electrocatalyzed by using different substrates. In systems involving molecular oxygen, Zn(II) chloride is normally employed as a source of Zn(II) ions [33,35]. Throughout the process, the low solubility of oxygen (8.3 mg·L^{-1} at 25 °C and 101.1 kPa), which significantly decreases as the temperature rises, is an important limitation. In general, with molecular oxygen, electrodeposition is performed using oxygen-saturated solution, during which slight oxygen bubbling is continuously maintained; such bubbling can dramatically affect the morphology and architecture of deposits and even make hard-template electrodeposition impractical [33,35].

(ii) **Nitrate ions**: The reduction of nitrate ions is an excellent source of hydroxide ions, one that can be especially useful for the hard-template electrodeposition of ZnO nanowires or

https://doi.org/10.1080/10408436.2021.1989663

even more complex nanostructures. The generation of hydroxide ions is based on Equations 7 and 8 [28,34,35,38–40]:

$$NO_{3\,(aq)}^{-} + H_2O_{(l)} + 2\,e^{-} \rightarrow NO_{2\,(aq)}^{-} + 2\,OH^{-}_{(aq\ and\ ads)} \qquad \text{(Eq. 7)}$$

$$NO_{3\,(aq)}^{-} + 7H_2O_{(l)} + 8\,e^{-} \rightarrow NH_{4\,(aq)}^{+} + 10\,OH^{-}_{(aq\ and\ ads)} \qquad \text{(Eq. 8)}$$

The standard potentials of those reactions versus the SHE are 0.010 and -0.356 V, respectively. The copious production of hydroxide ions can suppress the dehydration of $Zn(OH)_2$, however, thereby leading to the formation of Zn(II) nitrate hydroxide hydrate due to the dominance of the reaction [28]:

$$Zn(NO_3)_2 + 4\,Zn(OH)_2 \rightarrow Zn_5(NO_3)_2(OH)_8 \qquad \text{(Eq. 9)}$$

In systems involving nitrate ions, optimizing the kinetics of hydroxide ion production is pivotal to avoiding the suppression of the dehydration of $Zn(OH)_2$ and, consequently, the formation of undesirable byproducts. The production of nitrite and ammonia can also affect deposition due to their progressive accumulation in the deposition bath [28,34,35,40].

(iii) **Hydrogen peroxide**: Hydrogen peroxide is another outstanding source of hydroxide ions due to its typical electrochemical reduction (Eq. 10) [35,41,42].

$$H_2O_{2(aq)} + 2\,e^{-} \rightarrow 2\,OH^{-}_{(aq\ and\ ads)} \qquad \text{(Eq. 10)}$$

The standard potential of that reaction versus SHE is 0.940 V. Hydrogen peroxide can be an excellent alternative to molecular oxygen and nitrate ions, not only due to its high solubility in aqueous media but also because it does not generate unwanted byproducts during reduction. However, hydrogen peroxide is photosensitive and easily decomposes in the presence of various metallic ions and metals. In systems involving hydrogen peroxide, Zn(II) chloride is commonly used as a source of Zn(II) ions [35,41,43].

Critical Reviews in Solid State and Materials Sciences Volume 47, Issue 5, Pages 772 – 805, 2022

https://doi.org/10.1080/10408436.2021.1989663

In any case, because the standard potential for metallic Zn deposition is -0.760 V versus SHE, an exceptionally large potential window for ZnO deposition using molecular oxygen, nitrate ions, or hydrogen peroxide can be expected.

Alternatively, the deposition of ZnO in nonaqueous solutions such as dimethyl sulfoxide (DMSO) and tetrabutylammonium hydroxide may improve electrodeposition, not only because the deposition of metal hydroxide does not occur in nonaqueous systems but also because using higher deposition temperatures than in water is possible, which can enhance the state of crystallization [44–48]. According to the literature, the electrodeposition of ZnO in DMSO is based on the following mechanism [46,49,50]:

$$O_{2(sol)} + e^- \rightarrow O_2^-{}_{(sol)} \quad \text{(Eq. 11)}$$

$$2\,O_2^-{}_{(sol)} \rightarrow O_{2(sol)} + O_2^{2-}{}_{(sol)} \quad \text{(Eq. 12)}$$

$$O_2^{2-}{}_{(sol)} + Zn^{2+}{}_{(sol)} \rightarrow ZnO_{2(s)} \quad \text{(Eq. 13)}$$

$$ZnO_{2(s)} \rightarrow ZnO_{(s)} + \frac{1}{2}\,O_{2(sol)} \quad \text{(Eq. 14)}$$

Despite the advantages of using nonaqueous solvents to deposit ZnO, the strategy is rarely proposed due to the operation's complexity and high costs relative to the potential advantages.

Electrodeposition parameters

Several parameters of electrodeposition can affect the architecture, morphology, and properties of electrodeposited ZnO. This section focuses on how such parameters influence the electrodeposition of ZnO nanowires and nanorods using templateless or hard-template electrodeposition and an aqueous bath. The major parameters, their effects, and the optimal experimental conditions that should be considered prior to depositing ZnO nanowires or

https://doi.org/10.1080/10408436.2021.1989663

nanorods are summarized in **Table 1** [39,40,43,51–53]. Although additional parameters should be considered depending on the composition of the bath, the nature of the working electrode, the design of the reactor, and final application, those parameters are beyond the scope of this thesis work.

Table 1: Primary parameters of electrodeposition and their effects on the electrodeposition of ZnO nanowires and nanorods.

Electrodeposition parameter	**Effect**
Bath temperature	- Primarily controlled by bath temperature, the dehydration of the deposited $Zn(OH)_2$ starts at approximately 34 °C but increases considerably as the temperature rises. At temperatures of 60–70 °C, the dehydration and thus formation of ZnO are practically instantaneous [36,37,54]. - The solubility of molecular oxygen decreases as the bath temperature increases, which significantly reduces the kinetics of the formation of hydroxide ions [36,37,54]. - The kinetics of the decomposition of hydrogen peroxide increases considerably with bath temperature [36,37,54]. - Crystallinity increases as the bath temperature rises; at 40 °C, crystalline deposits can be obtained. The film's texturation with the *c-axis* perpendicular to the substrate surface is promoted at temperatures greater than 60 °C [36,37,54]. - Optimal bath temperatures range from 60 to 85 °C [36,37,54].
Potential	- Applied potential, both constant and pulsed, affects the concentration of hydroxide ions adsorbed on the working electrode and consequently the

https://doi.org/10.1080/10408436.2021.1989663

	nucleation and growth of ZnO. Owing to the effects of those processes, the orientation of ZnO at a constant temperature can be easily modified. In general, low and especially moderate applied potentials (i.e., >-1 V vs. SHE) promote the (002) preferred orientation, which is crucial for the templateless electrodeposition of ZnO nanowires [52]. A strong relationship between the directional growth along the (002) preferred orientation with the applied potential is expected independent of the precursor used [40,52,55–59]. - The diameter and density of ZnO nanowires in templateless electrodeposition increase as the applied potential increases; however, potential less than -1 V versus SHE can affect the nanowire or nanorod morphology [40,52,56,58,60–62]. - Potentiodynamic electrodeposition starting from the open circuit potential (OCP) to more negative potentials or between two potentials can enhance crystallinity. In potentiodynamic conditions, the rate of decreased or increased potential determines the number of nucleation sites and, in turn, nanowire density [40,52,56,58,60–62]. - The kinetics of hydroxide electrogeneration is controlled by the applied potential and concentration of the precursor (i.e., molecular oxygen, nitrate ions, or hydrogen peroxide) [40,52,56,58,60–62]. - The optimum applied potential ranges from -1 to -0.6 V versus SHE [40,52,56,58,60–62].
Precursor concentration	- The increased concentration of $Zn(NO_3)_2$ or H_2O_2 strongly affects the kinetics of hydroxide electrogeneration and thus the nucleation rate, saturated nucleation density, and crystallinity. For the templateless electrodeposition of ZnO nanowires and nanorods, the (002) preferred

https://doi.org/10.1080/10408436.2021.1989663

	orientation is promoted at low concentrations of the precursor, high bath temperatures, moderate potentials, and short deposition times. For the hard-template electrodeposition of ZnO nanowires or nanorods, higher concentrations of the precursor can be used [38,39,43,63–68]. - The optimal precursor concentrations for the templateless electrodeposition of ZnO nanowires and nanorods are a saturated solution for molecular oxygen, 2–5 mM for nitrate ions, and 2–10 mM for hydrogen peroxide [38,39,43,63,65,66,68–70].
Zn(II) concentration	- The increase of $[Zn^{2+}]$ provokes a decrease in nanowire density and an increase in nanowire diameter [38,39,43,63,65,66,68–73]. - The increase of $[Zn^{2+}]$ translates to a wider diameter distribution [38,39,43,63,65,66,68–70,72–74]. - High concentrations of $[Zn^{2+}]$ (i.e., >10 mM) are not suitable for the templateless electrodeposition of ZnO nanowires or nanorods [38,39,43,63,65,66,68–70,72–74].
Supporting electrolyte	- KCl, K_2SO_4, and KNO_3 are typically used as supporting electrolytes for the electrodeposition of ZnO nanorods and nanowires. The presence of such electrolytes influences the transport of Zn^{2+} to the working electrode. Whereas the increase of KCl and K_2SO_4 concentration prompts a decrease in nanowire or nanorod density, as well as slightly enhances crystallinity, KNO_3 affects the orientation and shape of the nanorods or nanowires and results in poor crystallinity [75–77].

Critical Reviews in Solid State and Materials Sciences Volume 47, Issue 5, Pages 772 – 805, 2022

https://doi.org/10.1080/10408436.2021.1989663

Templateless electrodeposition of ZnO nanowires

By permitting operational conditions to be fine-tuned, electrodeposition allows the synthesis of well-crystallized hexagonal ZnO nanowires and nanorods with an exceptionally high degree of verticality and orientation (**Figure 1**) [78–80]. In turn, ZnO nanowires and nanorods can be deposited onto a wide variety of conductive and semiconductor substrates. Although their definition, verticality, and orientation heavily depends upon the matching of the lattice parameters and the crystal structure of the nanowires or nanorods and substrates, high-quality, well-defined hexagonal ZnO nanowires and nanorods can indeed be directly electrodeposited onto various substrates, including glass coated with indium–tin oxide (ITO) or fluorine-doped–tin oxide (FTO). Moreover, such electrodeposition offers an easy, one-step process without the ZnO seeding layer normally required in most alternative techniques [12,30,80–87].

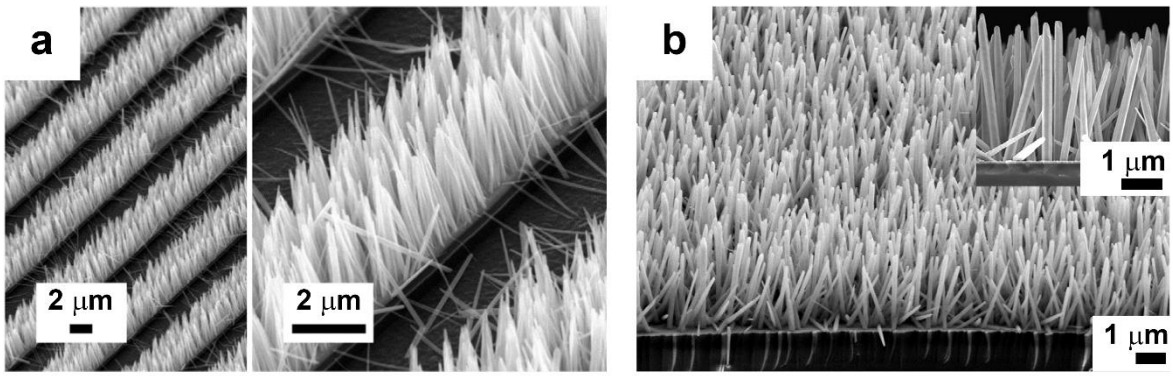

Figure 1: FE-SEM micrographs of templateless electrodeposited ZnO nanowires on (a) Au substrates (Adapted with permission from [87]) and (b) ITO glass (Adapted with permission from [81]).

By varying the operational conditions, many studies have focused on elucidating the degree to which dense hexagonal ZnO or ZnO nanowire and/or nanorod arrays can be

https://doi.org/10.1080/10408436.2021.1989663

successfully electrodeposited. Most of those studies have revealed that the key parameter of the origin of the different possible morphologies lies in the concentration of Zn(II) in the electrochemical media [83,86]. Overall, it has been concluded that the growth of such nanowires and nanorods occurs only along the longitudinal axis when the diffusion of Zn(II) species is significantly less than the rate at which hydroxide ions are generated (**Figure 2a**). By contrast, similar generation rates and diffusions of Zn(II) species have prompted the growth of ZnO along the longitudinal and transversal axes (**Figure 2b**) [86,88].

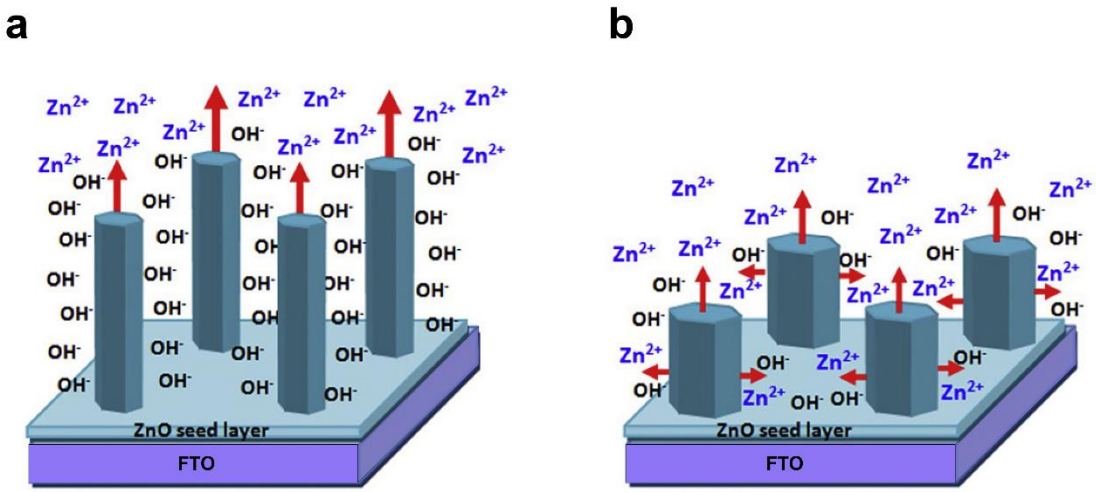

Figure 2: Growth mechanism of ZnO nanowires and nanorods by electrodeposition based on the model of the diffusion of Zn(II) species. (a) The diffusion of the Zn(II) ions is significantly less than the electrogeneration of hydroxide ions. (b) The diffusion of Zn(II) ions and the electrogeneration of hydroxide ions occur at a similar rate. Adapted with permission from [86].

However, that simple model cannot fully explain the formation of well-defined nanowires and nanorods when the concentration gradient of Zn(II) is maintained in the vicinity of the electrode, in which lateral growth is expected according to the model of the diffusion of Zn(II) species [12,86]. That occurrence suggests that the critical parameter for defining ZnO

https://doi.org/10.1080/10408436.2021.1989663

morphology is the local pH at the electrode–solution interface. The pH determines the speciation of the Zn(II) ions, which is pivotal to understanding their adsorption and electrodeposition [12]. The model suggests that the two morphologies are formed at different pH levels: dense films at pH close to neutral versus nanowires and nanorods in alkaline conditions. The basis of the model rests upon the different speciation and interaction of the Zn(II) species that coexist at different pH levels [12,30]. As shown in **Figure 3**, the primary Zn(II) species at a pH close to neutral in a typical bath using nitrate ions, molecular oxygen, or hydrogen peroxide as a precursor are Zn^{2+}, $ZnCl^{+}$, and $Zn(OH)^{+}$. By contrast, in alkaline conditions, the dominant species are hydroxide complexes such as $Zn(OH)_3^{-}$ and $Zn(OH)_4^{2-}$ [12,30]. It is supposed that the positively charged Zn(II) species are electrostatically attracted to the negatively polarized surface of the working electrode, which would facilitate the formation of ZnO nuclei, their longitudinal and transversal growth, and, in turn, the formation of dense ZnO films. In alkaline conditions, the predominant negatively charged Zn(II) species are not electrostatically attracted to the working electrode's surface, which translate to a low deposition faradic efficiency. However, it is also known that hexagonal ZnO has polar and nonpolar planes and that the top polar plane is positively charged and exhibits high surface energy. Consequently, it is possible that negatively charged Zn(II) species as well as the hydroxide ions are preferentially adsorbed on the top Zn-terminated (0001) polar plane of the hexagonal ZnO crystals, thereby resulting in rapid growth along the longitudinal axis [12,30].

Critical Reviews in Solid State and Materials Sciences Volume 47, Issue 5, Pages 772 – 805, 2022

https://doi.org/10.1080/10408436.2021.1989663

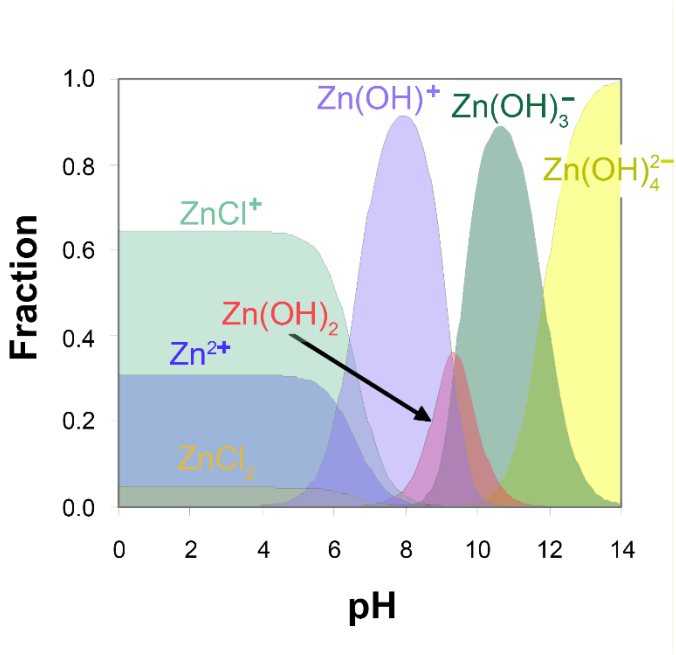

Figure 3: Speciation diagram of Zn(II) ions in 0.1 M of KCl at 70 °C. Adapted with permission from [30].

Although the templateless electrodeposition of ZnO nanowires and nanorods seems to necessitate the use of alkaline electrochemical media, the most widely used electrochemical media have pH levels of approximately 7. Otherwise, $Zn(OH)_2$ is precipitated [30]. Understanding why nanowires and nanorods can be deposited using non-alkaline electrochemical media requires holistic thinking focused on the mechanism of nucleation and growth as well as the conditions of the electrochemical bath. As shown in **Figure 4**, the first steps of the electrodeposition of ZnO nanowires and nanorods is the electrodeposition of ZnO nuclei [30]. The initial pH at the interface of the electrode is nearly neutral, which indicates that Zn^{2+} and $ZnCl^{+}$ are more relevant Zn(II) species. Under such conditions, the electrostatic attraction of positively charged Zn(II) species to the electrode's surface prompts the formation of ZnO nuclei, which grow along the longitudinal and transversal axes. By contrast, the polar (0001) faces of hexagonal ZnO nuclei promote the growth rate in the *c-axis* direction. Depending on the

https://doi.org/10.1080/10408436.2021.1989663

concentration of Zn(II) ions, two situations can be expected [12,30]. On the one hand, when the concentration of Zn(II) species is high, the electrogenerated hydroxide ions rapidly react with positively charged Zn(II) species attracted to the electrode's surface, which, following a sufficiently long deposition, cause the formation of dense, continuous ZnO films. On the other, when the concentration of Zn(II) species is significantly low in relation to the generation of hydroxide ions, the pH of the electrode's interface progressively increases, which provokes the dominance of $Zn(OH)_3^-$ and $Zn(OH)_4^{2-}$ ions and consequently results in the complete quenching of the lateral growth. The growth in the direction of the *c-axis* is maintained due to the reaction of negatively charged Zn(II) species with the positively charged tetrahedron corners of hexagonal crystals, which results in the formation of ZnO nanowires and nanorods [12,30].

In summary, the morphology of electrodeposited ZnO depends directly upon the pH near the electrode's surface, which is intrinsically linked to the concentration of Zn(II). At the same time, the depth of the nanowire or nanorod depends exclusively upon the time required to hinder lateral growth—that is, the increase of local pH at values greater than 9 [30,89]. According to the literature, smaller-diameter ZnO nanowires (i.e., 18–20 nm) obtained using templateless electrodeposition have involved an aqueous solution of Zn(II) chloride and molecular oxygen as a precursor. The aspect ratio of ZnO nanowires or nanorods is determined by the deposition time, whereas their density depends primarily upon the density of sites with energy favorable for the nucleation of ZnO (i.e., the properties, reactivity, and affinity of the working electrode's surface). In that context, the density of nanowires is significantly greater when nanowires or nanorods are electrodeposited onto a ZnO seed layer. Of course, the method has not been restricted only to the deposition of well-aligned ZnO nanowires and nanorods on flat substrates [30,81,89]. During the past two decades, it has been frequently used to create complex architectures based on the use of non-flat substrates or polymeric matrices covered with ZnO seed layers to create so-called "hairy lattices" and "sea urchins," among other elaborate architectures (**Figure**

https://doi.org/10.1080/10408436.2021.1989663

5) [90–94]. More recently, the hydrodynamic conditions during electrodeposition have been useful in producing fractal fern-like microstructures, for the turbulent regime allows the formation of new nuclei on the ZnO nanowires or nanorods. All of those factors can be modulated by controlling different electrochemical parameters, including deposition potential and concentration of electrolyte supports, and the hydrodynamic conditions during electrodeposition [17,80–82,95].

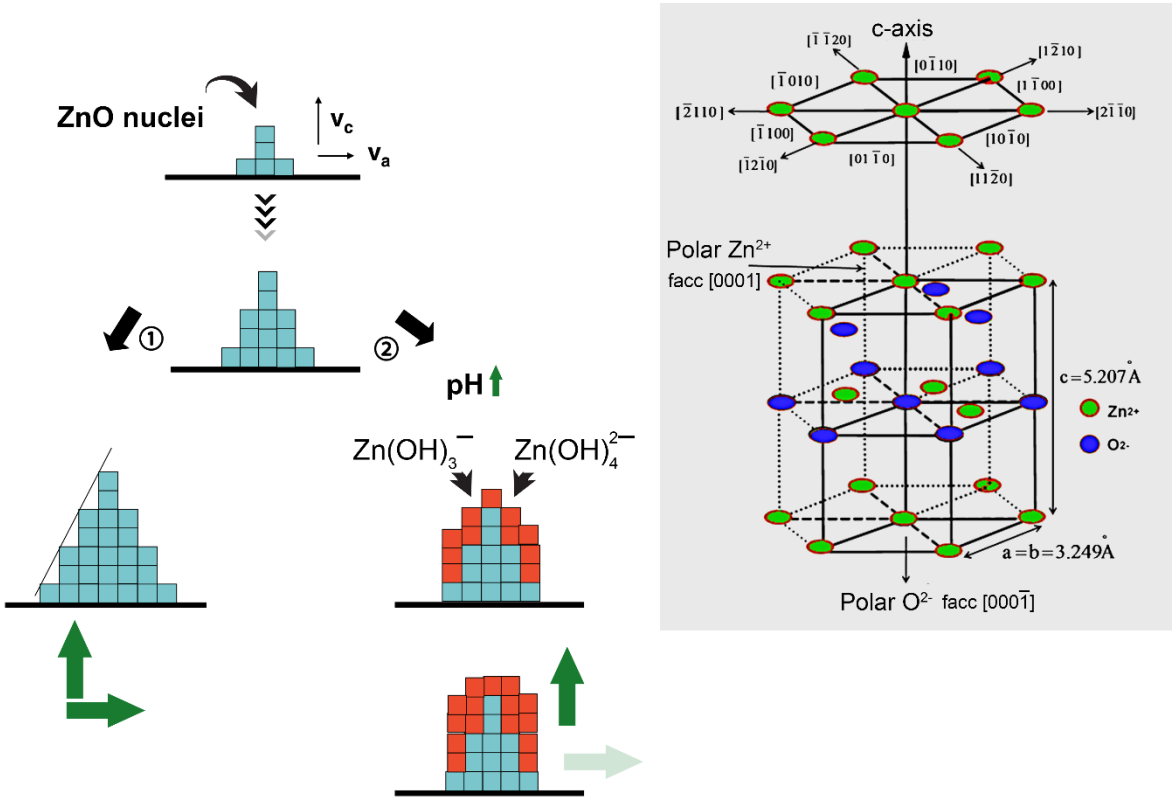

Figure 4: Mechanism of the electrochemical deposition of ZnO. Adapted with permission from [30] and [96].

Critical Reviews in Solid State and Materials Sciences Volume 47, Issue 5, Pages 772 – 805, 2022

https://doi.org/10.1080/10408436.2021.1989663

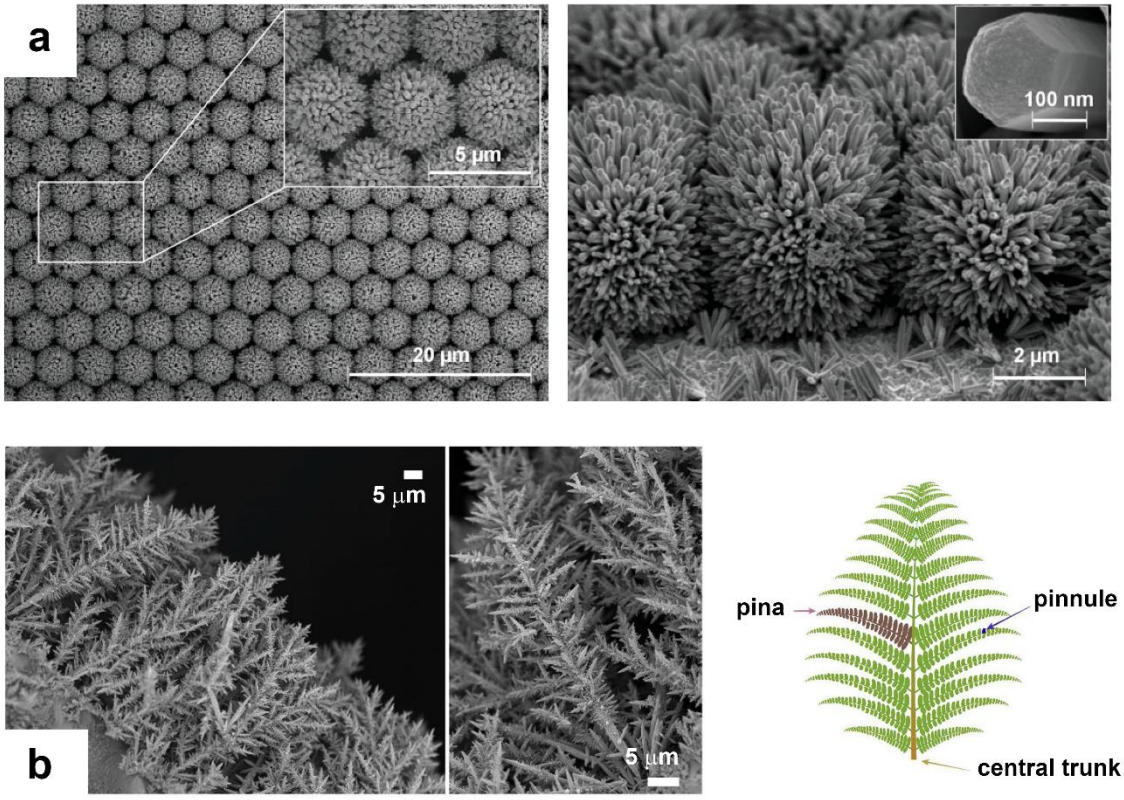

Figure 5: FE-SEM micrographs of (a) sea urchins (reproduced with permission from [91]), and (b) bioinspired microferns (reproduced with permission from [97]), all formed with ZnO nanowires and nanorods.

Hard-template electrodeposition of ZnO nanowires

Due to its simplicity and robustness, hard-template electrodeposition is the most widely applied strategy for electrosynthesizing polymeric, metallic, alloyed, or semiconducting nanowires or nanorods, one that offers controlled properties and the controlled definition of shape [29,98–105]. The method also poses disadvantages, however, including problems with scalability and costs associated with fabricating and removing templates [29,106]. In the context of ZnO, the hard-template electrodeposition is less significant than the template-free electrodeposition.

Critical Reviews in Solid State and Materials Sciences Volume 47, Issue 5, Pages 772 – 805, 2022

https://doi.org/10.1080/10408436.2021.1989663

Against that trend, two strategies have been investigated for the hard-template electrodeposition of ZnO nanowires. One entails electrodepositing Zn nanowires into hard templates, primarily anodic aluminum oxide (AAO) templates, which are posteriorly oxidized by a thermal route in air or oxygen atmospheres in order to obtain ZnO nanowires [15,107–109], as shown in **Figure 6**. That strategy simplifies experimental conditions by allowing electrodeposition to be performed at room temperature with significantly high rates of deposition, even up to 1 $\mu m \cdot min^{-1}$, depending on the bath's composition. Even so, the lengthy time (i.e., >30 h) required for posterior thermal treatment in oxidizing atmospheres at moderate temperatures to obtain pure ZnO nanowires limits the strategy's real applicability [48,110].

As an alternative, the other strategy entails the direct electrodeposition of ZnO using nitrate or hydrogen peroxide precursors in aqueous solutions at low concentrations of Zn(II) ions, as shown in **Figure 6** [27,58,111–114]. Although oxygen precursors are rarely used for ZnO's hard-template electrodeposition, the same limitations of its templateless electrodeposition, including moderate deposition rates and optimal bath temperatures ranging from 60 to 85 °C, occur nonetheless [58,111–114]. Moderate temperatures remain viable but promote the deposition of $Zn(OH)_2$, which generally reduces the purity and quality of ZnO nanowires. The aspect ratio of ZnO nanowires electrodeposited following that strategy usually ranges from 8 to 29 [115]. Meanwhile, the growth rates of ZnO nanowires for both templateless and hard-template electrodeposition are similar [116]. Non-aqueous solutions, especially when AAO membranes are used, have also been investigated in efforts to improve the quality and purity of ZnO depositions or their function at room temperature [46,48].

Critical Reviews in Solid State and Materials Sciences Volume 47, Issue 5, Pages 772 – 805, 2022

https://doi.org/10.1080/10408436.2021.1989663

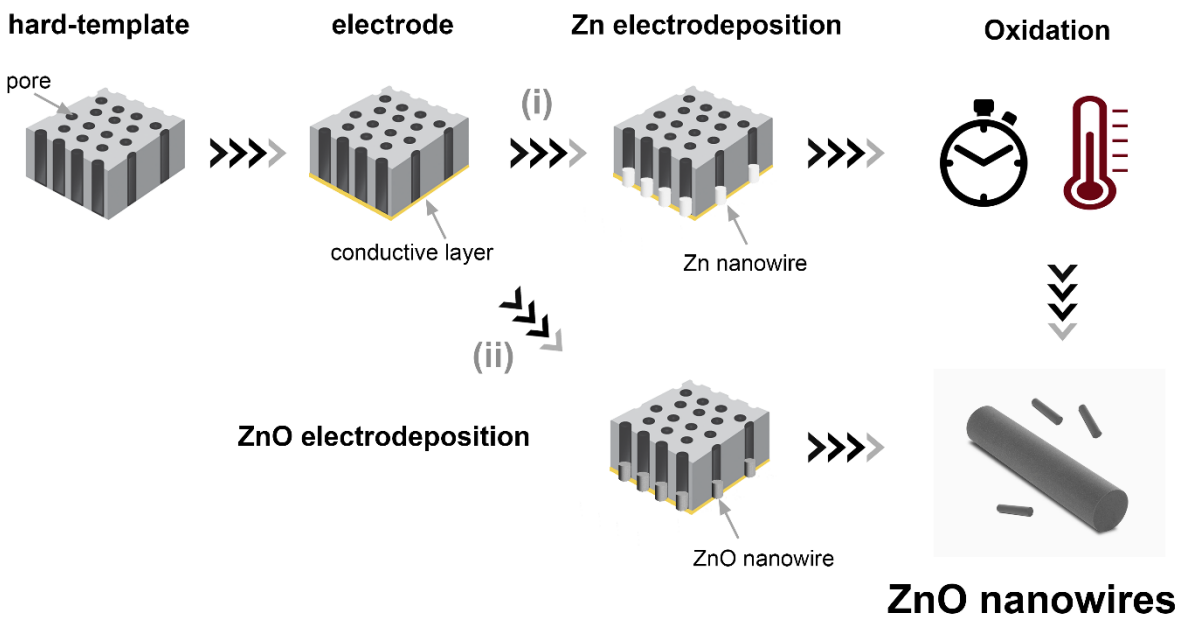

Figure 6: Schematic representation of the hard-template electrodeposition of ZnO via (i) Zn deposition and posterior oxidation and (ii) direct ZnO electrodeposition.

The growth of Zn or ZnO nanowires inside the nanopores of hard templates occurs in three stages that can be clearly identified in current–time curves (**Figure 7**). First, a nucleation process involves the deposition of Zn or ZnO on the conductive layer of the bottom part of the pores of hard templates, in a process usually identified by a drop in current density due to the mass transport limited processes (**Figure 7**, region I). Second, a steady state zone arises that is characterized by a pseudoconstant current density due to the spherical diffusion of Zn(II) (**Figure 7**, region II). Third and last, a progressive rise in current density occurs (**Figure 7**, region III) owing to the overgrowth of nanowires when they completely fill the template [112,117,118]. Well-defined current–time curves provide detailed evidence about that growth process.

Critical Reviews in Solid State and Materials Sciences Volume 47, Issue 5, Pages 772 – 805, 2022

https://doi.org/10.1080/10408436.2021.1989663

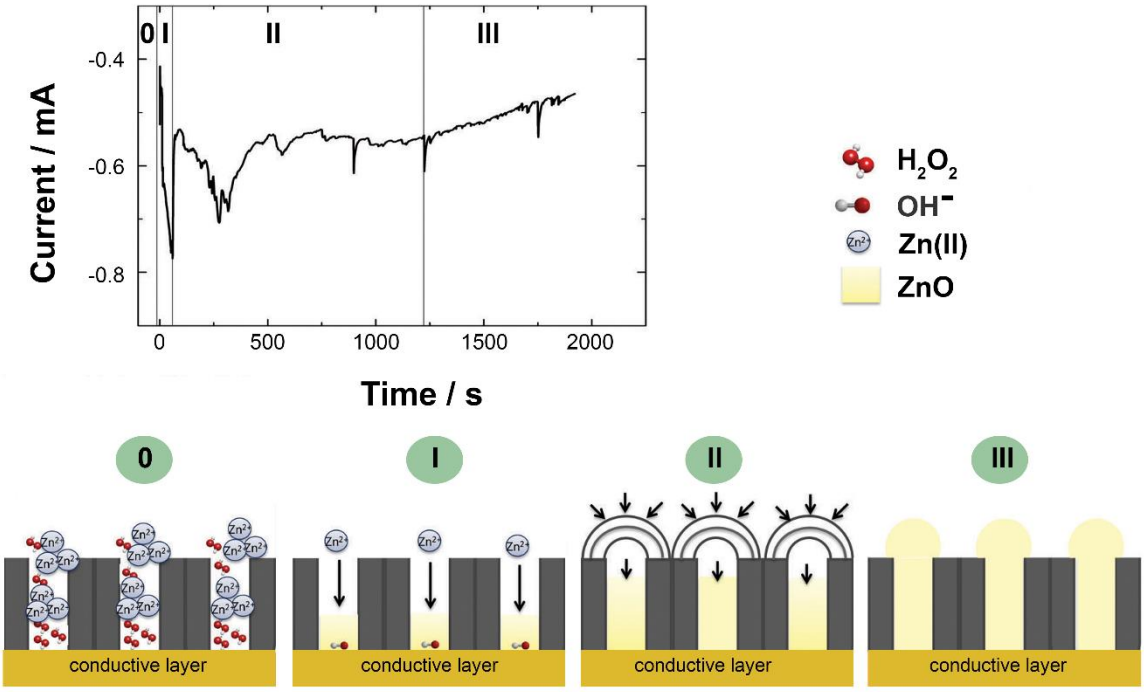

Figure 7: Current–time curve of ZnO nanowires deposited at 70 °C using an aqueous solution of 0.001 M $ZnCl_2$ + 0.04 M H_2O_2 + 0.1 M KCl at -0.8 V versus Ag|AgCl and a schematic representation of the diffusion mechanism of ZnO's deposition. Adapted from [112] with permission.

The shape and alignment of ZnO nanowires electrodeposited using hard templates are chiefly defined by the template's dimensions and shape, or else its pores, either of which translates into greater versatility. In the templateless electrodeposition of ZnO, electrochemical parameters are optimized to control of the architecture (i.e., shape and dimensions of nanowires or nanorods). By way of hard-template electrodeposition, the morphology, growth rate, and surface porosity, among other characteristics, of ZnO nanowires and nanorods can be significantly modified without affecting their architecture. A strong influence of experimental conditions on the crystallinity, morphology, and properties has been established by varying the deposition potential, precursor concentration, temperature, Zn(II) concentration, templated

Critical Reviews in Solid State and Materials Sciences Volume 47, Issue 5, Pages 772 – 805, 2022

https://doi.org/10.1080/10408436.2021.1989663

substrate, and deposition time. Importantly, by varying the electrodeposition parameters, well-defined ZnO nanotubes instead of nanowires or nanorods can be easily fabricated [106,112,118].

Electroless deposition of ZnO nanowires

Electroless deposition is a process of chemical reduction in which metallic ions are directly reduced to metal by a reducing agent without the use of external electrical energy. Since 1946, when Brenner and Riddel developed the first industrial version of the process, electroless deposition has been widely applied due to its ability to produce excellent coatings, including on nonconductive or irregular surfaces [119–121]. Unlike other electrochemical deposition approaches such as electrodeposition, it also allows the deposition of metallic coating on nonconductive materials such as plastics.

In the process (Eq. 15), electrons are transferred through a catalytic surface by a chemical reducing agent that acts as a simple electron donor. When metallic ions, acting as electron acceptors, react with the electrons, metal can be deposited without using external electrical energy [120–122].

$$M^{n+}_{(aq)} + Red_{(aq)} \rightarrow M_{(s)} + Ox_{(aq)} \qquad \text{(Eq. 15)}$$

Because the deposited metal acts as a catalytic surface for the subsequent deposition of metal, electroless deposition is an autocatalytic process. Therein, as the deposited material increasingly accelerates the deposition, the reducing agent becomes oxidized [120–122]. In classical electroless deposition, pure Ni, Co, Sn, Rh, Pt, Cu, Au, Ru, Pd, and Ag can be electrolessly deposited as well as electrolessly co-deposited with Ni. During the past five decades, numerous reducing agents have been extensively used, including amino boranes, sodium borohydride, hydrazine, and sodium hypophosphite [120–122]. Although electroless deposition was originally designed as a process for depositing metals, it has since emerged as a simple, scalable, low-cost

https://doi.org/10.1080/10408436.2021.1989663

process for depositing ZnO nanowires and nanorods, one especially relevant to growing nanowires or nanorods on irregular, nonconductive, internal, and natural surfaces [6,123,124].

Mechanism

In 1996, Izaki *et al.* first proposed using electroless deposition to grow ZnO deposits [125–127]. Compared with other strategies involving chemical bath deposition (e.g., hexamethylenetetramine-based processes), electroless deposition allows the direct preferential growth of nanowires and nanorods without needing the otherwise necessary ZnO seed layer on the substrate. The electroless deposition of ZnO nanowires and nanorods typically involves using zinc nitrate as a precursor and dimethylamine borane (DMAB)—that is, $(CH_3)_2NHBH_3$—as a reducing agent at 50–80 °C [6,127]. Thus, a plausible mechanism of deposition can be written as [124,125,127,128]:

$$(CH_3)_2NHBH_{3\,(aq)} + 2\,H_2O_{(l)} \xrightarrow{cat} HBO_{2\,(aq)} + (CH_3)_2NH_2^{+}{}_{(aq)} + 5\,H^{+}{}_{(aq)} + 6\,e^{-} \quad \text{(Eq. 16)}$$

$$NO_3^{-}{}_{(aq)} + H_2O_{(l)} + 2\,e^{-} \rightarrow NO_2^{-}{}_{(aq)} + 2\,OH^{-}{}_{(aq\ and\ ads)} \quad \text{(Eq. 17)}$$

$$O_{2(aq)} + 2\,H_2O_{(l)} + 4\,e^{-} \rightarrow 4\,OH^{-}{}_{(aq\ and\ ads)} \quad \text{(Eq. 18)}$$

$$Zn^{2+}{}_{(aq\ and\ ads)} + 2\,OH^{-} \xrightarrow{cat} Zn(OH)_{2\,(s)} \xrightarrow{\Delta} ZnO_{\,(s)} + H_2O_{(l)} \quad \text{(Eq. 19)}$$

Unlike electrodeposition, the electroless deposition of ZnO nanowires or nanorods is possible on nonconductive substrates, including glass, polymers, or natural surfaces. Although the oxidation of the chemical reducing agent (e.g., DMAB) requires a catalytic surface to be initiated, such a surface can be easily provided by palladization, a process frequently used for the electroless deposition of metals [122,129]. Pd nanoparticles play a dual role as not only a catalyst

https://doi.org/10.1080/10408436.2021.1989663

for oxidating DMAB but also a nucleus for growing ZnO nanowires. Because the process is autocatalytic, the previously deposited ZnO also catalyzes the oxidation of the chemical reducing agent. In that process, the six electrons conveyed through the substrate's catalytic surface (Eq. 16) reduce the nitrate ions (Eq. 17) and/or the dissolved molecular oxygen (Eq. 18), which induces the generation of hydroxide ions. In turn, the electrogenerated hydroxide ions drive the precipitation of $Zn(OH)_2$, which ZnO dehydrates in a solid–solid phase transformation at moderate temperatures [125–128]. In parallel, the electrogenerated HBO_2 (pK_a = 9.24) and $(CH_3)_2NH_2^+$ (pK_a = 10.77) can also help to maintain a pH near 9-10 in the substrate's vicinity. Although other precursors and chemical reducing agents can be used in the electroless deposition of ZnO nanowires and nanorods, most studies to date have involved using zinc nitrate and DMAB.

Electroless parameters

The chief parameters to be considered for the successful electroless deposition of ZnO nanowires and nanorods appear in **Table 2**. Although other chemical reducing agents can be used for the process, most published works report the use of DMAB. Likewise, the parameters in **Table 2** are based on the use of DMAB, because stronger reducing agents could suggest alternative conclusions [6,124,127,130–141].

Table 2: Primary parameters of electroless deposition and their effects on the electroless deposition of ZnO nanowires and nanorods

Electroless parameter	Effect
Concentration of DMAB	- The concentration of DMAB, at low or moderate values (i.e., <50 mM), does not affect the morphology of nanowires, which depends heavily on the concentration of Zn(II) ions.

https://doi.org/10.1080/10408436.2021.1989663

	- Longitudinal growth—that is, (002) preferred orientation growth—increased as the DMAB/Zn(II) ratio increased [139]. - The optimal concentration of DMAB ranges from 4 to 50 mM.
Catalyst	- Pd catalyzation is the most widely applied process for activating nonconductive substrates for the electroless deposition of ZnO. The deposition of Pd nanoparticles on substrates allows the successful growth of ZnO nanowires or nanorods, sometimes both, on Si, Au, glass, alumina, polyethylene terephthalate substrates, cotton fabrics, polyester textile materials, and polymeric spheres [136,138,139,142]. - More cost-effective than Pd, Cu also presents excellent catalytic activity for the oxidization of DMAB. Several studies have demonstrated that Cu is an excellent substrate for inducing the electroless deposition of well-defined ZnO nanowires and nanorods. Indeed, ZnO nanowires have been grown by using electrolessly deposited Cu or Cu fibers, cables, or other Cu substrates [6,127,141]. - To the best of our knowledge, other metals (e.g., Ni) that can catalyze the oxidation of DMAB can be used in the deposition of ZnO films. The optimization of experimental conditions for growing nanowires and nanorods remains to be investigated [129,143]. - Although deposited ZnO will also catalyzes DMAB's oxidation, the process is slower than with Pd or Cu.

https://doi.org/10.1080/10408436.2021.1989663

Bath temperature	- Longitudinal growth—that is, (002) preferred orientation growth—as well as crystallinity increases as the temperature of deposition rises [139] . Texturation with the c-axis perpendicular to the substrate's surface is promoted at temperatures exceeding 55 °C [140]. - Optimal bath temperatures range from 70 to 85 °C.
Precursor	- Cl^- and SO_4^{2-} ions adsorbed on Pd nanoparticles inhibit the oxidation of DMAB when those nanoparticles are used as catalysts [124]. - ClO_4^- and NO_3^- ions favor the increase of pH in the substrate's vicinity to approximately 9, which itself favors the preferred growth of nanowires in the c-axis direction. Meanwhile, Cl^- and SO_4^{2-} ions cause a slow increase in pH compared with NO_3^- ions, which is detrimental for the deposition of ZnO [124]. - Wurtzite ZnO with the (002) preferred orientation materializes when ClO_4^- and NO_3^- precursors are used, whereas double salt hydrates such as $Zn_5Cl_2(OH)_8 \cdot H_2O$ and $Zn_4(SO_4)(OH)_6 \cdot 5H_2O$ form when Cl^- and SO_4^{2-} precursors are used, respectively [124]. - The most adequate precursor for synthesizing well-defined ZnO nanowires or nanorods is $Zn(NO_3)_2$ [124,127], whereas both it and $Zn(ClO_4)_2$ can be used as precursors and as sources of Zn(II) ions. - The presence of dissolved oxygen affects the crystal growth of ZnO nanowires by reducing their diameters relative to the

https://doi.org/10.1080/10408436.2021.1989663

	diameters of nanowires created with deoxygenated solutions [124].
Zn(II) concentration	- The (002) preferred orientation growth is promoted at relatively low or moderate concentrations of $Zn(NO_3)_2$. Concentrations of Zn(II) ions exceeding 50 mM prompt the growth of dense, compact ZnO layers with microplatelet morphology [130,137]. - At low and moderate concentrations of $Zn(NO_3)_2$, the lengths of nanowires increase nonlinearly while their diameters decrease linearly [133]. - Optimal $Zn(NO_3)_2$ concentrations range from 1 to 50 mM.
Deposition time	- The length and diameter of ZnO nanowires and nanorods increase as deposition continues, and longer deposition times cause ZnO films to be more compact [133]. - The (002) preferred orientation is more important when ZnO nuclei are formed than on a fresh Pd or Cu surface.

Electroless deposition of ZnO nanowires and nanorods

Electroless deposition has been proven to be an efficient, scalable, low-cost process for growing ZnO nanowires and nanorods on various substrates, including nonconductive materials with irregular shapes. Despite the need for a catalytic surface to effectively oxidate DMAB (**Figure 8**), which plays an important role in the transfer of electrons in order to electrogenerate hydroxide ions, the columnar architecture of nanowires and nanorods depends heavily upon the pH in the substrate's vicinity. When the oxidation of DMAB is initiated (Eq. 16), the reduction of NO_3^- ions occurs (Eq. 17), and the pH in the substrate's vicinity rises The presence of dissolved oxygen also favors the increase of pH (Eq. 18) [124]. At temperatures ranging from 70 to

Critical Reviews in Solid State and Materials Sciences Volume 47, Issue 5, Pages 772 – 805, 2022

https://doi.org/10.1080/10408436.2021.1989663

85 °C and at low or moderate concentrations of Zn(II) ions (i.e., <50 mM), the pH in the substrate interface progressively increases and ultimately hovers between 9 to 11 owing to the multiple co-occurring processes. The formation of HBO_2 and $(CH_3)_2NH_2^+$ species also plays an important role in keeping the pH between 9 and 11; that fact is critical, for at pH levels higher to 9, the dominant Zn(II) species are $Zn(OH)_3^-$ and $Zn(OH)_4^{2-}$ ions (**Figure 3**), which effectively quench the lateral growth of the ZnO nucleus [12]. The dominant negatively charged Zn(II) species are electrostatically attracted to the positively charged tetrahedron corners of hexagonal crystals (**Figure 8**), which, in promoting growth in the direction of the c-axis, facilitates the formation of well-defined ZnO nanowires and nanorods [6,127,128,133,136,139].

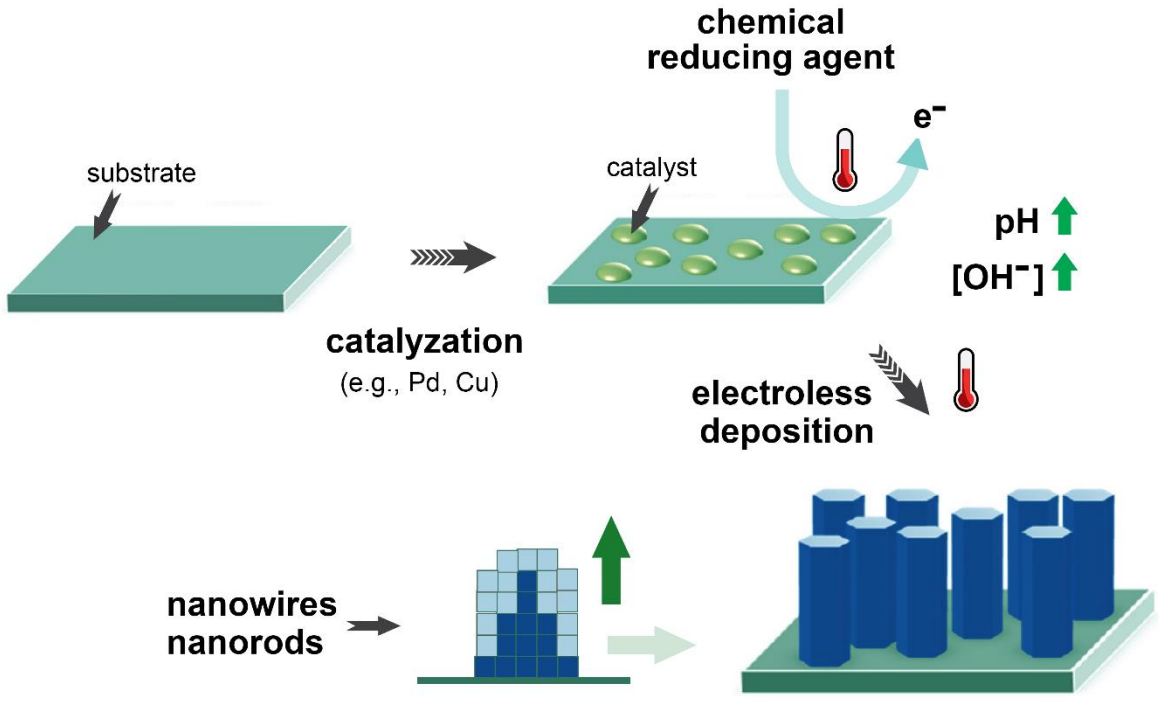

Figure 8: Schematic representation of the electroless deposition of ZnO nanowires or nanorods.

Variation in the parameters of electroless deposition allows excellent control over the length, diameter, aspect ratio, and growth density of ZnO nanowires and nanorods created. During the past three decades, the process has been extensively used to deposit well-defined

Critical Reviews in Solid State and Materials Sciences Volume 47, Issue 5, Pages 772 – 805, 2022

https://doi.org/10.1080/10408436.2021.1989663

nanowires on different materials, including Pd-catalyzed glass substrates (**Figure 9a**) [133], Cu mesh (**Figure 9b**) [127], Cu cables (Figure 9c) [6], cotton fabrics (**Figure 9d**) [136], and polymeric spheres (**Figure 9e**) [138]. In short, electroless deposition represents an industrially applicable strategy for synthesizing well-defined ZnO nanowires and nanorods.

Critical Reviews in Solid State and Materials Sciences Volume 47, Issue 5, Pages 772 – 805, 2022

https://doi.org/10.1080/10408436.2021.1989663

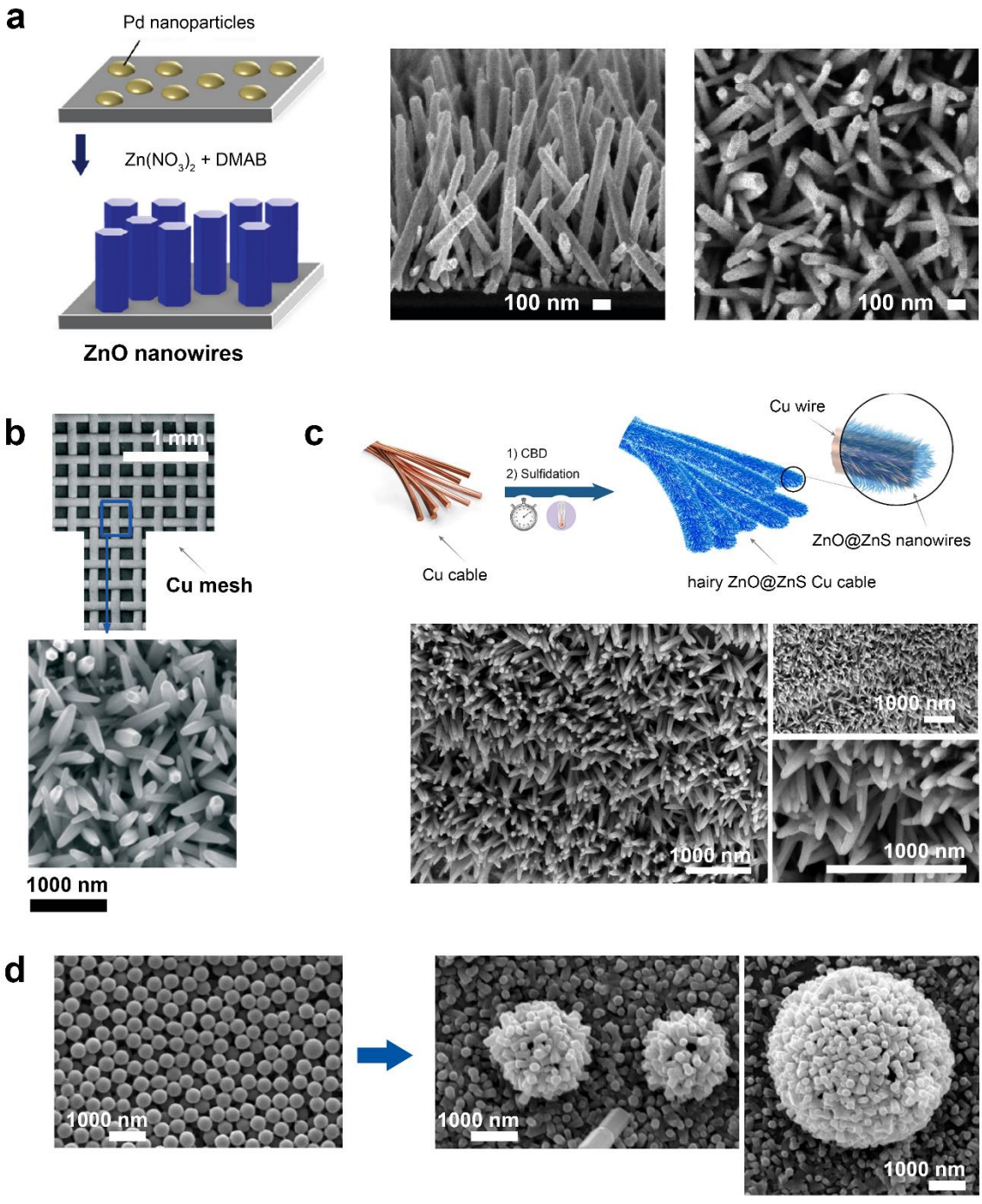

Figure 9: FE-SEM micrographs of ZnO nanowires deposited on (a) Pd-catalyzed glass substrates (adapted with permission from [133]), (b) Cu mesh (adapted with permission from [127]), (c) Cu cables (adapted with permission from [6]), (d) cotton fabrics (adapted with permission

https://doi.org/10.1080/10408436.2021.1989663

from [136]), and (e) polymeric spheres (adapted with permission from [138]).

Modification of ZnO nanowires

Despite the robust physical and chemical properties of ZnO nanowires and nanorods, the structures are often modified in order to improve their performance in different applications or to improve their stability, especially their photostability [144–146]. The modification of ZnO nanowires and nanorods can have various objectives, although primarily seeks to enhance their photosensitivity in the visible domain and to hinder the fast recombination of the photogenerated electrons and holes in order to improve their quantum yield and minimize wasted energy. The wide bandgap of ZnO nanowires and nanorods (E_g = approx. 36 eV) requires an excitation wavelength in the UV domain ($\lambda < 390$ nm), which is incompatible with the low percentage of UV light (<4.0%) in the solar spectra. Pure ZnO nanowires and nanorods are thus highly limited to sunlight-driven devices. Beyond that, considering the costs of energy consumption and concerns about sustainability, extending the photosensitivity of ZnO nanowires and nanorods to visible light (42–43% of the solar spectra) and improving their competiveness are both greatly needed undertakings [97,147–149]. The modification of ZnO is also popularly pursued to hinder its high photocorrosion activity, especially in aqueous media, or to tune its electrical or magnetic properties. Of course, modification can have other goals, but they are far less common [145,146].

Among the many strategies for modifying ZnO nanowires, the most widespread and effective are anionic doping (e.g., with C, N, and S), cationic doping (e.g., with Mn, Ni, Co, Bi, Fe, K, and Mg), rare earth doping (e.g., Ce, Dy, Er, Eu, Gd, Ho, and Nd), co-doping, semiconductor coupling, and surface decoration. In the context of the electrochemical deposition of ZnO nanowires and nanorods, the doping and co-doping processes are frequently performed simultaneously with the deposition of ZnO by modifying the composition of the

https://doi.org/10.1080/10408436.2021.1989663

electrochemical bath and the deposition conditions [97,145,150]. Surface decoration and semiconductor coupling, which result in the formation of heterostructured nanowires, are performed by subjecting the electrosynthesized nanowires or nanorods to an additional treatment based on electrochemical, physical, chemical, or photochemical processes [97,146,149].

Properties of ZnO nanowires

As it was shown before, ZnO nanowires can be obtained by different approaches, using templateless [97,151] or hard-templates as anodic aluminum oxide (AAO) templates [112] or polycarbonate membranes [152,153], etc... Depending on how ZnO nanowires are obtained, the structural, morphological, optical and electrical properties are different. The application which ZnO can be applied are directly connected by these properties. Furthermore, when ZnO is doped or form part of a heterojunctions different properties and application can be achieved. This section is focus on analyze the optical, photoluminescence, electrical and magnetic properties of ZnO nanowires. The properties of ZnO can be tuned by the electrosynthesis conditions as such as electrolyte, precursor concentration, bath temperature, applied potential, applied current density, pulsed electrodeposition, deposition time, etc...

Crystallographic structure

ZnO presents wurtzite structure with a hexagonal unit cell with two lattices parameters, *a* and *c*. In this structure, each Zn^{2+} is tetrahedrally linked to four O^{2-} ions. There are two polar faces, the [0 0 0 1] finished in Zn^{2+} and the [0 0 0 $\bar{1}$] finished in O^{2-}. The non-polar faces are the [1 1 $\bar{2}$ 0] and [1 0 $\bar{1}$ 0], which have the equal number of atoms of Zn^{2+} than O^{2-}. **Figure 10** shows the ZnO crystallographic structure and the example of one of the polar and non-polar faces of ZnO hexagonal structure.

Critical Reviews in Solid State and Materials Sciences Volume 47, Issue 5, Pages 772 – 805, 2022

https://doi.org/10.1080/10408436.2021.1989663

When ZnO presents a preferred orientation along the *c-axis*, the growth is perpendicular to the substrate's surface, the material presents the [0 0 0 1] direction. In this case, the semiconductor exhibits excellent electrical properties. It is well-known than in the case of nanowires, for applications as such as solar cells, UV-photodetectors, light emitting diodes (LED's), etc...it is essential that the ZnO nanowires are oriented along the *c-axis* of the structure, exhibits [0 0 0 1] direction, in order to have excellent electrical properties and then it can be formed part of efficient devices. In the case of ZnO nanowires grown by electrodeposition or electroless, the nanowires are normally polycrystalline, but in some cases the deposition conditions were tuned in order to obtain nanowires highly oriented along the *c-axis* of ZnO structure, in the [0 0 0 1] direction [6].

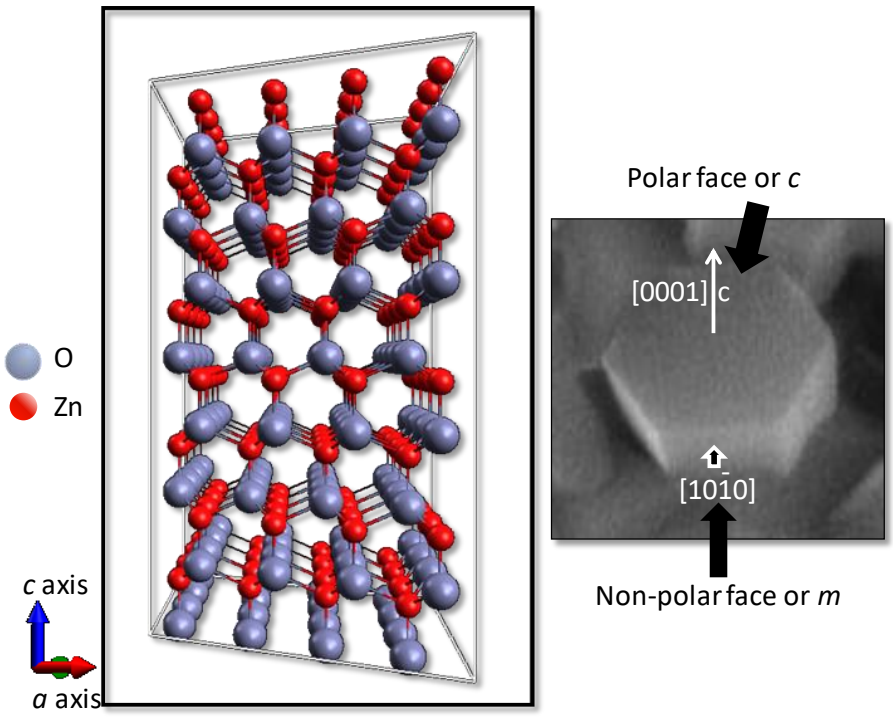

Figure 10: Crystallographic structure of ZnO and the example of one of the polar and non-polar faces of ZnO. Reproduced from [154] with permission.

Critical Reviews in Solid State and Materials Sciences Volume 47, Issue 5, Pages 772 – 805, 2022

https://doi.org/10.1080/10408436.2021.1989663

Optical properties

Due to the wide band gap of ZnO (E_g~3.36 eV), this material is a perfect candidate for UV applications and emission in the visible range. In this sense, it is important to study the optical properties of ZnO nanowires electrodeposited using different approaches on the UV and Vis ranges.

Referent to the optical properties of ZnO nanowires grown on flat substrate, different studies are found in the literature. In 2010, Xu *et al.* reported high transmittance (90%) in the visible wavelength range in ZnO nanorods vertically aligned arrays and a blue-shift in the band gap when these nanorods are comparing with ZnO films [155]. The same year, J. Elias *et al.* published an increment of 30% in the reflectance when ZnO hollow urchin-like thin films were compared with ZnO nanowires. These nanostructures were grown using polystyrene spheres (PS) [91] (see **Figure 11**). One year later, different band gap energies (3.23 and 3.29 eV) were obtained when the diameter of ZnO nanowire arrays changes from 40 to 250 nm. This variation in the diameter was due to the precursor used for the growth of the nanowires [156]. An increment in the reflectance from 10 to 20% was observed when ZnO nanowires were grown only longitudinally and longitudinally and laterally [78].

Critical Reviews in Solid State and Materials Sciences Volume 47, Issue 5, Pages 772 – 805, 2022

https://doi.org/10.1080/10408436.2021.1989663

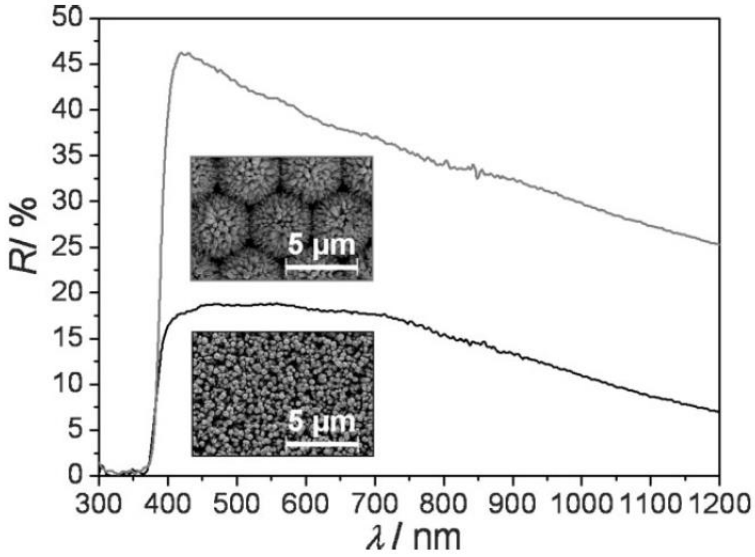

Figure 11. Total reflectance spectra of glass/SnO_2:F/ZnO free-standing nanowires samples and ordered hollow urchin-like structure arrays. Each SEM images corresponds to its spectrum above. Adapted from [75] with permission.

In the case of nanowires electrodeposited inside templates, the reflectance of ZnO nanowires grown inside polycarbonate (PC) membranes were compared depending on the applied potential used for the electrodeposition, obtaining a maximum value of 47% when more negative potential was applied. An increment from 10% to 47% was reported when the potential was reduced from -0.9V to -1.2V [157].

Respect to doped ZnO nanowires, Lupan *et al.* reported the optical properties for Eu-doped ZnO and Ag-doped ZnO nanowires. In the case of Eu, an increment of 10-15% in the transmission was observed [158]. However, when ZnO is doped with 3.7% of Ag, a reduction of 10% in the transmittance was reported compared with undoped ZnO [159]. A similar behavior was observed when Ag nanoparticles are used to decorate ZnO nanowires, a reduction in the transmittance of 40-55% was measured when different concentration of Ag were incorporated (from 1 to 3%) to ZnO nanowires [160].

Critical Reviews in Solid State and Materials Sciences Volume 47, Issue 5, Pages 772 – 805, 2022

https://doi.org/10.1080/10408436.2021.1989663

The optical properties of heterojunctions formed between ZnO and other materials as ZnS, ZnSe, Cu_2O, α-FeO_3 was also reported in the literature. An increment of 5% in the maximum absorbance was observed in the case of ZnO/ZnS core/shell nanowires compared to ZnO nanowires [161]. A reduction of 20% in the transmittance was obtained in the case of ZnO (80%) nanowires respect to ZnO/ZnSe (60%) core/shell nanowires [162]. A high reduction in the band gap, from 3.34 to 1.7 eV, was reported when ZnO nanowires were compared with ZnO/Cu_2O core/shell nanowires [163].

Photoluminescence properties

By photoluminescence measurements is possible to analyze the band gap of ZnO nanowires and the defects of the material [164,165]. ZnO nanowire arrays grown on ITO substrate exhibits a band gap of 3.27 eV and a wide emission band in the yellow-orange region due to interstitial oxygen [5]. In the case of urchin-like ZnO using PS spheres, three photoluminescence peaks were observed at 3.23, 3.00 and 2.30 eV, corresponded to the recombination of free excitons at the near-band edge of ZnO nanowires and the green emission associated with oxygen vacancies, respectively [166]. Additionally, the photoluminescence of ZnO nanowires before and after an annealing process under different conditions was investigated. ZnO nanowires before annealing present a band gap of 3.26 eV at room temperature; however, after an annealing at 400 ºC for 1 h in air, the intensity of the near band gap luminescence decreases and exhibits a narrower band. Also, two more band appears at 2.55 eV and 1.85 eV, the first band is associated to zinc vacancies and the second is due to an unidentified acceptor, which energy level is close to the middle of the band gap [167].

The photoluminescence of ZnO nanowires grown inside polycarbonate membranes was also analyzed. Three different peaks were observed, at 350 nm (3.52 eV) due to the impurities

https://doi.org/10.1080/10408436.2021.1989663

of the nanowires, at 364 nm associated to the band gap, and 382 nm attributed to structural defects in the crystal of ZnO [168].

Respect to the photoluminescence measurements of doped ZnO nanowires, few studies were published. In the case of Cu-doped ZnO nanowires, the band gap was shifted from 382 nm (for ZnO) to 394 nm (for Cu-doped ZnO). No visible emission due to deep defects was found in this kind of nanowires [169]. A red-shifted in the band gap was observed for chlorine-doped ZnO nanowires; additionally, a band located at ~ 600 nm (associated to surface defects) disappeared when the nanowires are doped with Cl [170].

In the case of heterojunctions, the photoluminescence of ZnO/PANI coaxial nanowires was measured observing an important PL intensity increment respect to ZnO nanowires. Two other peaks were also identified, at ~373 nm due to excite emission, and at 400 nm associated to oxygen vacancies or zinc interstitial defects [171]. For Ag-decorated ZnO nanowires, a red-shift in the band gap is observed and the PL intensity decreases [160]. However, when ZnO nanowires are coated with Ni, the green emission observed in ZnO nanowires is quenched [172]. In the case of a heterojunction between ZnO and α-FeO_3, ZnO/α-FeO_3 core/shell nanowires exhibits three peaks, at 387 nm related to the NBE emission in ZnO, at 515 nm due to green emission associated to the combined effect of the band edge emission in α-FeO_3 nanowires and zinc vacancies from ZnO, and at 556 nm (yellow-green region) attributed to oxygen vacancy defects in ZnO [173].

Building block properties

Exactly what do we mean when we talk about building blocks? A building block is a basic unit of a construction or composition from which a larger entity or more complex structure is developed. For future hierarchical architectures, ZnO nanowires are the most promising building blocks due to methods that allow precisely controlling their morphology, composition,

Critical Reviews in Solid State and Materials Sciences Volume 47, Issue 5, Pages 772 – 805, 2022

https://doi.org/10.1080/10408436.2021.1989663

growth, structure, doping, and assembly, as well as their potential incorporation into other materials [97,174,175]. During the past two decades, multiple complex architectures have been electrosynthesized using ZnO nanowires and generally show two interconnected, simultaneously occurring levels. At one, each nanowire is an individual element used to build a more complex structures, including urchin-like ZnO architectures; at the other, a set or array of nanowires act as an individual building block. As a result, once a structure with many nanowires is formed, it can later be integrated as a building block into a device [176–179].

To continue with the mentioned example, in urchin-like ZnO architectures each nanowire mimics the spine of a sea urchin as a building block of such complex systems (**Figure 12a**). Urchin-inspired ZnO structures can also serve as building blocks in real devices (e.g., dye-sensitized solar cells) thanks to their simple, scalable electrochemically based fabrication. The urchin-like organization of ZnO nanowires can improve light scattering and provide a larger surface area, both of which can be fine-tuned by controlling the dimensions of the nanowires.[174,175].

Critical Reviews in Solid State and Materials Sciences Volume 47, Issue 5, Pages 772 – 805, 2022

https://doi.org/10.1080/10408436.2021.1989663

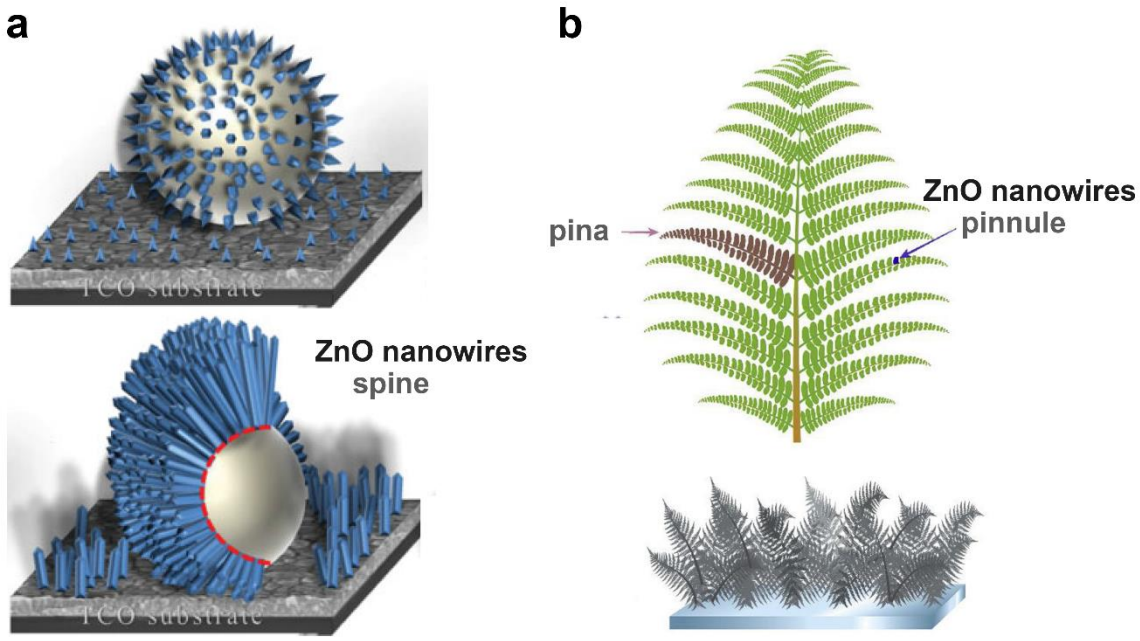

Figure 12: Schematic representation of (a) urchin-like ZnO (adapted from [151] with permission) and (b) ZnO microfern architectures (adapted from [97] with permission).

Another example is the creation of fractal and branched ZnO nanowire-based architectures frequently inspired by plants and/or leaves (**Figure 12b**). Those complex architectures can be grown directly via electrodeposition in controlled conditions or result from the assembly of individual ZnO nanowires [97,144,180]. . In either case, the branched architectures are formed by nanowire units and can be used globally as a building block for photochemical and photoelectrochemical devices [97,181]. The fractal and branched architecture of those units can translate into the important enhancement of light trapping and absorption as well as improve the architecture's surface-to-volume ratio [97].

Possibilities for forming more complex architectures based on ZnO nanowires abound. In particular, the simplicity of electrochemical methods, especially electroless processes, affords

https://doi.org/10.1080/10408436.2021.1989663

a wide range of possibilities for significantly improving the efficiency of new devices, especially in applications that need to improve light absorption or increase the surface area.

Electrical properties

Since ZnO is a n-type semiconductor, in this section the electrical properties of this semiconductor will be analyzed. Most of the electrical properties of ZnO nanowires were measured in nanowires grown inside templates, doped-ZnO or heterojunctions due to in the first case more uniform and large nanowires can be obtained. Respect to the ZnO nanowires grown on a flat substrate, the intensity-voltage (I-V) curve was measured in ZnO nanowire arrays grown on ITO, another ITO layer was deposited on the top of the nanowires, the electrical resistivity was found to be between KΩ-MΩ [182].

Respect to the electrical properties of ZnO nanowires grown inside templates, it was reported the growth of ZnO nanowires in PMMA lithography templates, these nanowires were perfectly oriented along [0001] direction, and the contact for the electrical properties was made using nanopillars of 100 μm in length and 50 nm thickness of Ag. The intensity-voltage curves show a non-linear behavior due to the Schottky contact at the Au-ZnO interfaces reaching $5 \cdot 10^{-6}$ A when 1 V was applied [168]. Also, ZnO nanowires grown inside PC membranes were measured, a single nanowire was measured and aligned by electrophoresis, the electrical resistivity was found to be $2.2\text{-}3.4 \cdot 10^{-3}$ Ω·m, in this case the electrical resistivity is very low comparing with ZnO nanorods (ρ=10 Ω·m) due to the electrophoresis process to suspense the nanowires on the chip [183]. In 2014, another study about the electrical properties of ZnO inside PC membranes was published, the measurements were also performed in a single wire. In order to increase such properties, several annealing treatments were applied at different temperatures, 200, 350 and 450 ºC; an improvement in the transport properties was observed. For temperatures lower of 350 ºC the I-V curves are not linear, while for temperature higher than 350 ºC a strange

https://doi.org/10.1080/10408436.2021.1989663

decrease of electrical conductivity was observed. The best results in terms of devices behavior was obtained when the annealed temperature was 350 ºC [157].

In order to improve the transport properties of ZnO different elements were studied for doping as such as Sn, Cl and Ag. Sn-doped ZnO nanowires exhibit an excellent emission current stability and ~ 10 μA for 6h. The sheet resistance was 3 and 13 KΩ for 0.5% and 2% Sn, respectively [145]. In the case of Cl-doped ZnO nanowires, the I-V curves were measured using a SPM (Scanning Probe Microscope) with a Pt-coated tip. For all ZnO:Cl nanowires quasi-symmetric I-V response was observed common in semiconductors. A decrease of two orders of magnitude in the electrical resistivity was obtained for the maximum Cl doping in ZnO. The electrical resistivity was found to be 1.9, 1.81, 1.79, 0.25, 0.051 and 0.019 Ω·cm when a concentration of NH_4Cl used was 0, 0.005, 0.02, 0.05, 0.07 and 0.1 M, respectively [170]. In the case of Ag-decorated ZnO nanowires, the I-V curves show a rectifying behavior and a lower current was measured for this king of nanostructures [159].

Different heterojunctions based on ZnO nanowires can be found in the literature. I-V curves of PEDOT:PSS and ZnO nanowires show a good rectifying behavior with a rectification factor of 25 ± 5 V [5]. Another heterojunction is the one composed of ZnO/α-FeO_3 core/shell nanowires, the I-V curves were obtained using an AFM tip (Pt-Ir). The electrical resistivity of this kind of nanowires was found to be $3.1 \cdot 10^2$ Ω·m [173].

Magnetic properties

ZnO is a non-magnetic material, but can exhibit a magnetic character when ZnO is doped with different magnetic materials as such as Cu, Co, Mn, Ni, Fe_2O_3. In this section, the magnetic properties of ZnO nanowires doped with different materials and heterojunctions will be studied.

Critical Reviews in Solid State and Materials Sciences Volume 47, Issue 5, Pages 772 – 805, 2022

https://doi.org/10.1080/10408436.2021.1989663

Respect to the magnetic properties of ZnO nanowires deposited on flat substrates, the magnetic hysteresis was compared between ZnO doped with Co, Mn and Cu. Saturation was observed at ~ 2 KG for Mn and Co, and at ~ 1 KG for Cu. The observed response can be identified as superparamagnetic; this behavior is interpreted as a ferromagnetic response of small ferromagnetism domains whose Neel relaxation time is smaller than the typical measurement time [184].

In the case of ZnO nanowires electrodeposited using a template, J-J. Gu *et al.* reported the magnetic response of Co- doped ZnO nanowires using AAO templates after the deposition and applying different annealed temperatures (400, 500 and 600 ºC). The magnetic hysteresis loops were measured in the parallel and perpendicular direction to the nanowire growth. H_c in the parallel and perpendicular direction to the nanowire growth was found to be 1000, 590 and 925 Oe for as deposited nanowires, at 400 ºC and 500 ºC annealed temperatures, respectively. Mr/Ms was 44% and 69% for nanowires annealed at 400 ºC and 500 ºC, respectively[150].

Referent to the heterojunctions, the magnetic properties of Ni-coated ZnO nanowires were studied. The coercivity field and remanence ratio were 930 Oe and 15% while the magnetic field was parallel to the sample surface, and 740 Oe and 9.2% for perpendicular to the surface. In general, the ferromagnetic properties of ZnO/Ni core/shell nanowires are lower than to ZnO/Co nanowires [185].

Piezoelectrical properties

ZnO nanostructures, especially nanowires, have significant potential for creating nanoscale piezoelectric devices, the piezoelectric effect of which can convert a mechanical vibration into an electrical signal, or vice versa [186–188]. Owing to the nature of ZnO semiconductors, the piezoelectric effect, the formation of Schottky barriers between the metal or conductive

https://doi.org/10.1080/10408436.2021.1989663

polymers and ZnO contacts, and ZnO's relatively low toxicity, ZnO nanowires are excellent candidates for designing nanogenerators [189–191].

Piezoelectric nanogenerators based on ZnO nanowires with an estimated efficiency of 17–30% have been designed by Wang [189]. Because the piezoelectric coefficient of nanowires and nanorods exceeds the value obtained for bulk wurtzite ZnO up to their free boundaries [187], the piezoelectric energy output of an individual nanowire in one discharge event was approximately 0.05 fJ, whereas the output voltage on the load was approximately 8 mV. Those values could be significantly enhanced if the resonance of nanowires could be induced [189,192]. Growing ZnO nanowires on flexible polymeric substrates such as polyethylene terephthalate (PET) substrates can be an efficient strategy for improving the piezoelectric outcome. For example, ZnO nanowires on PET substrate yield $5 \cdot 10^{-10}$A without vibration, whereas a sample with 2% bending with vibration at a low frequency yields approximately $2.5 \cdot 10^{-7}$A, thereby demonstrating that slightly bending a flexible substrate can improve the piezoelectric performance [193]. That approach possesses potential for powering nanodevices; however, the output power of most developed direct current nanogenerators is remains too low to satisfy the requirements for microelectronic devices. Recently, Sun et al. demonstrated that direct current nanogenerators based on an array of two-layer ZnO nanorods with an equal c-axis direction can significantly enhance the peak voltage and current density compared with pure ZnO-based nanogenerators, thereby yielding a voltage output of 1.6 V and a current output of approximately $16.4 \cdot 10^{-6}$A. That improvement is due to the formation of Schottky and Ohmic contact at the top and bottom electrodes, respectively [194]. Alternatively, the piezoelectrical properties of ZnO nanowires can enhance the photocatalytic degradation of organic pollutants via the piezo-driven separation of photo-generated electron-hole pairs due to the significant suppression of the recombination process [190]. When a deformation is applied to ZnO nanowires, electron-hole pairs migrate to the surface in the opposite direction due to the piezoelectric field.

Critical Reviews in Solid State and Materials Sciences Volume 47, Issue 5, Pages 772 – 805, 2022

https://doi.org/10.1080/10408436.2021.1989663

By coupling the piezoelectric and photocatalytic character of ZnO-based nanowires, that dynamic is highly promising for water decontamination process [190].

Pyroelectrical properties

The pyroelectric effect is defined as the change in the spontaneous polarization of materials as a function of temperature [195]. ZnO-based nanostructures, especially nanowires and nanorods, are of special interest in research due to the non-centrosymmetric wurtzite structure. In the specific case of nanowires and nanorods, that effect is more important because changes in pyroelectric polarization are generated at both ends of the c-axis of nanowires and/or nanorods via time-dependent changes in temperature [196]. Those characteristics afford the possibility of using ZnO nanowires and nanorods for designing more efficient photodetectors [197,198]. Alternatively, the pyroelectric properties of ZnO nanowires can be used in thermocatalysis by combing of pyroelectricity with electrochemical oxidation to decompose organic pollutants such as rhodamine B, in which the pyroelectric effect enhances the efficiency of electrochemical oxidation [199].

Applications

Due to their properties, ZnO nanowires can be used in a wide range of applications, including photocatalytic water treatment, photoelectrocatalytic water oxidation, antibacterial agents, solar cells, UV-photodetectors, supercapacitators, batteries, nanosensing, hydrogen evolution, and LEDs applications. This section discusses, the various applications of ZnO nanowires grown by electrodeposition.

Critical Reviews in Solid State and Materials Sciences Volume 47, Issue 5, Pages 772 – 805, 2022

https://doi.org/10.1080/10408436.2021.1989663

Photocatalytic water treatment

ZnO nanowires rank among the most promising photocatalysts for water-decontaminating technologies, owing mostly to their high photocatalytic performance, low cost, and green properties. However, the wide bandgap of ZnO nanowires, which limits the use of sunlight, and fast recombination of photoinduced electron–hole pairs, as well as their highly photocorrosive activity, hinder the practical application of ZnO nanowires. The fundamental principle of photocatalysis relies upon the photoexcitation of electrons (e_{CB}^-) from the filled valence band (VB) to the empty conduction band (CB), as shown in **Figure 13**, which forms positive holes (h_{VB}^+) and electrons on the surface of ZnO nanowires, as capture in Eq. 20 [6].

$$ZnO + hv \rightarrow e_{CB}^- + h_{VB}^+ \qquad (Eq.20)$$

That process is initiated when the ZnO nanowires or nanorods adsorb photons with energies greater than the bandgap energies. Therefore, ZnO nanowires require an excitation wavelength in the UV domain (i.e., $\lambda < 390$ nm), which limits the inexpensive use of solar light irradiation, because less than 5% of the solar spectra is UV [6]. The photocatalytic performance of ZnO nanowires can be improved and extended to the visible spectrum, however, by doping or another modification strategy (e.g., semiconductor coupling). Such modifications not only extend the photosensitivity of ZnO nanowires to the visible domain but also reduce the high recombination of electron–hole pairs as well as improve the properties of photostability. Although intensive research has been performed to materialize solar-driven ZnO-based photocatalysts during the past two decades, additional modifications remain necessary in order to improve their photocatalytic activity under direct sunlight irradiation by reducing their bandgap energies as well as minimizing their recombination losses [6].

Critical Reviews in Solid State and Materials Sciences Volume 47, Issue 5, Pages 772 – 805, 2022

https://doi.org/10.1080/10408436.2021.1989663

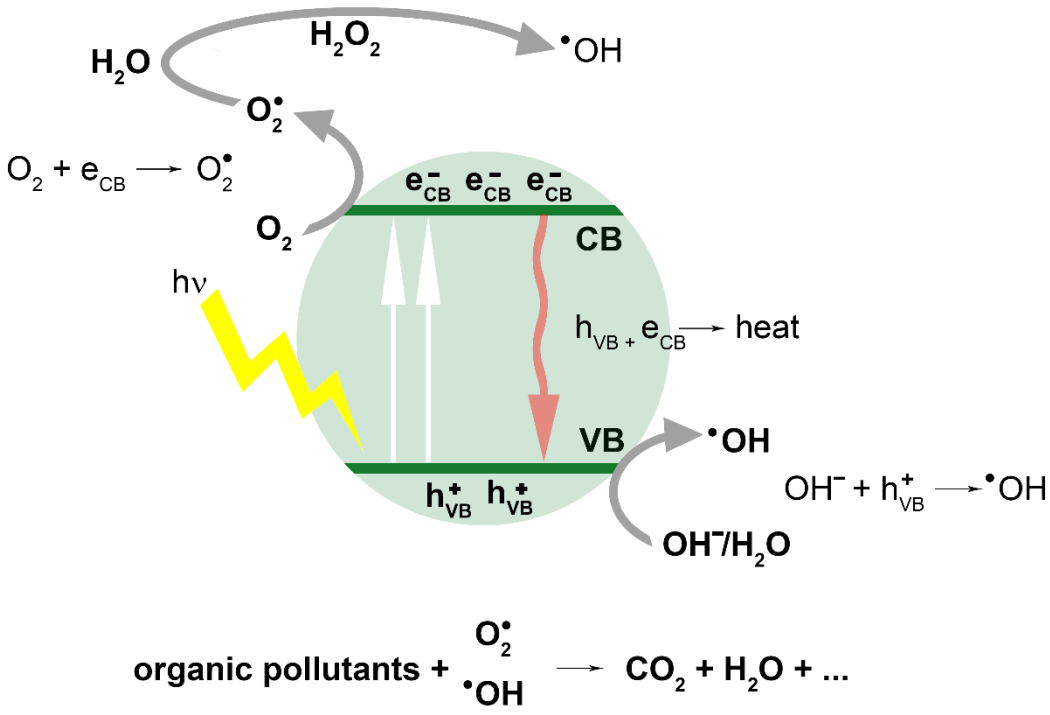

Figure 13: General mechanism of the photocatalysis of ZnO nanowires.

Organic pollutants can be directly oxidized and mineralized into carbon dioxide, water, and mineral acids by means of photogenerated holes or else indirectly oxidized and mineralized in a reaction with the highly oxidizing reactive oxygen species previously formed (e.g., hydroxyl or superoxide radicals). Although the magnitude of publications and varying natures of organic pollutants make it impossible to summarize even the major results of the effective (i.e., photodegradation and/or mineralization close to 100%) use of ZnO-based nanowires for water-decontaminating applications, most of those publications focus on the total photo-oxidation of organic dyes, phenolic compounds, drugs, pesticides, and persistent organic pollutants, because they are difficult, if not impossible, to remove with conventional water treatment technologies [6,144]. Beyond that, because inorganic ions found in industrial wastewater are also toxic in some of their valence states, the photoreduction of metals to nontoxic forms or

https://doi.org/10.1080/10408436.2021.1989663

their removal from waste streams is also relevant to water decontamination, in which various toxic heavy metals, including Ag(I), Cr(VI), Hg(II), and Pt(II), can be directly reduced into less toxic species by reacting with the photogenerated electrons [144].

The photocatalytic performance of ZnO nanowires depends not only upon their optoelectronic properties but also ZnO's loading and structure, the concentration of pollutants, the pH of the medium, the light's wavelength and intensity, the temperature, and the effect of other species on the reaction medium, among other factors. Although the general effect of those variables is quite similar from one nanostructured material to the next, the photocatalytic performance of ZnO-based photocatalysts is strongly affected by their architecture, including in terms of shape and dimensions, which determines the specific surface area and hence the light-trapping ability as well as ability to interact with pollutants. Within the range of nanostructured materials, nanowires offer important advantages that significantly improve their global photocatalytic performance as well as facilitate their integration into photoreactors. Nanowires generally have lower specific surface areas than nanoparticles, whereas their growth can be easily achieved on an array of substrates, including irregular surfaces. The possibility of growing and being easily fixed on substrates significantly facilitates their reuse, thereby bypassing the complicated recovery and pretreatment processes required by most nanostructured materials, which are generally suspended in the reactant media [6]. Likewise, nanowires can be building blocks for creating more effective architectures such as fractal structures or biomimetic systems (e.g., fern microleaves and sea urchins), as described in Section 5.4 [92,97,200,201]. Composed of multiple nanowires, those complex architectures improve the light-trapping ability of photocatalysts, facilitate pollutants' access to the photocatalyst's surface, and enhance absorption independent of incident angles, which is especially important for sunlight-driven devices.

Critical Reviews in Solid State and Materials Sciences Volume 47, Issue 5, Pages 772 – 805, 2022

https://doi.org/10.1080/10408436.2021.1989663

Despite intensive research during the past two decades on using ZnO-based nanowires, further studies are needed to clarify and improve the performance of solar photocatalysts in large volumes of real water as well as the incorporation of those nanostructures into the design of effective photoreactors.

Photoelectrocatalytic water oxidation or reduction

The sunlight-driven photoelectrochemical splitting of water into hydrogen and oxygen on ZnO nanowires and nanorods has attracted considerable attention in relation to overcoming the technological limitations of producing hydrogen from carbon-free sources (e.g., H_2O). ZnO nanowires are promising photoanode candidates due to their wide bandgaps, high electron mobility, low onset potential, simple fabrication, and low cost [7,202–205]. However, the rapid recombination of photogenerated electrons and holes, slow carrier transfer kinetics, and high photocorrosive activity of ZnO nanowires result in poor energy conversion efficiencies [202,203]. The photoelectrochemical process involves two electrodes: the photocathode and photoanode. Whereas the photoanode is irradiated by light during the process, the photocathode is not, or at least not necessarily. Instead, the photoanode adsorbs light to drive water oxidation, which forms oxygen and protons, while protons are simultaneously reduced to form hydrogen at the photocathode. The fundamental principle of photoelectrochemical water oxidation also relies upon the photoexcitation of electrons from the filled VB to the empty CB when the photoanode is irradiated by light that has energy greater than the bandgap of the ZnO nanowires or nanorods[7].

The limitations of ZnO nanowires can be overcome by modifying them via doping or semiconductor coupling [7,204–206]. Thus, extensive research has been conducted on synthesizing effective ZnO-based nanowire arrays photoanodes using various methods [204]. According to the literature, to electrosynthesize ZnO nanowires, the formation of heterostructured ZnO-based

https://doi.org/10.1080/10408436.2021.1989663

nanowires or the decoration of their surfaces with metal nanoparticles or nanostructured oxides seems to be more efficient than doping in terms of the performance of photoelectrochemical water oxidation [205,206]. Nevertheless, doping approaches have demonstrated remarkable effectiveness when other routes of synthesis are employed [207]. For example, doping with Al ions has been shown to improve the electrical conductivity of ZnO nanowires, whereas the photoelectrochemical performance remained unchanged [205]. Even so, Mo-doped ZnO nanorods, especially when assisted with cobalt phosphate, can significantly increase the photocurrent up to 250%, relative to pristine ZnO nanorods [7]. At the same time, the formation of ZnO@TiO_2–FeOOH core@shell nanowire arrays was shown to improve the photostability and photocurrent density of nanowires, which were nearly 180% and 690% times higher than that of ZnO@TiO_2 core@shell nanowires and ZnO nanowires, respectively [208]. Surface decoration is another promising approach to modification, as demonstrated by the preparation of ZnO nanorods decorated with cobalt acetate, which effectively lowers the onset potential of the oxygen evolution reaction and improves the photo-oxidation current of the oxygen evolution reaction by fourfold [203]. Last, electrodepositing Co_3O_4 nanocrystals on ZnO nanorods is another possibility, one which exhibits enhanced oxygen evolution reaction activity with less overpotential and more favorable kinetics [206].

ZnO nanowires have also been applied for hydrogen evolution applications while decorated with MoS_2 [209] and in the case of ZnO/CdS/$CuSbS_2$ core/shell nanowire arrays [210]. In the first case, Mo_2S/ZnO achieved an efficiency of hydrogen evolution of 2.38 times higher than ZnO nanowires [209].

Antibacterial agents

Recent investigations into ZnO-nanostructured materials, especially nanoparticles, as antibacterial agents with potential applicability in the food industry have shown that ZnO

https://doi.org/10.1080/10408436.2021.1989663

nanowires and nanorods exhibit not only significant antibacterial and antimicrobial activity but also good biocompatibility with human cells. However, the various mechanisms proposed to explain the antibacterial activity of such materials continue to be debated [211–214].

According to the literature, four mechanisms may explain the antibacterial activity of ZnO-based nanomaterials. The first involves the formation of reactive oxygen species such as hydroxyl radicals, superoxide ions, or hydrogen peroxide, all of which can attack cell walls (e.g., lipids and proteins), penetrate cells, and, in turn, inhibit or kill micro-organisms. In view of that mechanism, numerous researchers have characterized the formation of reactive oxygen species as the major cause of ZnO's nanotoxicity. The second is the release of Zn(II) ions, which significantly inhibits the active transport and disrupts the metabolism of amino acids and the enzyme system. Several other researchers have demonstrated the potential effect of Zn(II) ions in media, in which their release depends heavily upon the physicochemical properties of ZnO nanowires or nanorods, the media's chemistry (e.g., pH and ionic strength), and external stimuli (e.g., light irradiation). The third proposed mechanism maintains that the internalization of nanowires or nanorods into bacteria effectively inhibits the energy metabolism of bacteria and may cause mechanical damage, especially if external stimuli are applied. Fourth and finally, electrostatic interactions between nanowires or nanorods and microorganisms may inhibit the growth of microorganisms and can damage cell membranes [104,211–215]. Of all of those mechanisms, the most relevant seem to be the first and second—that is, the formation of reactive oxygen species and the release of Zn(II) ions [211]. Although nanowires and nanorods indeed exhibit great potential, nanoparticles are far more effective, because their antimicrobial activity largely stems from the interaction of microorganisms and nanostructures, which is more involved in the case of nanoparticles [212–214].

Critical Reviews in Solid State and Materials Sciences Volume 47, Issue 5, Pages 772 – 805, 2022

https://doi.org/10.1080/10408436.2021.1989663

Solar cells

As it was explained in the section 5.2, due to the wide band gap of ZnO, the optical properties of this semiconductor on the UV and VIS ranges are excellent for different applications as solar cells, UV-photodetectors or light emitting diodes (LED's). Depending on the architecture of ZnO nanowires the light absorption can be improved. In this section, the solar efficiency of these different architectures is analyzed.

ZnO nanowires grown by electrodeposition were extensively used as dyes sensitized solar cell (DSSCs). **Table 4** collected the solar cells characteristics of electrodeposited ZnO nanostructures. In 2011, a comparison of the solar cell characteristics between bare ZnO nanowires and branched ZnO nanowire arrays observing the highest solar efficiency (0.88%) for branched ZnO nanowire arrays was reported [2]. One year later, a comparison between ZnO nanowires and ZnO hierarchical nanowires measured with different dye loading times (2 and 12 h) was studied, the efficiency was higher in the case of ZnO hierarchical nanowires and the highest value (1.65%) was observed in the case of 2 h of dye loading time [3]. In the literature, a study where ZnO nanowires were deposited on ITO and an annealing at 150 ºC for 1h was reported, with a solar efficiency of 0.66% [81]. The highest solar efficiency value, considering only ZnO, published was 2.73% for ZnO nanoparticles network, this value was compared with the solar efficiency (0.88%) of 5 μm thickness ZnO nanowires [11]. A solar efficiency of 0.66% was observed for ZnO wires in nanosheets [216]. For urchin-ZnO and ordered network of ZnO hierarchical urchin, solar efficiencies of 1.33% [175] and 0.80% [217] were reported, respectively. A high solar efficiency value of 2.1% was observed of ZnO/ZnO core/shell nanowires [218]. Also, in the literature ZnO nanowires were deposited on a flexible substrate formed by PEN-ITO with an efficiency of 1.48% [219]. The solar efficiency of ZnO nanowires electrodeposited into AAO templates was also studied, measuring a value of 1.23% [4]. Other approaches were investigated in order to increase the solar cell characteristics of ZnO nanowires as introducing HTMA in the

https://doi.org/10.1080/10408436.2021.1989663

electrolyte for performing the electrodeposition, a solar efficiency of 1.02% was reported when 9 M of HTMA was used for the growth of ZnO nanowires [220].

Table 4. Solar cells characteristics of electrodeposited ZnO nanostructures.

Type of nanostructure	JSC / mA cm^{-2}	VOC / V	FF	η/ %	Reference
Bare ZnO nanowires	3.04	0.37	0.29	0.32	[2]
Branched ZnO nanowire arrays	5.79	0.51	0.3	0.88	[2]
ZnO nanowires (2h)	4.09	-	0.58	1.45	[3]
ZnO nanowires (12h)	2.30	-	0.48	0.68	[3]
ZnO hierarchical nanowires (2h)	4.63	.	0.64	1.65	[3]
ZnO hierarchical nanowires (12h)	5.10	-	0.54	1.63	[3]
ZnO nanowires/ITO (150 ºC, 1h)	0.606	3.28	0.333	0.66	[81]
ZnO nanoparticles network	9.65	0.635	0.45	2.73	[11]
ZnO nanowires (5 µm)	4.23	0.554	0.37	0.88	[11]
ZnO wires in nanosheets	7.35	0.23	0.40	0.66	[216]
Urchin- ZnO	-	0.44	0.34	1.33	[175]
Ordered network of ZnO hierarchical urchin	2.97	0.57	0.47	0.80	[217]
ZnO/ ZnO Core/shell nanowires	5.9	0.846	0.42	2.1	[218]
ZnO nanowires	1.5743	0.6688	0.3012	0.320	[221]

https://doi.org/10.1080/10408436.2021.1989663

ZnO nanowires/ PEN-ITO	1.78	0.606	0.453	1.48	[219]
ZnO nanowires into AAO (ordered nanowires)	4.8	0.64	0.4	1.23	[4]
ZnO nanowires grown in HTMA (9M)	3.91	0.655	0.44	1.02	[220]

Several works have been published in the literature respect to the fabrication of dyes sensitized solar cell (DSSCs) made by a heterojunction formed between ZnO and CuO/CuO_2 nanowires (see **Table 5**). K. P. Musselman *et al.* reported from 2010 to 2012 different studies where CuO_2 films were electrodeposited on ZnO nanowires grown by electrodeposition on a flat substrate. In this studies, different thicknesses of CuO_2 films were analyzed (between 2 to 3.5μm) [222–224]. The maximum solar efficiency (0.47%) was reached for a thickness of 3 μm CuO_2 films [223]. However, a maximum solar efficiency (0.85%) was observed when a ZnO bilayer was grown instead ZnO nanowires [224]. Nevertheless, the highest solar efficiency (1.26%) reported in the literature for this kind of heterojunctions was found when ZnO nanowires were deposited on Cu_2O film [225]. Additionally, CuO film was grown on ZnO nanowires/ZnO film, this film was deposited by ALD, the solar efficiency is not given by the authors; however, the fill factor (FF) reported was 0.25 [163].

Table 5. Solar cells characteristics of electrodeposited heterojunction formed between ZnO and CuO/CuO_2 nanowires

Type of nanostructure	**JSC / mA· cm^{-2}**	**VOC / V**	**FF**	**η / %**	**Reference**

https://doi.org/10.1080/10408436.2021.1989663

Cu_2O (2µm)/ ZnO nanowires	5.4	0.21	0.32	0.36	[222]
Cu_2O (3µm)/ ZnO nanowires	4.4	0.28	0.39	0.47	[223]
Cu_2O (2-3.5µm)/ZnO nanowires	-	-	0.34	0.38	[224]
Cu_2O (2-4.5µm)/ZnO bilayer	-	-	0.48	0.85	[224]
ZnO nanowires/Cu_2O	7.1	0.35	0.52	1.26	[225]
CuO/ZnO nanowires/ZnO ALD	0.025	0.058	0.25	-	[163]

Other materials as CdSe [226,227], CdS [227], perovskite [228], PMMA spheres [219] or Pt [229] were also used to form a heterojunction with ZnO in order to analyze the solar cells properties (see **Table 6**). In the case of CdSe deposited conformal on ZnO nanowires, a solar efficiency of 0.5% was reported [226]. A comparative study of the solar cell characteristics between CdSe/ZnO nanowires and a passivation layer deposited on the top of these nanostructures, CdS/CdSe/ZnO nanowires, was performed observing an increment of 83.47% in the efficiency, from 0.39% without the CdS passivation layer to 2.36% after the deposition of CdS [227]. A solar efficiency of 1.48% was published for ZnO nanowires electrodeposited on PMMA spheres [219]. Nevertheless, the highest solar efficiency was observed for ZnO nanowires electrodeposited on a perovskite ($CH_3NH_3PbI_3$) and in the case of Pt-decorated ZnO nanowires with solar efficiencies of 10.28% [228] and 7.2±0.2% [229], respectively.

Table 6. Solar cells characteristics of electrodeposited heterojunction based on ZnO nanowires.

Type of nanostructure	**JSC / mA cm^{-2}**	**VOC / V**	**FF**	**η / %**	**Reference**
CdSe/ZnO nanowires conformal	0.41	0.23	-	0.5%	[226]

https://doi.org/10.1080/10408436.2021.1989663

CdSe/ZnO nanowires	3.56	0.325	0.51	0.39	[227]
CdS/CdSe/ZnO nanowires	8.36	0.555	0.51	2.36	[227]
ZnO nanowires/PMMA spheres	5.33	0.606	0.453	1.48	[219]
ZnO nanowires/$CH_3NH_3PbI_3$ (Perovskite)	2.2	-	-	10.28	[228]
Pt-decorated ZnO nanowires	19 ± 1	0.74	0.52±0.04	7.2±0.2	[229]

UV-Photodetectors

In the literature, there are few studies where the UV photodetector response of ZnO nanowires was analyzed, most of the studies are referent to hybrid materials based on ZnO. A. Lamouchi e*t al.* published a comparative study between the photocurrent intensity of ZnO nanowires grown on a flat substrate and ZnO nanowires grown on a ZnO seed layer. The photocurrent density values were 0.13 $mA \cdot cm^{-2}$ without the seed layer and 0.25 $mA \cdot cm^{-2}$ without the seed layer [230]. The UV photoresponse of ZnO urchins have been compared to ZnO nanowires grown on a flat substrate. The photocurrent was 20.51 ± 0.25 and 36.81 ± 0.16 A/W for ZnO nanowires and ZnO urchins, respectively. This increment in the UV photoresponse was attributed to an excess on oxygen/photodesorbed on barrier highs on grain boundaries under UV light [231].

Respect to the hybrid materials, the photoelectrochemical response was increased with the incorporation of Ag (1, 1.5, 2 and 3%) in ZnO nanowires. The maximum photoelectrochemical response was observed for the maximum Ag concentration (3%). An increment from 0.05 to 0.13 $mA \cdot cm^{-2}$ was observed under UV illumination [160]. An UV photoresponse of $I_{UV}on/I_{UV}off$ ~ 1.48 was observed for ZnO:Ag rod-wire. Fast response and recovery time of 0.98 and 0.87 s, respectively, was observed [232]. An enhancement in the photocurrent was observed when Au nanoparticles were deposited between ITO and ZnO

https://doi.org/10.1080/10408436.2021.1989663

nanowires [233]. Different concentrations of Al (0, 0.1, 0.5, 1, 2 and 5%) were deposited by ALD (Atomic Layer Deposition) on ZnO in order to see the effect of Al on the photocurrent, the maximum photocurrent value was found to be 11.1 mA when 0.1% of Al was deposited on ZnO nanowires [234]. The UV photoresponse of CdSe/ZnO and ZnO nanowires was compared observing a maximum photocurrent value for ZnO nanowires [235]. Furthermore, the photocurrent of In_2Se_3 was deposited on the top of ZnO nanowires forming a core-shell nanostructure was analyzed. The photocurrent was enhanced from 2.3 to 5 $mA \cdot cm^{-2}$ when In_2Se_3 was deposited on the top of ZnO nanowires [149]. In addition, ZnO nanowires were used as sacrificial substrate for the deposition of Cu_2O inside CdSe nanowires. A photocurrent of 470 $\mu A \cdot cm^{-2}$ was reported, with three times better photosensibility [236].

Supercapacitators

In the literature, a comparative study based on the supercapacitator response of ZnO nanocones and nanowires was reported. ZnO nanocones exhibits a specific capacitance of 378.5 F/g at 20 mV/s of scan rate, which is almost twice that of ZnO nanowires (191.5 F/g) [237]. In another study, Ni_3S_2 coated ZnO array present a specific of 1529 F/g at a current density of 2 A/g [238].

Respect to heterojunctions, high-performance supercapacitators were reported for $Ni(OH_2)$ nanoflakes on ZnO nanowires grown by pulsed electrodeposition with a large specific capacitance of 1830 F/g, high energy density of 51.5 W·h/Kg and a high power density of 9 KW/Kg [239]. The specific capacitances of 3D ZnO/MnO2 core/shell nanocables were found to be 537.8 and 613.5 F/g at a scan rate of 5 mV/s and a current density of 1 A/g, respectively [146]. In addition, ZnO microrods were used as sacrificial substrate in order to generate the microstructure for Carbon nanospheres/Ni core/shell nanowires measuring the capacitance properties of these nanostructure [240].

Critical Reviews in Solid State and Materials Sciences Volume 47, Issue 5, Pages 772 – 805, 2022

https://doi.org/10.1080/10408436.2021.1989663

Other applications

Batteries: ZnO nanowires were also used for batteries application as sacrificial substrate [240]. Co_3O_4/Ni core/branch nanowires were evaluated as the anode for Li ion batteries [241].

Nanosensing : Nanosensing is another application of ZnO nanowires, these nanostructures were applied as vacuum [182], glucose [242], melamine [243], NO_2 gas [244] or hydrogen sensors [245]. As NO_2 gas sensing, a response time of 120 s, a value four times higher than in the case of thin films or nanorods, was reported [244]. A sensitive value of 19.5 μA/Mm·cm^2 was published when ZnO nanowires were used as glucose biosensor [242]. Respect to doped ZnO nanowires, Al-ZnO was also used for NO_2 gas sensing [246].

Light Emitting Diodes (LED's): Due to the optical properties of ZnO nanowires, these nanostructures are commonly used as light emitting diodes (LED's). For such application, it is necessary another material to have a n-p type union, where ZnO is the n type material. A good rectifying behavior, with a rectifying factor of 25 ± 5 V, was reported when ZnO nanowires were grown with PEDOT:PSS. This union was perfect for white-light LEDs [5]. Cu-doped ZnO was also tested as color-tunable light emitting nanodevices observing a violet-blue emission due to the shift in the band gap of 40 nm when ZnO is doped with Cu respect to ZnO nanowires [169]. Moreover, Ag-doped ZnO nanowires with 3.7% of Ag was analyzed as LED's observing a UV-blue emission. Low emission threshold of 5 V and a red-shift due to the Ag in the band gap was found [159]. An efficiency of 8.3% was measured for scintillator with light-guiding effect in ZnO nanowires [1].

Textile industry: ZnO nanowires applied to on cotton fabrics via electroless deposition can serve as an ideal multifunctional coating for textiles [136], because incorporating ZnO

Critical Reviews in Solid State and Materials Sciences Volume 47, Issue 5, Pages 772 – 805, 2022

https://doi.org/10.1080/10408436.2021.1989663

nanowires into fabrics and fibers in general takes advantage of the nanowires' self-cleaning, superhydrophobic, and UV blocking properties. Self-cleaning, water-repellent textiles are highly promising for military applications as well as to prevent unwelcome stains on clothes. The significant decrease in the transmission of UV radiation into fabrics covered with ZnO nanowires is another important emerging area in the textile industry, one aimed at protecting the human body from harmful UV sunlight irradiation [136].

Critical Reviews in Solid State and Materials Sciences Volume 47, Issue 5, Pages 772 – 805, 2022

https://doi.org/10.1080/10408436.2021.1989663

Future scope and conclusions

This paper reviewed the synthesis of ZnO nanowires grown using electrodeposition and electroless explaining both growth mechanism. ZnO nanowires can be electrosynthesis by different approaches based on the use of templateless or hard-templates, these growth mechanisms and approaches resulted in different morphologies/architectures of ZnO nanowires. In conclusion, for the synthesis of ZnO nanowires, three electrolytes can be used, molecular oxygen, nitrate ions and hydrogen peroxide. The electrodeposition parameters, which can be changed in order to tune the architecture of ZnO nanowires are bath temperature, applied potential, precursor concentration, Zn(II) concentration and supporting electrolyte. In the case of templateless electrodeposition ZnO nanowires, the morphology depends on pH at the electrode's surface, and consequently, on the Zn(II) concentration. The aspect ratio of the nanostructures depends on the electrodeposition time. By hard-templates electrodeposition of ZnO nanowires, the morphology, growth rate, filling ratio, and other characteristics of ZnO nanostructures can be modified without affecting their architecture. Respect to the electroless technique for growing ZnO nanostructures, their parameters allows an excellent control over length, diameter, aspect ratio and growth density of ZnO nanowires and nanorods. This technique represents a perfect industrial process for producing such nanostructures. In addition, doped ZnO and heterojunctions based on ZnO are good candidates for extend even more the properties of this material. The properties of these nanostructures depend strongly on the architectures of the materials, consequently, also affect to the applications. In this review, the crystallographic structure, optical properties, photoluminescence, electrical and magnetic properties, and the stability of ZnO nanowires were analyzed. ZnO nanowires have been shown to be a potential candidate for many applications as such as photocatalytic water treatment, photoelectrocatalytic water oxidation or reduction, antibacterial agents, solar cells, UV-photodetectors, supercapacitators, batteries, nanosensing, LED's and for their use in textile

https://doi.org/10.1080/10408436.2021.1989663

industry. In conclusion, this work reviewed the electrosynthesis (electrodeposition and electroless) of ZnO nanowires, and their properties and applications.

Acknowledgements, This work was supported by the Metrohm foundation. C.V. M. would like to acknowledge funding from “Atracción de Talento Investigador” de la Comunidad de Madrid, contract No. 2019-T1/IND-13541. We acknowledge support of the publication fee by the CSIC Open Access Publication Support Initiative through its Unit of Information Resources for Research (URICI).

REFERENCES

1. M. Izaki, M. Kobayashi, T. Shinagawa, T. Koyama, K. Uesugi, and A. Takeuchi, Electrochemically Grown ZnO Vertical Nanowire Scintillator with Light-Guiding Effect. *Phys. Status Solidi Appl. Mater. Sci.* **214**(11), 1–7 ((2017)).
2. J. Qiu, M. Guo, Y. Feng, and X. Wang, Electrochemical deposition of branched hierarchical ZnO nanowire arrays and its photoelectrochemical properties. *Electrochim. Acta* **56**(16), 5776–5782 ((2011)).
3. Y. T. Kim, J. Park, S. Kim, D. W. Park, and J. Choi, Fabrication of hierarchical ZnO nanostructures for dye-sensitized solar cells. *Electrochim. Acta* **78**, 417–421 ((2012)).
4. H. Gómez, S. Cantillana, F. A. Cataño, H. Altamirano, and A. Burgos, Template assisted electrodeposition of highly oriented ZnO nanowire arrays and their integration in dye sensitized solar cells. *J. Chil. Chem. Soc.* **59**(2), 2447–2450 ((2014)).
5. A. El-Shaer, A. Dev, J. P. Richters, S. R. Waldvogel, J. Waltermann, W. Schade, and T. Voss, Hybrid LEDs based on ZnO-nanowire arrays. *Phys. Status Solidi Basic Res.* **247**(6), 1564–1567 ((2010)).
6. A. Serrà, and L. Philippe, Simple and scalable fabrication of hairy ZnO@ZnS core@shell Cu cables for continuous sunlight-driven photocatalytic water remediation. *Chem. Eng. J.* **401**(June) ((2020)).
7. Y. G. Lin, Y. K. Hsu, Y. C. Chen, B. W. Lee, J. S. Hwang, L. C. Chen, and K. H. Chen, Cobalt-

https://doi.org/10.1080/10408436.2021.1989663

Phosphate-Assisted Photoelectrochemical Water Oxidation by Arrays of Molybdenum-Doped Zinc Oxide Nanorods. *ChemSusChem* **7**(9), 2748–2754 ((2014)).

8. Ü. Özgür, Y. I. Alivov, C. Liu, A. Teke, M. A. Reshchikov, S. Doğan, V. Avrutin, S. J. Cho, and H. Morkoç, A comprehensive review of ZnO materials and devices. *J. Appl. Phys.* **98**(4), 1–103 ((2005)).

9. A. Janotti, and C. G. Van De Walle, Fundamentals of zinc oxide as a semiconductor. *Reports Prog. Phys.* **72**(12) ((2009)).

10. Z. L. Wang, Zinc oxide nanostructures: Growth, properties and applications. *J. Phys. Condens. Matter* **16**(25) ((2004)).

11. E. Guillén, E. Azaceta, L. M. Peter, A. Zukal, R. Tena-Zaera, and J. A. Anta, ZnO solar cells with an indoline sensitizer: A comparison between nanoparticulate films and electrodeposited nanowire arrays. *Energy Environ. Sci.* **4**(9), 3400–3407 ((2011)).

12. M. Skompska, and K. Zarębska, Electrodeposition of ZnO nanorod arrays on transparent conducting substrates-a review. *Electrochim. Acta* **127**, 467–488 ((2014)).

13. S. Sun, S. Jiao, K. Zhang, D. Wang, S. Gao, H. Li, J. Wang, Q. Yu, F. Guo, and L. Zhao, Nucleation effect and growth mechanism of ZnO nanostructures by electrodeposition from aqueous zinc nitrate baths. *J. Cryst. Growth* **359**(1), 15–19 ((2012)).

14. N. P. Dasgupta, J. Sun, C. Liu, S. Brittman, S. C. Andrews, J. Lim, H. Gao, R. Yan, and P. Yang, 25th anniversary article: Semiconductor nanowires - Synthesis, characterization, and applications. *Adv. Mater.* **26**(14), 2137–2183 ((2014)).

15. C. V. Manzano, O. Caballero-Calero, S. Hormeño, M. Penedo, M. Luna, and M. S. Martín-González, ZnO morphology control by pulsed electrodeposition. *J. Phys. Chem. C* **117**(3), 1502–1508 ((2013)).

16. J. Elias, J. Michler, L. Philippe, M. Y. Lin, C. Couteau, G. Lerondel, and C. Lévy-Clément, ZnO nanowires, nanotubes, and complex hierarchical structures obtained by electrochemical deposition. *J. Electron. Mater.* **40**(5), 728–732 ((2011)).

17. S. Sun, S. Jiao, K. Zhang, D. Wang, S. Gao, H. Li, J. Wang, Q. Yu, F. Guo, and L. Zhao,

https://doi.org/10.1080/10408436.2021.1989663

Nucleation effect and growth mechanism of ZnO nanostructures by electrodeposition from aqueous zinc nitrate baths. *J. Cryst. Growth* **359**(1), 15–19 ((2012)).

18. M. J. Haque, M. M. Bellah, M. R. Hassan, and S. Rahman, Synthesis of ZnO nanoparticles by two different methods & comparison of their structural, antibacterial, photocatalytic and optical properties. *Nano Express* **1**(1), 010007 ((2020)).

19. Z. Sun, T. Liao, J. G. Kim, K. Liu, L. Jiang, J. H. Kim, and S. X. Dou, Architecture designed ZnO hollow microspheres with wide-range visible-light photoresponses. *J. Mater. Chem. C* **1**(42), 6924–6929 ((2013)).

20. Z. Sun, T. Liao, K. Liu, L. Jiang, J. H. Kim, and S. X. Dou, Fly-eye inspired superhydrophobic anti-fogging inorganic nanostructures. *Small* **10**(15), 3001–3006 ((2014)).

21. Z. Sun, T. Liao, W. Li, Y. Dou, K. Liu, L. Jiang, S. W. Kim, J. H. Kim, and S. Xue Dou, Fish-scale bio-inspired multifunctional ZnO nanostructures. *NPG Asia Mater.* **7**(June) ((2015)).

22. Z. Sun, T. Liao, K. Liu, L. Jiang, J. H. Kim, and S. X. Dou, Robust superhydrophobicity of hierarchical ZnO hollow microspheres fabricated by two-step self-assembly. *Nano Res.* **6**(10), 726–735 ((2013)).

23. B. Y. Xia, P. Yang, Y. Sun, Y. Wu, B. Mayers, B. Gates, Y. Yin, F. Kim, and H. Yan, One-Dimensional Nanostructures : Synthesis , Characterization , and Applications **. No. 5, 353–389 ((2003)).

24. Z. L. Wang, ZnO nanowire and nanobelt platform for nanotechnology. *Mater. Sci. Eng. R Reports* **64**(3–4), 33–71 ((2009)).

25. P. Yang, H. Yan, S. Mao, R. Russo, J. Johnson, R. Saykally, N. Morris, J. Pham, R. He, and H. J. Choi, Controlled growth of ZnO nanowires and their optical properties. *Adv. Funct. Mater.* **12**(5), 323–331 ((2002)).

26. Z. Sun, T. Liao, and L. Kou, Strategies for designing metal oxide nanostructures. *Sci. China Mater.* **60**(1), 1–24 ((2017)).

27. M. J. Zheng, L. D. Zhang, G. H. Li, and W. Z. Shen, Fabrication and optical properties of large-scale uniform zinc oxide nanowire arrays by one-step electrochemical deposition technique.

https://doi.org/10.1080/10408436.2021.1989663

Chem. Phys. Lett. **363**(1–2), 123–128 ((2002)).

28. M. Izaki, and T. Omi, Transparent zinc oxide films prepared by electrochemical reaction. *Appl. Phys. Lett.* **2439**(October 1995), 2439 ((1995)).

29. A. Serrà, and E. Vallés, Advanced electrochemical synthesis of multicomponent metallic nanorods and nanowires: Fundamentals and applications. *Appl. Mater. Today* **12**, 207–234 ((2018)).

30. H. El Belghiti, T. Pauporté, and D. Lincot, Mechanistic study of ZnO nanorod array electrodeposition. *Phys. Status Solidi Appl. Mater. Sci.* **205**(10), 2360–2364 ((2008)).

31. I. Gurrappa, and L. Binder, Electrodeposition of nanostructured coatings and their characterization - A review. *Sci. Technol. Adv. Mater.* **9**(4) ((2008)).

32. I. Zhitomirsky, Cathodic electrodeposition of ceramic and organoceramic materials. Fundamental aspects. *Adv. Colloid Interface Sci.* **97**(1–3), 279–317 ((2002)).

33. T. Pauporté, R. Cortès, M. Froment, B. Beaumont, and D. Lincot, Electrocrystallization of epitaxial zinc oxide onto gallium nitride. *Chem. Mater.* **14**(11), 4702–4708 ((2002)).

34. M. Izaki, and T. Omi, Electrolyte Optimization for Cathodic Growth of Zinc Oxide Films. *J. Electrochem. Soc.* **143**(3), L53–L55 ((2019)).

35. G. H. A. Therese, and P. V. Kamath, Electrochemical synthesis of metal oxides and hydroxides. *Chem. Mater.* **12**(5), 1195–1204 ((2000)).

36. A. Goux, T. Pauporté, J. Chivot, and D. Lincot, Temperature effects on ZnO electrodeposition. *Electrochim. Acta* **50**(11), 2239–2248 ((2005)).

37. S. Hori, T. Suzuki, T. Suzuki, S. Miura, and S. Nonomura, Effects of deposition temperature on the electrochemical deposition of zinc oxide thin films from a chloride solution. *Mater. Trans.* **55**(4), 728–734 ((2014)).

38. M. L. Lifson, C. G. Levey, and U. J. Gibson, Diameter and location control of ZnO nanowires using electrodeposition and sodium citrate. *Appl. Phys. A Mater. Sci. Process.* **113**(1), 243–247 ((2013)).

39. B. E. Prasad, P. V. Kamath, and S. Ranganath, Electrodeposition of ZnO coatings from aqueous

https://doi.org/10.1080/10408436.2021.1989663

Zn(NO3) 2 baths: Effect of Zn concentration, deposition temperature, and time on orientation. *J. Solid State Electrochem.* **16**(12), 3715–3722 ((2012)).

40. J. Lee, and Y. Tak, Electrodeposition of ZnO on ITO electrode by potential modulation method. *Electrochem. Solid-State Lett.* **4**(9), 63–66 ((2001)).

41. T. Pauporté, and D. Lincot, Hydrogen peroxide oxygen precursor for zinc oxide electrodeposition II - Mechanistic aspects. *J. Electroanal. Chem.* **517**(1–2), 54–62 ((2001)).

42. F. Jamali Sheini, I. S. Mulla, D. S. Joag, and M. A. More, Influence of process variables on growth of ZnO nanowires by cathodic electrodeposition on zinc substrate. *Thin Solid Films* **517**(24), 6605–6611 ((2009)).

43. F. Jamali Sheini, I. S. Mulla, D. S. Joag, and M. A. More, Influence of process variables on growth of ZnO nanowires by cathodic electrodeposition on zinc substrate. *Thin Solid Films* **517**(24), 6605–6611 ((2009)).

44. B. O'Regan, V. Sklover, and M. Grätzel, Electrochemical Deposition of Smooth and Homogeneously Mesoporous ZnO Films from Propylene Carbonate Electrolytes. *J. Electrochem. Soc.* **148**(7), C498 ((2001)).

45. R. Jayakrishnan, and G. Hodes, Non-aqueous electrodeposition of ZnO and CdO films. *Thin Solid Films* **440**(1–2), 19–25 ((2003)).

46. H. Gomez, G. Riveros, D. Ramirez, R. Henriquez, R. Schrebler, R. Marotti, and E. Dalchiele, Growth and characterization of ZnO nanowire arrays electrodeposited into anodic alumina templates in DMSO solution. *J. Solid State Electrochem.* **16**(1), 197–204 ((2012)).

47. Z. Li, A. Shkilnyy, and A. Taubert, Room temperature ZnO mesocrystal formation in the hydrated ionic liquid precursor (ILP) tetrabutylammonium hydroxide. *Cryst. Growth Des.* **8**(12), 4526–4532 ((2008)).

48. Q. Wang, G. Wang, B. Xu, J. Jie, X. Han, G. Li, Q. Li, and J. G. Hou, Non-aqueous cathodic electrodeposition of large-scale uniform ZnO nanowire arrays embedded in anodic alumina membrane. *Mater. Lett.* **59**(11), 1378–1382 ((2005)).

49. D. Gal, G. Hodes, D. Lincot, and H. W. Schock, Electrochemical deposition of zinc oxide films

https://doi.org/10.1080/10408436.2021.1989663

from non-aqueous solution: A new buffer/window process for thin film solar cells. *Thin Solid Films* **361**, 79–83 ((2000)).

50. G. Riveros, D. Ramírez, A. Tello, R. Schrebler, R. Henríquez, and H. Gómez, Electrodeposition of ZnO from DMSO solution: Influence of anion nature and its concentration in the nucleation and growth mechanisms. *J. Braz. Chem. Soc.* **23**(3), 505–512 ((2012)).

51. E. Akbari, N. Ayati, and S. P. Marashi, Influence of deposition voltage on growth of ZnO nanowires by cathodic electrodeposition. *Adv. Mater. Res.* **829**, 732–736 ((2014)).

52. J. Li, Z. Liu, E. Lei, and Z. Zhu, Effects of potential and temperature on the electrodeposited porous zinc oxide films. *J. Wuhan Univ. Technol. Mater. Sci. Ed.* **26**(1), 47–51 ((2011)).

53. J. Elias, R. Tena-Zaera, and C. Lévy-Clément, Effect of the chemical nature of the anions on the electrodeposition of ZnO nanowire arrays. *J. Phys. Chem. C* **112**(15), 5736–5741 ((2008)).

54. A. I. Inamdar, S. H. Mujawar, S. R. Barman, P. N. Bhosale, and P. S. Patil, The effect of bath temperature on the electrodeposition of zinc oxide thin films via an acetate medium. *Semicond. Sci. Technol.* **23**(8), 085013 ((2008)).

55. E. Matei, M. Enculescu, N. Preda, and I. Enculescu, ZnO morphological, structural and optical properties control by electrodeposition potential sweep rate. *Mater. Chem. Phys.* **134**(2–3), 988–993 ((2012)).

56. A. S. Rodzi, M. H. Mamat, M. M. Zahidi, Y. Mohd, M. N. Berhan, and M. Rusop, Effect of annealing process on ZnO nanorod prepared at different potentials using electrodeposition technique. *AIP Conf. Proc.* **1341**(May), 77–81 ((2011)).

57. A. Henni, A. Merrouche, L. Telli, A. Azizi, and R. Nechache, Effect of potential on the early stages of nucleation and properties of the electrochemically synthesized ZnO nanorods. *Mater. Sci. Semicond. Process.* **31**(1), 380–385 ((2015)).

58. A. Prună, D. Pullini, and D. B. Mataix, Influence of Deposition Potential on Structure of ZnO Nanowires Synthesized in Track-Etched Membranes. *J. Electrochem. Soc.* **159**(4), E92–E98 ((2012)).

59. N. Nouzu, A. Ashida, T. Yoshimura, and N. Fujimura, Control of cathodic potential for

https://doi.org/10.1080/10408436.2021.1989663

deposition of ZnO by constant-current electrochemical method. *Thin Solid Films* **518**(11), 2957–2960 ((2010)).

60. E. Matei, M. Enculescu, N. Preda, and I. Enculescu, ZnO morphological, structural and optical properties control by electrodeposition potential sweep rate. *Mater. Chem. Phys.* **134**(2–3), 988–993 ((2012)).

61. A. Henni, A. Merrouche, L. Telli, A. Azizi, and R. Nechache, Effect of potential on the early stages of nucleation and properties of the electrochemically synthesized ZnO nanorods. *Mater. Sci. Semicond. Process.* **31**(1), 380–385 ((2015)).

62. N. Nouzu, A. Ashida, T. Yoshimura, and N. Fujimura, Control of cathodic potential for deposition of ZnO by constant-current electrochemical method. *Thin Solid Films* **518**(11), 2957–2960 ((2010)).

63. K. Dakhsi, R. Belkhamina, M. E. Touhami, Z. El Khalidi, B. Hartiti, A. Ridah, and P. Thevenin, Effect study of precursor concentration of ZnO crystals obtained by electrode position. *Proc. 2015 IEEE Int. Renew. Sustain. Energy Conf. IRSEC 2015* 3–5 ((2016)).

64. A. Henni, A. Merrouche, L. Telli, S. Walter, A. Azizi, and N. Fenineche, Effect of H2O2 concentration on electrochemical growth and properties of vertically oriented ZnO nanorods electrodeposited from chloride solutions. *Mater. Sci. Semicond. Process.* **40**, 585–590 ((2015)).

65. L. Mentar, O. Baka, M. R. Khelladi, A. Azizi, S. Velumani, G. Schmerber, and A. Dinia, Effect of nitrate concentration on the electrochemical growth and properties of ZnO nanostructures. *J. Mater. Sci. Mater. Electron.* **26**(2), 1217–1224 ((2014)).

66. H. Y. Yang, S. H. Lee, and T. W. Kim, Effect of zinc nitrate concentration on the structural and the optical properties of ZnO nanostructures. *Appl. Surf. Sci.* **256**(20), 6117–6120 ((2010)).

67. A. El Hichou, N. Stein, C. Boulanger, and L. Johann, Structural and spectroscopic ellipsometry characterization for electrodeposited ZnO growth at different hydrogen peroxide concentration. *Thin Solid Films* **518**(15), 4150–4155 ((2010)).

68. Q. P. Chen, M. Z. Xue, Q. R. Sheng, Y. G. Liu, and Z. F. Ma, Electrochemical growth of nanopillar zinc oxide films by applying a low concentration of zinc nitrate precursor.

https://doi.org/10.1080/10408436.2021.1989663

Electrochem. Solid-State Lett. **9**(3), 0–4 ((2006)).

69. A. Henni, A. Merrouche, L. Telli, S. Walter, A. Azizi, and N. Fenineche, Effect of H2O2 concentration on electrochemical growth and properties of vertically oriented ZnO nanorods electrodeposited from chloride solutions. *Mater. Sci. Semicond. Process.* **40**, 585–590 ((2015)).

70. A. El Hichou, N. Stein, C. Boulanger, and L. Johann, Structural and spectroscopic ellipsometry characterization for electrodeposited ZnO growth at different hydrogen peroxide concentration. *Thin Solid Films* **518**(15), 4150–4155 ((2010)).

71. H. Kim, J. Y. Moon, and H. S. Lee, Effect of ZnCl2 concentration on the growth of ZnO by electrochemical deposition. *Curr. Appl. Phys.* **12**(SUPPL.4), S35–S38 ((2012)).

72. K. Lovchinov, G. Marinov, M. Petrov, N. Tyutyundzhiev, and T. Babeva, Influence of ZnCl 2 concentration on the structural and optical properties of electrochemically deposited nanostructured ZnO. *Appl. Surf. Sci.* **456**(April), 69–74 ((2018)).

73. Y. Park, G. Nam, and J. Y. Leem, Effect of a Sn seed layer and ZnCl2 concentration on electrodeposited ZnO nanostructures. *J. Korean Phys. Soc.* **66**(8), 1253–1258 ((2015)).

74. H. Kim, J. Y. Moon, and H. S. Lee, Effect of ZnCl2 concentration on the growth of ZnO by electrochemical deposition. *Curr. Appl. Phys.* **12**(SUPPL.4), S35–S38 ((2012)).

75. T. Singh, D. K. Pandya, and R. Singh, Effect of supporting electrolytes on the growth and optical properties of electrochemically deposited ZnO nanorods. *Opt. Mater. (Amst).* **35**(7), 1493–1497 ((2013)).

76. R. Tena-Zaera, J. Elias, C. Lévy-Clément, C. Bekeny, T. Voss, I. Mora-Seró, and J. Bisquert, Influence of the potassium chloride concentration on the physical properties of electrodeposited ZnO nanowire arrays. *J. Phys. Chem. C* **112**(42), 16318–16323 ((2008)).

77. H. Y. Yang, Y. S. No, J. Y. Kim, and T. W. Kim, Effect of potassium chloride concentration on the structural and optical properties of ZnO nanorods grown on glass substrates coated with indium tin oxide film. *Jpn. J. Appl. Phys.* **51**(6 PART 2), 0–4 ((2012)).

78. M. R. Khajavi, D. J. Blackwood, G. Cabanero, and R. Tena-Zaera, New insight into growth mechanism of ZnO nanowires electrodeposited from nitrate-based solutions. *Electrochim. Acta*

69(3), 181–189 ((2012)).

79. E. Matei, A. Costas, C. Florica, M. Enculescu, I. Pintilie, L. Pintilie, and I. Enculescu, Electrical properties of templateless electrodeposited ZnO nanowires. *Mater. Sci. Semicond. Process.* **42**, 364–372 ((2016)).

80. V. A. Antohe, L. Gence, S. K. Srivastava, and L. Piraux, Template-free electrodeposition of highly oriented and aspect-ratio controlled ZnO hexagonal columnar arrays. *Nanotechnology* **23**(25), 0–6 ((2012)).

81. O. Lupan, V. M. Guérin, I. M. Tiginyanu, V. V. Ursaki, L. Chow, H. Heinrich, and T. Pauporté, Well-aligned arrays of vertically oriented ZnO nanowires electrodeposited on ITO-coated glass and their integration in dye sensitized solar cells. *J. Photochem. Photobiol. A Chem.* **211**(1), 65–73 ((2010)).

82. D. Pradhan, and K. T. Leung, Controlled growth of two-dimensional and one-dimensional ZnO nanostructures on indium tin oxide coated glass by direct electrodeposition. *Langmuir* **24**(17), 9707–9716 ((2008)).

83. J. Lee, S. C. Nam, and Y. Tak, On the origin of electrodeposition mechanism of ZnO on ITO substrate. *Korean J. Chem. Eng.* **22**(1), 161–164 ((2005)).

84. V. M. Guérin, and T. Pauporté, From nanowires to hierarchical structures of template-free electrodeposited ZnO for efficient dye-sensitized solar cells. *Energy Environ. Sci.* **4**(8), 2971–2979 ((2011)).

85. Z. Liu, L. E, J. Ya, and Y. Xin, Growth of ZnO nanorods by aqueous solution method with electrodeposited ZnO seed layers. *Appl. Surf. Sci.* **255**(12), 6415–6420 ((2009)).

86. M. R. Khajavi, D. J. Blackwood, G. Cabanero, and R. Tena-Zaera, New insight into growth mechanism of ZnO nanowires electrodeposited from nitrate-based solutions. *Electrochim. Acta* **69**(3), 181–189 ((2012)).

87. E. Matei, A. Costas, C. Florica, M. Enculescu, I. Pintilie, L. Pintilie, and I. Enculescu, Electrical properties of templateless electrodeposited ZnO nanowires. *Mater. Sci. Semicond. Process.* **42**, 364–372 ((2016)).

https://doi.org/10.1080/10408436.2021.1989663

88. F. Xu, Y. Lu, Y. Xie, and Y. Liu, Controllable morphology evolution of electrodeposited ZnO nano/micro-scale structures in aqueous solution. *Mater. Des.* **30**(5), 1704–1711 ((2009)).

89. A. I. Inamdar, S. H. Mujawar, S. B. Sadale, A. C. Sonavane, M. B. Shelar, P. S. Shinde, and P. S. Patil, Electrodeposited zinc oxide thin films: Nucleation and growth mechanism. *Sol. Energy Mater. Sol. Cells* **91**(10), 864–870 ((2007)).

90. J. Elias, I. Utke, S. Yoon, M. Bechelany, A. Weidenkaff, J. Michler, and L. Philippe, Electrochemical growth of ZnO nanowires on atomic layer deposition coated polystyrene sphere templates. *Electrochim. Acta* **110**, 387–392 ((2013)).

91. J. Elias, C. Léuy-Clément, M. Bechelany, J. Michler, G. Y. Wang, Z. Wang, and L. Philippe, Hollow urchin-like ZnO thin films by electrochemical deposition. *Adv. Mater.* **22**(14), 1607–1612 ((2010)).

92. V. M. Guérin, J. Elias, T. T. Nguyen, L. Philippe, and T. Pauporté, Ordered networks of ZnO-nanowire hierarchical urchin-like structures for improved dye-sensitized solar cells. *Phys. Chem. Chem. Phys.* **14**(37), 12948–12955 ((2012)).

93. J. Elias, M. Bechelany, I. Utke, R. Erni, D. Hosseini, J. Michler, and L. Philippe, Urchin-inspired zinc oxide as building blocks for nanostructured solar cells. *Nano Energy* **1**(5), 696–705 ((2012)).

94. J. Elias, L. Philippe, J. Michler, and C. Lévy-Clément, Mechanism of formation of urchin-like ZnO. *Electrochim. Acta* **56**(26), 9532–9536 ((2011)).

95. J. Elias, I. Utke, S. Yoon, M. Bechelany, A. Weidenkaff, J. Michler, and L. Philippe, Electrochemical growth of ZnO nanowires on atomic layer deposition coated polystyrene sphere templates. *Electrochim. Acta* **110**, 387–392 ((2013)).

96. R. Kumar, A. Umar, G. Kumar, H. S. Nalwa, A. Kumar, and M. S. Akhtar, Zinc oxide nanostructure-based dye-sensitized solar cells. *J. Mater. Sci.* **52**(9), 4743–4795 ((2017)).

97. A. Serrà, Y. Zhang, B. Sepúlveda, E. Gómez, J. Nogués, J. Michler, and L. Philippe, Highly active ZnO-based biomimetic fern-like microleaves for photocatalytic water decontamination using sunlight. *Appl. Catal. B Environ.* **248**(October 2018), 129–146 ((2019)).

98. J. Martín, C. V. Manzano, O. Caballero-Calero, and M. Martín-González, High-aspect-ratio and

https://doi.org/10.1080/10408436.2021.1989663

highly ordered 15-nm porous alumina templates. *ACS Appl. Mater. Interfaces* **5**(1), 72–79 ((2013)).

99. E. Bertero, C. V. Manzano, G. Bürki, and L. Philippe, Stainless steel-like FeCrNi nanostructures via electrodeposition into AAO templates using a mixed-solvent Cr(III)-based electrolyte. *Mater. Des.* **190**, 108559 ((2020)).

100. C. V. Manzano, M. N. Polyakov, J. Maiz, M. H. Aguirre, X. Maeder, and M. Martín-González, Pulsed current-voltage electrodeposition of stoichiometric Bi2Te3 nanowires and their crystallographic characterization by transmission electron backscatter diffraction. *Sci. Technol. Adv. Mater.* **20**(1), 1022–1030 ((2019)).

101. C. Frantz, A. Lauria, C. V. Manzano, C. Guerra-Nuñez, M. Niederberger, C. Storrer, J. Michler, and L. Philippe, Nonaqueous Sol-Gel Synthesis of Anatase Nanoparticles and Their Electrophoretic Deposition in Porous Alumina. *Langmuir* **33**(43), 12404–12418 ((2017)).

102. J. García-Torres, A. Serrà, P. Tierno, X. Alcobé, and E. Vallés, Magnetic Propulsion of Recyclable Catalytic Nanocleaners for Pollutant Degradation. *ACS Appl. Mater. Interfaces* **9**(28), 23859–23868 ((2017)).

103. A. Serrà, S. Grau, C. Gimbert-Suriñach, J. Sort, J. Nogués, and E. Vallés, Magnetically-actuated mesoporous nanowires for enhanced heterogeneous catalysis. *Appl. Catal. B Environ.* **217**, 81–91 ((2017)).

104. A. Serrà, N. Gimeno, E. Gómez, M. Mora, M. L. Sagristá, and E. Vallés, Magnetic Mesoporous Nanocarriers for Drug Delivery with Improved Therapeutic Efficacy. *Adv. Funct. Mater.* **26**(36), 6601–6611 ((2016)).

105. A. Serrà, E. Gómez, M. Montiel, and E. Vallés, Effective new method for synthesizing Pt and $CoPt_3$ mesoporous nanorods. New catalysts for ethanol electro-oxidation in alkaline medium. *RSC Adv.* **6**(53), 47931–47939 ((2016)).

106. S. J. Hurst, E. K. Payne, L. Qin, and C. A. Mirkin, Multisegmented one-dimensional nanorods prepared by hard-template synthetic methods. *Angew. Chemie - Int. Ed.* **45**(17), 2672–2692 ((2006)).

https://doi.org/10.1080/10408436.2021.1989663

107. Y. Li, G. W. Meng, L. D. Zhang, and F. Phillipp, Ordered semiconductor ZnO nanowire arrays and their photoluminescence properties. *Appl. Phys. Lett.* **76**(15), 2011–2013 ((2000)).

108. Y. Li, G. S. Cheng, and L. D. Zhang, Fabrication of highly ordered ZnO nanowire arrays in anodic alumina membranes. *J. Mater. Res.* **15**(11), 2305–2308 ((2000)).

109. J. B. Yi, H. Pan, J. Y. Lin, J. Ding, Y. P. Feng, S. Thongmee, T. Liu, H. Gong, and L. Wang, Ferromagnetism in ZnO nanowires derived from electro-deposition on AAO template and subsequent oxidation. *Adv. Mater.* **20**(6), 1170–1174 ((2008)).

110. D. L. Wang, Y. F. Ruan, L. C. Zhang, C. X. Qiu, D. Y. Fang, and H. B. Yang, Study on preparation of ZnO nanowires in AAO template by electrodeposition method. *Rengong Jingti Xuebao/Journal Synth. Cryst.* **39**(5), 1166–1170 ((2010)).

111. J. Sunday, K. Amoah, and G. Slaughter, Growth of electrodeposited ZnO nanowires. *Proc. IEEE Sensors* 1–3 ((2012)).

112. C. V. Manzano, G. Bürki, L. Pethö, J. Michler, and L. Philippe, Determining the diffusion mechanism for high aspect ratio ZnO nanowires electrodeposited into anodic aluminum oxide. *J. Mater. Chem. C* **5**(7), 1706–1713 ((2017)).

113. N. S. Ayati, E. Akbari, S. P. Marashi, and S. Saramad, Template assisted growth of zinc oxide-based nanowires and piezoelectric properties. *Adv. Mater. Res.* **829**, 757–761 ((2014)).

114. M. G. Maas, E. J. B. Rodijk, A. Wouter Maijenburg, D. H. A. Blank, and J. E. Ten Elshof, Microstructure development in zinc oxide nanowires and iron oxohydroxide nanotubes by cathodic electrodeposition in nanopores. *J. Mater. Res.* **26**(17), 2261–2267 ((2011)).

115. Y. H. Chen, Y. M. Shen, S. C. Wang, and J. L. Huang, Fabrication of one-dimensional ZnO nanotube and nanowire arrays with an anodic alumina oxide template via electrochemical deposition. *Thin Solid Films* **570**(PB), 303–309 ((2014)).

116. S. K. Sharma, A. Rammohan, and A. Sharma, Templated one step electrodeposition of high aspect ratio n-type ZnO nanowire arrays. *J. Colloid Interface Sci.* **344**(1), 1–9 ((2010)).

117. D. Ramirez, T. Pauporte, H. Gomez, and D. Lincot, Electrochemical growth of ZnO nanowires inside nanoporous alumina templates. A comparison with metallic Zn nanowires growth. *Phys.*

https://doi.org/10.1080/10408436.2021.1989663

Status Solidi Appl. Mater. Sci. **205**(10), 2371–2375 ((2008)).

118. N. Kumar, A. K. Srivastava, R. Nath, B. K. Gupta, and G. D. Varma, Probing the highly efficient room temperature ammonia gas sensing properties of a luminescent ZnO nanowire array prepared via an AAO-assisted template route. *Dalt. Trans.* **43**(15), 5713–5720 ((2014)).

119. J. Sudagar, J. Lian, and W. Sha, Electroless nickel, alloy, composite and nano coatings - A critical review. *J. Alloys Compd.* **571**, 183–204 ((2013)).

120. J. N. Balaraju, S. K. Seshadri, M. S. Division, N. A. Laboratories, and M. Centre, Electroless Ni – P composite coatings. 807–816 ((2003)).

121. H. Miyake, S. Ye, and M. Osawa, Electroless deposition of gold thin films on silicon for surface-enhanced infrared spectroelectrochemistry. *Electrochem. commun.* **4**(12), 973–977 ((2002)).

122. J. Sudagar, J. Lian, and W. Sha, Electroless nickel, alloy, composite and nano coatings - A critical review. *J. Alloys Compd.* **571**, 183–204 ((2013)).

123. T. Shinagawa, H. Takahashi, and M. Izaki, Direct growth of ZnO crystals on various Cu substrates by Cu-catalyzed chemical bath deposition. *CrystEngComm* **21**(15), 2476–2480 ((2019)).

124. T. Shinagawa, K. Murase, S. Otomo, J. Katayama, and M. Izaki, Effects of Counteranions and Dissolved Oxygen on Chemical ZnO Deposition from Aqueous Solutions. *J. Electrochem. Soc.* **156**(5), H320 ((2009)).

125. M. Izaki, and T. Omi, Transparent Zinc Oxide Films Chemically Prepared from Aqueous Solution. *J. Electrochem. Soc.* **144**(1), L3–L5 ((2019)).

126. M. Izaki, and J. Katayama, Characterization of Boron-Incorporated Zinc Oxide Film Chemically Prepared from an Aqueous Solution. *J. Electrochem. Soc.* **147**(1), 210 ((2000)).

127. T. Shinagawa, H. Takahashi, and M. Izaki, Direct growth of ZnO crystals on various Cu substrates by Cu-catalyzed chemical bath deposition. *CrystEngComm* **21**(15), 2476–2480 ((2019)).

128. K. Murase, H. Tada, T. Shinagawa, M. Izaki, and Y. Awakura, QCM Studies of Chemical Solution Deposition of ZnO in Aqueous Media Containing Zinc Nitrate and

https://doi.org/10.1080/10408436.2021.1989663

Dimethylamineborane. *J. Electrochem. Soc.* **153**(11), C735 ((2006)).

129. A. Serrà, R. Artal, J. García-Amorós, B. Sepúlveda, E. Gómez, J. Nogués, and L. Philippe, Hybrid Ni@ZnO@ZnS-Microalgae for Circular Economy: A Smart Route to the Efficient Integration of Solar Photocatalytic Water Decontamination and Bioethanol Production. *Adv. Sci.* **7**(3), 1–9 ((2020)).

130. Z. Fu, Z. Pan, D. Sun, G. Zhan, H. Zhang, X. Zeng, G. Hu, C. Xiao, and Z. Wei, Multiple morphologies of ZnO films synthesized on flexible poly(ethylene terephthalate) by electroless deposition. *Mater. Lett.* **184**, 185–188 ((2016)).

131. T. Shinagawa, M. Watanabe, M. Chigane, and H. Takahashi, Surface study of sintered alumina substrates using solution-processed ZnO nanorods as a microscopic wettability indicator. *Surf. Interface Anal.* **49**(3), 216–222 ((2017)).

132. N. Saito, H. Haneda, and K. Koumoto, fåÑäìÉåÅÉë çÑ dêçïíÜ ` çåÇáíáçåë íç jçêéÜçäçÖó çÑ wål qÜáå cáäãë bäÉÅíêçäÉëëáó aÉéçëáíÉÇ çå mÇ `~ í ~ äóëí. **855**, 850–855 ((2007)).

133. T. Shinagawa, S. Watase, and M. Izaki, Size-controllable growth of vertical ZnO nanorod arrays by a Pd-catalyzed chemical solution process. *Cryst. Growth Des.* **11**(12), 5533–5539 ((2011)).

134. N. Preda, A. Costas, M. Beregoi, and I. Enculescu, A straightforward route to obtain organic/inorganic hybrid network from bio-waste: Electroless deposition of ZnO nanostructures on eggshell membranes. *Chem. Phys. Lett.* **706**, 24–30 ((2018)).

135. N. Preda, M. Enculescu, I. Zgura, M. Socol, E. Matei, V. Vasilache, and I. Enculescu, Superhydrophobic properties of cotton fabrics functionalized with ZnO by electroless deposition. *Mater. Chem. Phys.* **138**(1), 253–261 ((2013)).

136. L. Frunza, N. Preda, E. Matei, S. Frunza, C. P. Ganea, A. M. Vlaicu, L. Diamandescu, and A. Dorogan, Synthetic fabrics coated with zinc oxide nanoparticles by electroless deposition: Structural characterization and wetting properties. *J. Polym. Sci. Part B Polym. Phys.* **51**(19), 1427–1437 ((2013)).

137. T. Shinagawa, S. Otomo, J. ichi Katayama, and M. Izaki, Electroless deposition of transparent conducting and ⟨0 0 0 1⟩-oriented ZnO films from aqueous solutions. *Electrochim. Acta* **53**(3

https://doi.org/10.1080/10408436.2021.1989663

SPEC. ISS.), 1170–1174 ((2007)).

138. N. Preda, M. Enculescu, and I. Enculescu, Polymer sphere array assisted ZnO electroless deposition. *Soft Mater.* **11**(4), 457–464 ((2013)).

139. J. Y. Lee, S. Horiuchi, and H. K. Choi, Effects of deposition temperature and chemical composition on the ZnO crystal growth on the surface of Pd catalyst through electroless chemical reaction. *Mater. Chem. Phys.* **101**(2–3), 387–394 ((2007)).

140. J. Y. Kim, C. H. Noh, K. Y. Song, S. H. Cho, M. Y. Kim, and J. M. Kim, Low-temperature fabrication of zinc oxide micropatterns using selective electroless deposition. *Electrochem. Solid-State Lett.* **8**(9) ((2005)).

141. W. T. Chiou, W. Y. Wu, and J. M. Ting, Effect of electroless copper on the growth of ZnO nanowires. *J. Mater. Res.* **20**(9), 2348–2353 ((2005)).

142. N. Preda, M. Enculescu, I. Zgura, M. Socol, E. Matei, V. Vasilache, and I. Enculescu, Superhydrophobic properties of cotton fabrics functionalized with ZnO by electroless deposition. *Mater. Chem. Phys.* **138**(1), 253–261 ((2013)).

143. A. Serrà, P. Pip, E. Gómez, and L. Philippe, Efficient magnetic hybrid ZnO-based photocatalysts for visible-light-driven removal of toxic cyanobacteria blooms and cyanotoxins. *Appl. Catal. B Environ.* **268**(January) ((2020)).

144. A. Serrà, E. Gómez, and L. Philippe, Bioinspired ZnO-based solar photocatalysts for the efficient decontamination of persistent organic pollutants and hexavalent chromium in wastewater. *Catalysts* **9**(12), 1–16 ((2019)).

145. F. J. Sheini, D. S. Joag, and M. A. More, Electrochemical synthesis of Sn doped ZnO nanowires on zinc foil and their field emission studies. *Thin Solid Films* **519**(1), 184–189 ((2010)).

146. C. Yuan, H. Lin, H. Lu, E. Xing, Y. Zhang, and B. Xie, Electrodeposition of three-dimensional ZnO@MnO2 coreeshell nanocables as high-performance electrode material for supercapacitors. *Energy* **93**, 1259–1266 ((2015)).

147. A. A. Yaqoob, N. H. binti M. Noor, A. Serrà, and M. N. M. Ibrahim, Advances and Challenges in Developing Efficient Graphene Oxide-Based ZnO Photocatalysts for Dye Photo-Oxidation.

Nanomaterials **10**(5), 932 ((2020)).

148. A. Serrà, Y. Zhang, B. Sepúlveda, E. Gómez, J. Nogués, J. Michler, and L. Philippe, Highly reduced ecotoxicity of ZnO-based micro/nanostructures on aquatic biota: Influence of architecture, chemical composition, fixation, and photocatalytic efficiency. *Water Res.* **169** ((2020)).

149. Z. Braiek, A. Brayek, M. Ghoul, S. Ben Taieb, M. Gannouni, I. Ben Assaker, A. Souissi, and R. Chtourou, Electrochemical synthesis of ZnO/In2S3 core-shell nanowires for enhanced photoelectrochemical properties. *J. Alloys Compd.* **653**, 395–401 ((2015)).

150. J. J. Gu, L. H. Liu, H. T. Li, Q. Xu, and H. Y. Sun, Annealing effects on structural and magnetic properties of Co-doped ZnO nanowires synthesized by an electrodeposition process. *J. Alloys Compd.* **508**(2), 516–519 ((2010)).

151. J. Elias, C. Léuy-Clément, M. Bechelany, J. Michler, G. Y. Wang, Z. Wang, and L. Philippe, Hollow urchin-like ZnO thin films by electrochemical deposition. *Adv. Mater.* **22**(14), 1607–1612 ((2010)).

152. L. Movsesyan, I. Schubert, L. Yeranyan, C. Trautmann, and M. E. Toimil-Molares, Influence of electrodeposition parameters on the structure and morphology of ZnO nanowire arrays and networks synthesized in etched ion-track membranes. *Semicond. Sci. Technol.* **31**(1), 14006 ((2015)).

153. L. Movsesyan, A. W. Maijenburg, N. Goethals, W. Sigle, A. Spende, F. Yang, B. Kaiser, W. Jaegermann, S. Y. Park, G. Mul, C. Trautmann, and M. E. Toimil-Molares, ZnO nanowire networks as photoanode model systems for photoelectrochemical applications. *Nanomaterials* **8**(9) ((2018)).

154. C. De Bolonia, F. Filippini, and C. De Estudios, Universidad Complutense de Madrid 1-. 1–16 ((2011)).

155. F. Xu, Y. Lu, Y. Xie, and Y. Liu, Seed layer-free electrodeposition and characterization of vertically aligned ZnO nanorod array film. *J. Solid State Electrochem.* **14**(1), 63–70 ((2010)).

156. C. D. Bojorge, V. R. Kent, E. Teliz, H. R. Cánepa, R. Henríquez, H. Gõmez, R. E. Marotti, and E.

https://doi.org/10.1080/10408436.2021.1989663

A. Dalchiele, Zinc-oxide nanowires electrochemically grown onto sol-gel spin-coated seed layers. *Phys. Status Solidi Appl. Mater. Sci.* **208**(7), 1662–1669 ((2011)).

157. C. Florica, E. Matei, A. Costas, M. E. T. Molares, and I. Enculescu, Field effect transistor with electrodeposited ZnO nanowire channel. *Electrochim. Acta* **137**, 290–297 ((2014)).

158. O. Lupan, T. Pauporté, B. Viana, P. Aschehoug, M. Ahmadi, B. R. Cuenya, Y. Rudzevich, Y. Lin, and L. Chow, Eu-doped ZnO nanowire arrays grown by electrodeposition. *Appl. Surf. Sci.* **282**, 782–788 ((2013)).

159. T. Pauporté, O. Lupan, J. Zhang, T. Tugsuz, I. Ciofini, F. Labat, and B. Viana, Low-Temperature Preparation of Ag-Doped ZnO Nanowire Arrays, DFT Study, and Application to Light-Emitting Diode. *ACS Appl. Mater. Interfaces* **7**(22), 11871–11880 ((2015)).

160. B. Slimi, I. Ben Assaker, A. Kriaa, B. Marí, and R. Chtourou, One-step electrodeposition of Ag-decorated ZnO nanowires. *J. Solid State Electrochem.* **21**(5), 1253–1261 ((2017)).

161. S. K. Arora, A. Devi, V. S. Jaswal, J. Singh, M. Kinger, and V. D. Gupta, Synthesis and characterization of ZnO nanoparticles. *Orient. J. Chem.* **30**(4), 1671–1679 ((2014)).

162. M. Ghoul, Z. Braiek, A. Brayek, I. Ben Assaker, N. Khalifa, J. Ben Naceur, A. Souissi, A. Lamouchi, S. Ammar, and R. Chtourou, Synthesis of core/shell ZnO/ZnSe nanowires using novel low cost two-steps electrochemical deposition technique. *J. Alloys Compd.* **647**, 660–664 ((2015)).

163. O. Messaoudi, H. Makhlouf, A. Souissi, I. Ben Assaker, G. Amiri, A. Bardaoui, M. Oueslati, M. Bechelany, and R. Chtourou, Synthesis and characterization of ZnO/Cu 2 O core-shell nanowires grown by two-step electrodeposition method. *Appl. Surf. Sci.* **343**, 148–152 ((2015)).

164. C. Manzano, A. Serrano, Á. Muñoz-Noval, J. Fernandez, and M. Martín-González, Crystal Defects and Optical Emissionsof Pulse Electrodeposited ZnO Films. *Electrochim. Acta* **357**, 136662 ((2020)).

165. C. V. Manzano, D. Alegre, O. Caballero-Calero, B. Alén, and M. S. Martín-González, Synthesis and luminescence properties of electrodeposited ZnO films. *J. Appl. Phys.* **110**(4) ((2011)).

166. J. Elias, J. Michler, L. Philippe, M. Y. Lin, C. Couteau, G. Lerondel, and C. Lévy-Clément, ZnO

https://doi.org/10.1080/10408436.2021.1989663

nanowires, nanotubes, and complex hierarchical structures obtained by electrochemical deposition. *J. Electron. Mater.* **40**(5), 728–732 ((2011)).

167. O. Lupan, T. Pauporté, I. M. Tiginyanu, V. V. Ursaki, H. Heinrich, and L. Chow, Optical properties of ZnO nanowire arrays electrodeposited on n- and p-type Si(1 1 1): Effects of thermal annealing. *Mater. Sci. Eng. B Solid-State Mater. Adv. Technol.* **176**(16), 1277–1284 ((2011)).

168. Y. Leprince-Wang, S. Bouchaib, T. Brouri, M. Capo-Chichi, K. Laurent, J. Leopoldes, S. Tusseau-Nenez, L. Lei, and Y. Chen, Fabrication of ZnO micro- and nano-structures by electrodeposition using nanoporous and lithography defined templates. *Mater. Sci. Eng. B Solid-State Mater. Adv. Technol.* **170**(1–3), 107–112 ((2010)).

169. O. Lupan, T. Pauporté, T. Le Bahers, B. Viana, and I. Ciofini, Wavelength-emission tuning of zno nanowire-based light-emitting diodes by Cu doping: Experimental and computational insights. *Adv. Funct. Mater.* **21**(18), 3564–3572 ((2011)).

170. J. Fan, A. Shavel, R. Zamani, C. Fábrega, J. Rousset, S. Haller, F. Güell, A. Carrete, T. Andreu, J. Arbiol, J. R. Morante, and A. Cabot, Control of the doping concentration, morphology and optoelectronic properties of vertically aligned chlorine-doped ZnO nanowires. *Acta Mater.* **59**(17), 6790–6800 ((2011)).

171. N. Saurakhiya, S. K. Sharma, R. Kumar, and A. Sharma, Templated electrochemical synthesis of polyaniline/ZnO coaxial nanowires with enhanced photoluminescence. *Ind. Eng. Chem. Res.* **53**(49), 18884–18890 ((2014)).

172. Y. Tang, D. Zhao, J. Zhang, and D. Shen, Quenching of the surface-state-related photoluminescence in Ni-coated ZnO nanowires. *Phys. B Condens. Matter* **405**(21), 4551–4555 ((2010)).

173. D. Sarkar, G. G. Khan, A. K. Singh, and K. Mandal, Enhanced electrical, optical, and magnetic properties in multifunctional ZnO/α-Fe 2O 3 semiconductor nanoheterostructures by heterojunction engineering. *J. Phys. Chem. C* **116**(44), 23540–23546 ((2012)).

174. C. Karam, C. Guerra-Nuñez, R. Habchi, Z. Herro, N. Abboud, A. Khoury, S. Tingry, P. Miele, I. Utke, and M. Bechelany, Urchin-inspired ZnO-TiO2 core-shell as building blocks for dye

https://doi.org/10.1080/10408436.2021.1989663

sensitized solar cells. *Mater. Des.* **126**(February), 314–321 ((2017)).

175. J. Elias, M. Bechelany, I. Utke, R. Erni, D. Hosseini, J. Michler, and L. Philippe, Urchin-inspired zinc oxide as building blocks for nanostructured solar cells. *Nano Energy* **1**(5), 696–705 ((2012)).

176. C. Zhu, G. Meng, Q. Huang, X. Wang, Y. Qian, X. Hu, H. Tang, and N. Wu, ZnO-nanotaper array sacrificial templated synthesis of noble-metal building-block assembled nanotube arrays as 3D SERS-substrates. *Nano Res.* **8**(3), 957–966 ((2015)).

177. J. L. Pau, C. G. Nunez, A. G. Marin, E. Ruiz, and J. Piqueras, Metal oxide nanowires as building blocks for light detectors, gas sensors and biosensors. *Proc. 2013 Spanish Conf. Electron Devices, CDE 2013* 171–174 ((2013)).

178. Z. Guo, H. Li, L. Zhou, D. Zhao, Y. Wu, Z. Zhang, W. Zhang, C. Li, and J. Yao, Large-scale horizontally aligned ZnO microrod arrays with controlled orientation, periodic distribution as building blocks for chip-in piezo-phototronic LEDs. *Small* **11**(4), 438–445 ((2015)).

179. M. Grundmann, Architecture of nano-and microdimensional building blocks. *Phys. Status Solidi Basic Res.* **247**(6), 1257–1264 ((2010)).

180. W. Chen, Y. Qiu, and S. Yang, Branched ZnO nanostructures as building blocks of photoelectrodes for efficient solar energy conversion. *Phys. Chem. Chem. Phys.* **14**(31), 10872–10881 ((2012)).

181. X. Chen, X. Chuai, L. Yang, and H. Zhao, Climatic warming and overgrazing induced the high concentration of organic matter in Lake Hulun, a large shallow eutrophic steppe lake in northern China. *Sci. Total Environ.* **431**, 332–338 ((2012)).

182. L. Wu, F. Song, X. Fang, Z. X. Guo, and S. Liang, A practical vacuum sensor based on a ZnO nanowire array. *Nanotechnology* **21**(47) ((2010)).

183. A. W. Maijenburg, M. G. Maas, E. J. B. Rodijk, W. Ahmed, E. S. Kooij, E. T. Carlen, D. H. A. Blank, and J. E. ten Elshof, Dielectrophoretic alignment of metal and metal oxide nanowires and nanotubes: A universal set of parameters for bridging prepatterned microelectrodes. *J. Colloid Interface Sci.* **355**(2), 486–493 ((2011)).

184. A. Nadarajah, and R. Könenkamp, Dilute magnetic semiconductors from electrodeposited ZnO

https://doi.org/10.1080/10408436.2021.1989663

nanowires. *Phys. Status Solidi Basic Res.* **248**(2), 334–338 ((2011)).

185. H. T. Pham, T. D. Nguyen, M. E. Islam, D. Q. Tran, and M. Akabori, Enhanced ferromagnetism of ZnO@Co/Ni hybrid core@shell nanowires grown by electrochemical deposition method. *RSC Adv.* **8**(2), 632–639 ((2018)).

186. G. Stan, C. V. Ciobanu, P. M. Parthangal, and R. F. Cook, Diameter-dependent radial and tangential elastic moduli of ZnO nanowires. *Nano Lett.* **7**(12), 3691–3697 ((2007)).

187. H. J. Xiang, J. Yang, J. G. Hou, and Q. Zhu, Piezoelectricity in ZnO nanowires: A first-principles study. *Appl. Phys. Lett.* **89**(22), 1–3 ((2006)).

188. J. F. Conley, L. Stecker, and Y. Ono, Directed assembly of ZnO nanowires on a Si substrate without a metal catalyst using a patterned ZnO seed layer. *Nanotechnology* **16**(2), 292–296 ((2005)).

189. Z. L. Wang, and J. Song, Piezoelectric nanogenerators based on zinc oxide nanowire arrays. *Science (80-.).* **312**(5771), 242–246 ((2006)).

190. X. Xue, W. Zang, P. Deng, Q. Wang, L. Xing, Y. Zhang, and Z. L. Wang, Piezo-potential enhanced photocatalytic degradation of organic dye using ZnO nanowires. *Nano Energy* **13**, 414–422 ((2015)).

191. S. Yang, L. Wang, X. Tian, Z. Xu, W. Wang, X. Bai, and E. Wang, The piezotronic effect of zinc oxide nanowires studied by in situ TEM. *Adv. Mater.* **24**(34), 4676–4682 ((2012)).

192. S. Kaps, S. Bhowmick, J. Gröttrup, V. Hrkac, D. Stauffer, H. Guo, O. L. Warren, J. Adam, L. Kienle, A. M. Minor, R. Adelung, and Y. K. Mishra, Piezoresistive Response of Quasi-One-Dimensional ZnO Nanowires Using an in Situ Electromechanical Device. *ACS Omega* **2**(6), 2985–2993 ((2017)).

193. C. L. Hsu, and K. C. Chen, Improving piezoelectric nanogenerator comprises ZnO nanowires by bending the flexible PET substrate at low vibration frequency. *J. Phys. Chem. C* **116**(16), 9351–9355 ((2012)).

194. Y. Sun, Y. Zheng, R. Wang, J. Fan, and Y. Liu, Direct-current piezoelectric nanogenerator based on two-layer zinc oxide nanorod arrays with equal c-axis orientation for energy harvesting. *Chem.*

Eng. J. **426**(July) ((2021)).

195. K. M. Ok, E. O. Chi, and P. S. Halasyamani, Bulk characterization methods for non-centrosymmetric materials: Second-harmonic generation, piezoelectricity, pyroelectricity, and ferroelectricity. *Chem. Soc. Rev.* **35**(8), 710–717 ((2006)).

196. Y. Zhu, B. Wang, C. Deng, Y. Wang, and X. Wang, Photothermal-pyroelectric-plasmonic coupling for high performance and tunable band-selective photodetector. *Nano Energy* **83**(January) ((2021)).

197. J. Dong, Z. Wang, X. Wang, and Z. L. Wang, Temperature dependence of the pyro-phototronic effect in self-powered p-Si/n-ZnO nanowires heterojuncted ultraviolet sensors. *Nano Today* **29** ((2019)).

198. Z. Xu, Y. Zhang, and Z. Wang, ZnO-based photodetector: From photon detector to pyro-phototronic effect enhanced detector. *J. Phys. D. Appl. Phys.* **52**(22), ab0728 ((2019)).

199. W. Qian, Z. Wu, Y. Jia, Y. Hong, X. Xu, H. You, Y. Zheng, and Y. Xia, Thermo-electrochemical coupling for room temperature thermocatalysis in pyroelectric ZnO nanorods. *Electrochem. commun.* **81**(May), 124–127 ((2017)).

200. A. Serrà, L. Philippe, F. Perreault, and S. Garcia-Segura, Photocatalytic treatment of natural waters. Reality or hype? The case of cyanotoxins remediation. *Water Res.* **188** ((2021)).

201. S. Ghimire, M. Flury, E. J. Scheenstra, and C. A. Miles, Jo ur na l P re of. *Sci. Total Environ.* 135577 ((2019)).

202. S. B. A. Hamid, S. J. Teh, and C. W. Lai, Photocatalytic water oxidation on ZnO: A review. *Catalysts* **7**(3) ((2017)).

203. A. Irshad, and N. Munichandraiah, Photochemical Deposition of Co-Ac Catalyst on ZnO Nanorods for Solar Water Oxidation. *J. Electrochem. Soc.* **162**(4), H235–H243 ((2015)).

204. C. Liu, Y. Qiu, F. Wang, L. Li, Q. Liang, and Z. Chen, Electrodeposition of ZnO nanoflake-based photoanode sensitized by carbon quantum dots for photoelectrochemical water oxidation. *Ceram. Int.* **43**(6), 5329–5333 ((2017)).

205. M. Fekete, W. Ludwig, S. Gledhill, J. Chen, A. Patti, and L. Spiccia, Al-Modified zinc oxide

nanorods for photoelectrochemical water oxidation. *Eur. J. Inorg. Chem.* No. 4, 750–759 ((2014)).

206. H. Wu, S. Li, X. Lu, C. Y. Toe, H. Y. Chung, Y. Tang, X. Lu, R. Amal, L. Li, and Y. H. Ng, Pulsed Electrodeposition of Co3O4 Nanocrystals on One-Dimensional ZnO Scaffolds for Enhanced Electrochemical Water Oxidation. *Chempluschem* **83**(10), 934–940 ((2018)).

207. C. Meng, Y. F. Gao, X. M. Chen, Y. X. Li, M. C. Lin, and Y. Zhou, Activating Inert ZnO by Surface Cobalt Doping for Efficient Water Oxidation in Neutral Media. *ACS Sustain. Chem. Eng.* **7**(21), 18055–18060 ((2019)).

208. Z. Li, S. Feng, S. Liu, X. Li, L. Wang, and W. Lu, A three-dimensional interconnected hierarchical FeOOH/TiO2/ZnO nanostructural photoanode for enhancing the performance of photoelectrochemical water oxidation. *Nanoscale* **7**(45), 19178–19183 ((2015)).

209. A. Lamouchi, I. Ben Assaker, and R. Chtourou, Enhanced photoelectrochemical activity of MoS 2 -decorated ZnO nanowires electrodeposited onto stainless steel mesh for hydrogen production. *Appl. Surf. Sci.* **478**(October 2018), 937–945 ((2019)).

210. R. R. Su, Y. X. Yu, Y. H. Xiao, X. F. Yang, and W. De Zhang, Earth abundant ZnO/CdS/CuSbS2 core-shell nanowire arrays as highly efficient photoanode for hydrogen evolution. *Int. J. Hydrogen Energy* **43**(12), 6040–6048 ((2018)).

211. A. Sirelkhatim, S. Mahmud, A. Seeni, N. H. M. Kaus, L. C. Ann, S. K. M. Bakhori, H. Hasan, and D. Mohamad, Review on zinc oxide nanoparticles: Antibacterial activity and toxicity mechanism. *Nano-Micro Lett.* **7**(3), 219–242 ((2015)).

212. A. Hatamie, A. Khan, M. Golabi, A. P. F. Turner, V. Beni, W. C. Mak, A. Sadollahkhani, H. Alnoor, B. Zargar, S. Bano, O. Nur, and M. Willander, Zinc Oxide Nanostructure-Modified Textile and Its Application to Biosensing, Photocatalysis, and as Antibacterial Material. *Langmuir* **31**(39), 10913–10921 ((2015)).

213. I. Chauhan, S. Aggrawal, and P. Mohanty, ZnO nanowire-immobilized paper matrices for visible light-induced antibacterial activity against Escherichia coli. *Environ. Sci. Nano* **2**(3), 273–279 ((2015)).

https://doi.org/10.1080/10408436.2021.1989663

214. J. M. Wu, and L. Y. Tsay, ZnO quantum dots-decorated ZnO nanowires for the enhancement of antibacterial and photocatalytic performances. *Nanotechnology* **26**(39), 395704 ((2015)).

215. A. Serrà, G. Vázquez-Mariño, J. García-Torres, M. Bosch, and E. Vallés, Magnetic Actuation of Multifunctional Nanorobotic Platforms to Induce Cancer Cell Death. *Adv. Biosyst.* **1700220**, 1700220 ((2018)).

216. H. Chen, L. Zhu, M. Wang, H. Liu, and W. Li, Wire-shaped quantum dots-sensitized solar cells based on nanosheets and nanowires. *Nanotechnology* **22**(47), 0–8 ((2011)).

217. V. M. Guérin, J. Elias, T. T. Nguyen, L. Philippe, and T. Pauporté, Ordered networks of ZnO-nanowire hierarchical urchin-like structures for improved dye-sensitized solar cells. *Phys. Chem. Chem. Phys.* **14**(37), 12948–12955 ((2012)).

218. E. Guillén, E. Azaceta, A. Vega-Poot, J. Idígoras, J. Echeberría, J. A. Anta, and R. Tena-Zaera, ZnO/ZnO core-shell nanowire array electrodes: Blocking of recombination and impressive enhancement of photovoltage in dye-sensitized solar cells. *J. Phys. Chem. C* **117**(26), 13365–13373 ((2013)).

219. P. Labouchere, A. K. Chandiran, T. Moehl, H. Harms, S. Chavhan, R. Tena-Zaera, M. K. Nazeeruddin, M. Graetzel, and N. Tetreault, Passivation of ZnO nanowire guests and 3D inverse opal host photoanodes for dye-sensitized solar cells. *Adv. Energy Mater.* **4**(12) ((2014)).

220. T. Marimuthu, N. Anandhan, R. Thangamuthu, and S. Surya, Effect of hexamethylenetetramine on the properties of electrodeposited ZnO thin films for dye sensitized solar cell applications. *J. Mater. Sci. Mater. Electron.* **29**(15), 12830–12841 ((2018)).

221. M. Zi, M. Zhu, L. Chen, H. Wei, X. Yang, and B. Cao, ZnO photoanodes with different morphologies grown by electrochemical deposition and their dye-sensitized solar cell properties. *Ceram. Int.* **40**(6), 7965–7970 ((2014)).

222. K. P. Musselman, A. Wisnet, D. C. Iza, H. C. Hesse, C. Scheu, J. L. MacManus-Driscoll, and L. Schmidt-Mende, Strong efficiency improvements in ultra-low-cost inorganic nanowire solar cells. *Adv. Mater.* **22**(35), 254–258 ((2010)).

223. K. P. Musselman, A. Marin, A. Wisnet, C. Scheu, J. L. MacManus-Driscoll, and L. Schmidt-

https://doi.org/10.1080/10408436.2021.1989663

Mende, A novel buffering technique for aqueous processing of zinc oxide nanostructures and interfaces, and corresponding improvement of electrodeposited ZnO-Cu2O photovoltaics. *Adv. Funct. Mater.* **21**(3), 573–582 ((2011)).

224. K. P. Musselman, A. Marin, L. Schmidt-Mende, and J. L. MacManus-Driscoll, Incompatible length scales in nanostructured Cu 2O solar cells. *Adv. Funct. Mater.* **22**(10), 2202–2208 ((2012)).

225. M. Izaki, T. Ohta, M. Kondo, T. Takahashi, F. B. Mohamad, M. Zamzuri, J. Sasano, T. Shinagawa, and T. Pauporté, Electrodeposited ZnO-nanowire/Cu2O photovoltaic device with highly resistive ZnO intermediate layer. *ACS Appl. Mater. Interfaces* **6**(16), 13461–13469 ((2014)).

226. H. Majidi, and J. B. Baxter, Electrodeposition of CdSe coatings on ZnO nanowire arrays for extremely thin absorber solar cells. *Electrochim. Acta* **56**(6), 2703–2711 ((2011)).

227. J. Zhang, C. Sun, S. Bai, R. Luo, A. Chen, L. Sun, and Y. Lin, Interfacial passivation of CdS layer to CdSe quantum dots-sensitized electrodeposited ZnO nanowire thin films. *Electrochim. Acta* **106**, 121–126 ((2013)).

228. J. Zhang, P. Barboux, and T. Pauporté, Electrochemical design of nanostructured ZnO charge carrier layers for efficient solid-state perovskite-sensitized solar cells. *Adv. Energy Mater.* **4**(18), 1–8 ((2014)).

229. G. Syrrokostas, K. Govatsi, G. Leftheriotis, and S. N. Yannopoulos, Platinum decorated zinc oxide nanowires as an efficient counter electrode for dye sensitized solar cells. *J. Electroanal. Chem.* **835**(October 2018), 86–95 ((2019)).

230. A. Lamouchi, B. Slimi, I. Ben Assaker, M. Gannouni, and R. Chtourou, Correlation between SSM substrate effect and physical properties of ZnO nanowires electrodeposited with or without seed layer for enhanced photoelectrochemical applications. *Eur. Phys. J. Plus* **131**(6) ((2016)).

231. H. Makhlouf, C. Karam, A. Lamouchi, S. Tingry, P. Miele, R. Habchi, R. Chtourou, and M. Bechelany, Analysis of ultraviolet photo-response of ZnO nanostructures prepared by electrodeposition and atomic layer deposition. *Appl. Surf. Sci.* **444**, 253–259 ((2018)).

https://doi.org/10.1080/10408436.2021.1989663

232. O. Lupan, V. Cretu, V. Postica, M. Ahmadi, B. R. Cuenya, L. Chow, I. Tiginyanu, B. Viana, T. Pauporté, and R. Adelung, Silver-doped zinc oxide single nanowire multifunctional nanosensor with a significant enhancement in response. *Sensors Actuators, B Chem.* **223**, 893–903 ((2016)).

233. J. Li, J. Wang, Z. Dai, and H. Li, Disordered photonics coupled with embedded nano-Au plasmonics inducing efficient photocurrent enhancement. *Talanta* **176**(August 2017), 428–436 ((2018)).

234. R. Alchaar, H. Makhlouf, N. Abboud, S. Tingry, R. Chtourou, M. Weber, and M. Bechelany, Enhanced UV photosensing properties of ZnO nanowires prepared by electrodeposition and atomic layer deposition. *J. Solid State Electrochem.* 1–10 ((2017)).

235. S. Choi, Y. Chae, S. Ham, W. Lee, N. Myung, and K. Rajeshwar, CdSe/ZnO composite via galvanic displacement followed by photocathodic deposition: Hybrid electrosynthesis and characterization. *J. Phys. Chem. C* **116**(38), 20146–20153 ((2012)).

236. J. Debgupta, R. Devarapalli, S. Rahman, M. V. Shelke, and V. K. Pillai, Electrochemical preparation of vertically aligned, hollow CdSe nanotubes and their p-n junction hybrids with electrodeposited Cu2O. *Nanoscale* **6**(15), 9148–9156 ((2014)).

237. X. He, J. E. Yoo, M. H. Lee, and J. Bae, Morphology engineering of ZnO nanostructures for high performance supercapacitors: Enhanced electrochemistry of ZnO nanocones compared to ZnO nanowires. *Nanotechnology* **28**(24), 245402 ((2017)).

238. Z. Xing, Q. Chu, X. Ren, C. Ge, A. H. Qusti, A. M. Asiri, A. O. Al-Youbi, and X. Sun, Ni3S2 coated ZnO array for high-performance supercapacitors. *J. Power Sources* **245**, 463–467 ((2014)).

239. I. H. Lo, J. Y. Wang, K. Y. Huang, J. H. Huang, and W. P. Kang, Synthesis of Ni(OH)2 nanoflakes on ZnO nanowires by pulse electrodeposition for high-performance supercapacitors. *J. Power Sources* **308**, 29–36 ((2016)).

240. X. Xia, Y. Zhang, Z. Fan, D. Chao, Q. Xiong, J. Tu, H. Zhang, and H. J. Fan, Novel Metal@CARBON spheres core-shell arrays by controlled self-assembly of carbon nanospheres: A stable and flexible supercapacitor electrode. *Adv. Energy Mater.* **5**(6) ((2015)).

https://doi.org/10.1080/10408436.2021.1989663

241. X. Xia, Q. Xiong, Y. Zhang, J. Tu, C. F. Ng, and H. J. Fan, Oxide nanostructures hyperbranched with thin and hollow metal shells for high-performance nanostructured battery electrodes. *Small* **10**(12), 2419–2428 ((2014)).

242. D. Pradhan, F. Niroui, and K. T. Leung, High-performance, flexible enzymatic glucose biosensor based on ZnO nanowires supported on a gold-coated polyester substrate. *ACS Appl. Mater. Interfaces* **2**(8), 2409–2412 ((2010)).

243. D. K. Sarfo, E. L. Izake, A. P. O'Mullane, T. Wang, H. Wang, T. Tesfamichael, and G. A. Ayoko, Fabrication of dual function disposable substrates for spectroelectrochemical nanosensing. *Sensors Actuators, B Chem.* **287**(July 2018), 9–17 ((2019)).

244. S. Öztürk, N. Kilinç, N. Taşaltin, and Z. Z. Öztürk, A comparative study on the NO2 gas sensing properties of ZnO thin films, nanowires and nanorods. *Thin Solid Films* **520**(3), 932–938 ((2011)).

245. O. Lupan, L. Chow, T. Pauporté, L. K. Ono, B. Roldan Cuenya, and G. Chai, Highly sensitive and selective hydrogen single-nanowire nanosensor. *Sensors Actuators, B Chem.* **173**, 772–780 ((2012)).

246. W. Maziarz, A. Rydosz, T. Pisarkiewicz, K. Domański, and P. Grabiec, Gas-sensitive properties of Zno nanorods/nanowires obtained by electrodeposition and electrospinning methods. *Procedia Eng.* **47**, 841–844 ((2012)).

Critical Reviews in Solid State and Materials Sciences Volume 47, Issue 5, Pages 772 – 805, 2022

https://doi.org/10.1080/10408436.2021.1989663

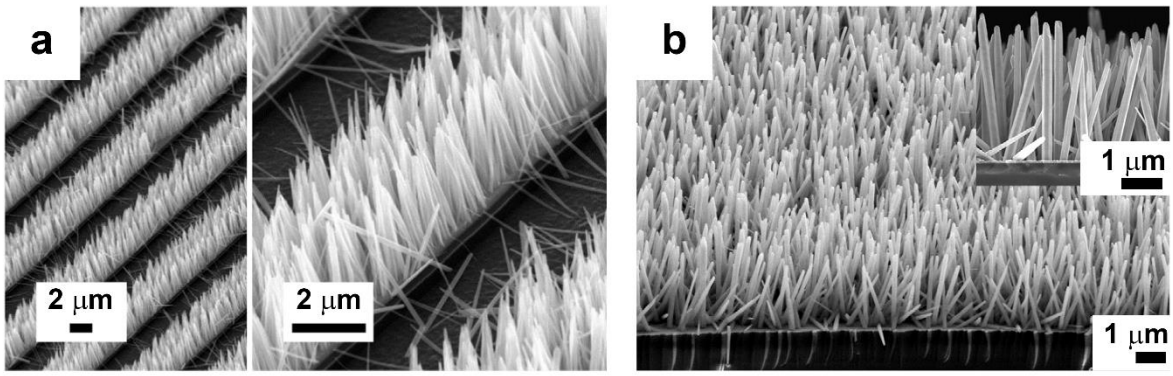

Figure 1: FE-SEM micrographs of templateless electrodeposited ZnO nanowires on (a) Au substrates (Adapted with permission from [87]) and (b) ITO glass (Adapted with permission from [81]).

Critical Reviews in Solid State and Materials Sciences Volume 47, Issue 5, Pages 772 – 805, 2022

https://doi.org/10.1080/10408436.2021.1989663

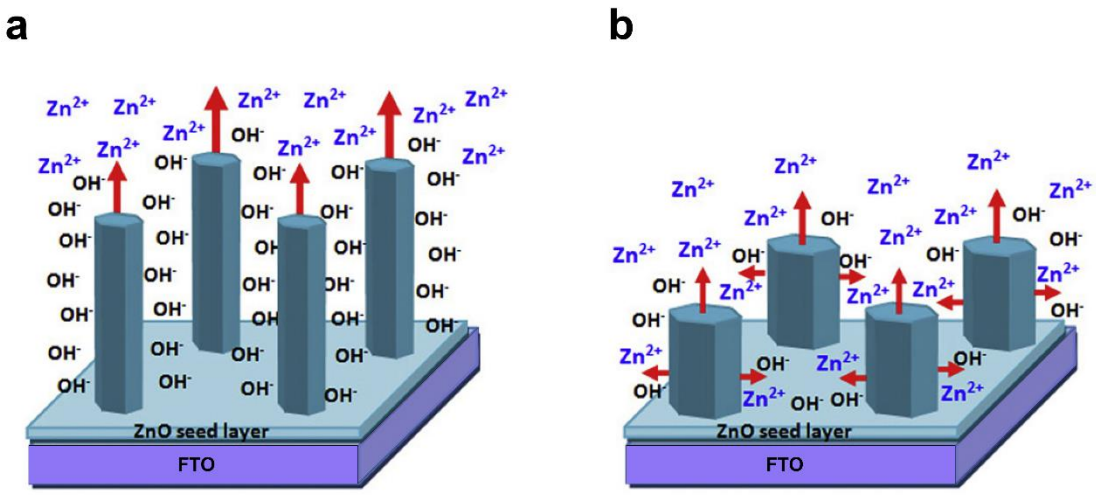

Figure 2: Growth mechanism of ZnO nanowires and nanorods by electrodeposition based on the model of the diffusion of Zn(II) species. (a) The diffusion of the Zn(II) ions is significantly less than the electrogeneration of hydroxide ions. (b) The diffusion of Zn(II) ions and the electrogeneration of hydroxide ions occur at a similar rate. Adapted with permission from [86].

Critical Reviews in Solid State and Materials Sciences Volume 47, Issue 5, Pages 772 – 805, 2022

https://doi.org/10.1080/10408436.2021.1989663

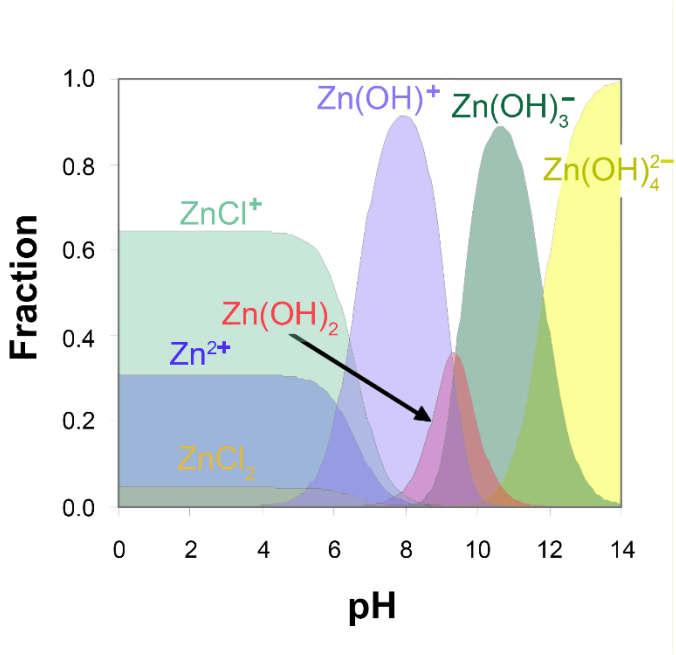

Figure 3: Speciation diagram of Zn(II) ions in 0.1 M of KCl at 70 °C. Adapted with permission from [30].

Critical Reviews in Solid State and Materials Sciences Volume 47, Issue 5, Pages 772 – 805, 2022

https://doi.org/10.1080/10408436.2021.1989663

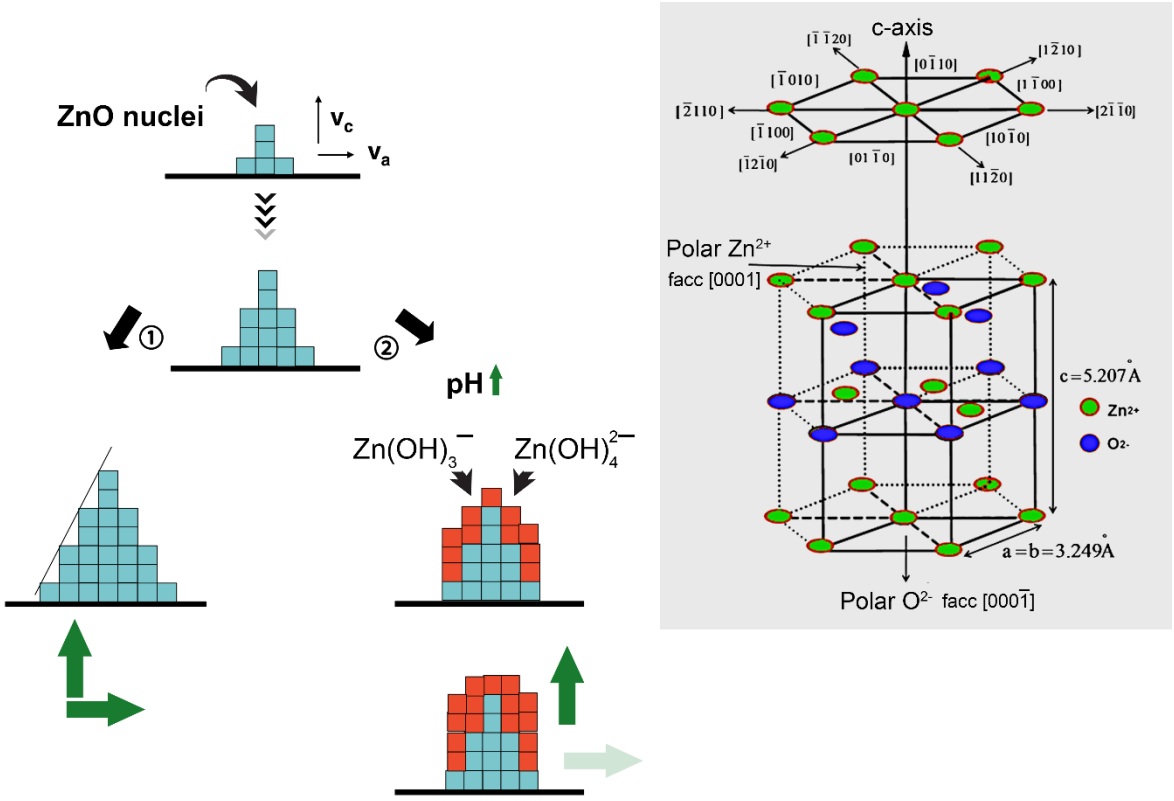

Figure 4: Mechanism of the electrochemical deposition of ZnO. Adapted with permission from [30] and [96].

Critical Reviews in Solid State and Materials Sciences Volume 47, Issue 5, Pages 772 – 805, 2022

https://doi.org/10.1080/10408436.2021.1989663

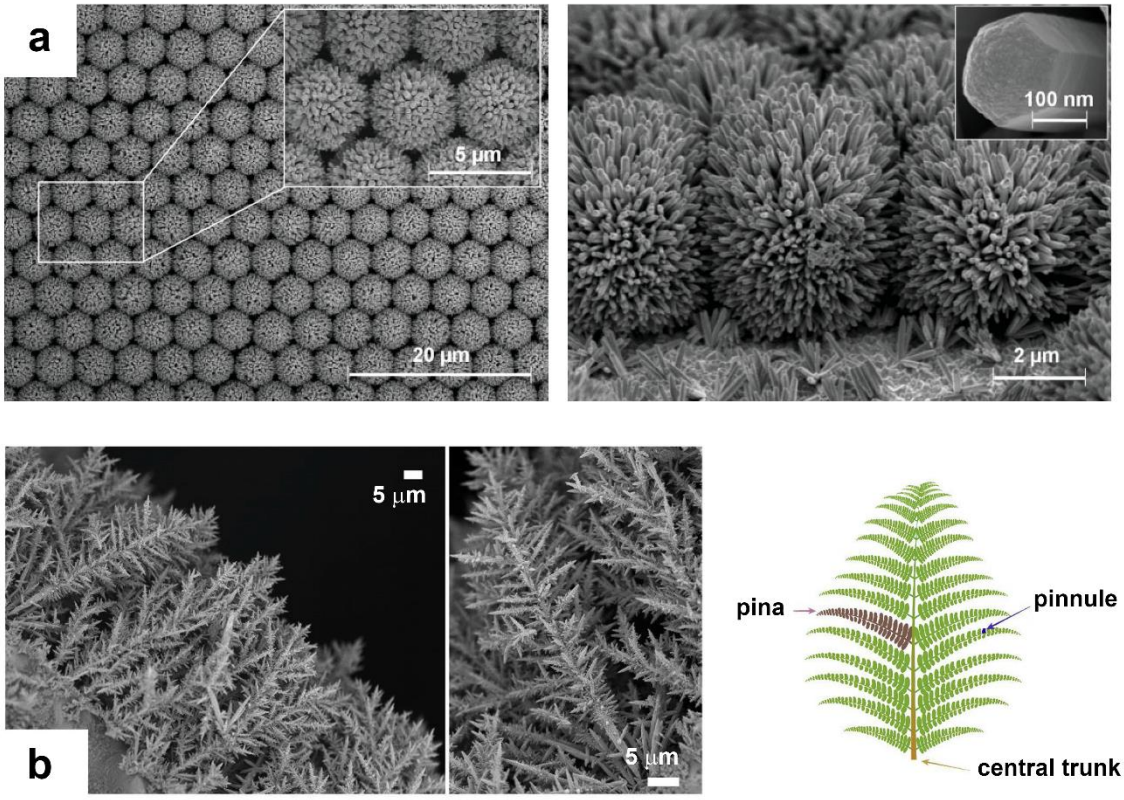

Figure 5: FE-SEM micrographs of (a) sea urchins (reproduced with permission from [91]), and (b) bioinspired microferns (reproduced with permission from [97]), all formed with ZnO nanowires and nanorods.

Critical Reviews in Solid State and Materials Sciences Volume 47, Issue 5, Pages 772 – 805, 2022

https://doi.org/10.1080/10408436.2021.1989663

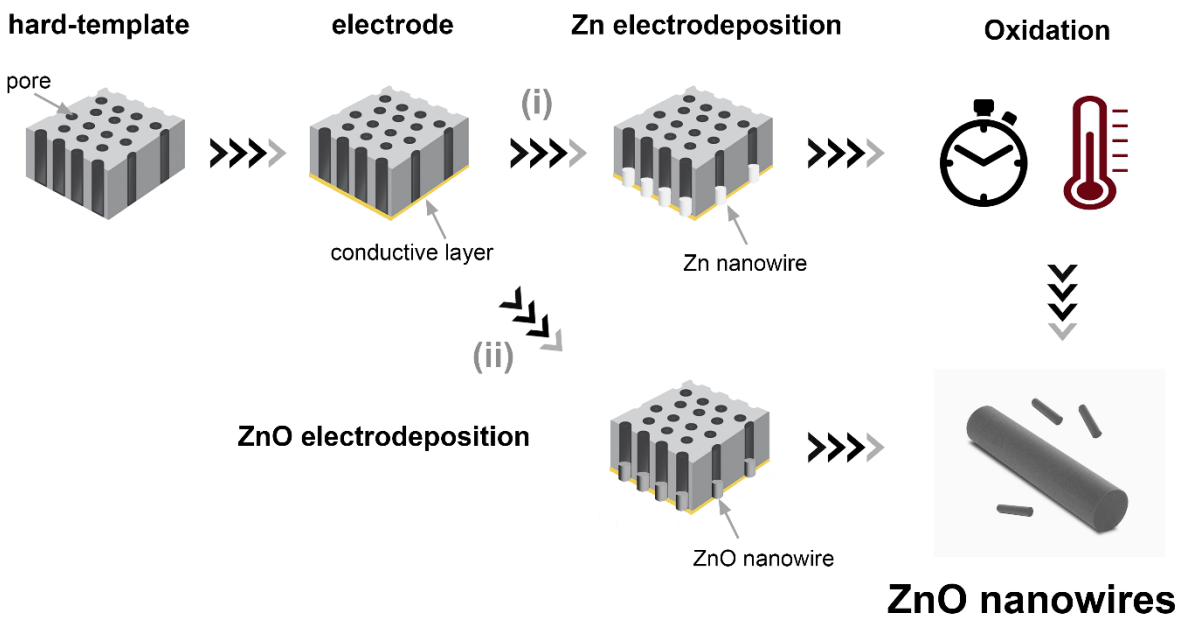

Figure 6: Schematic representation of the hard-template electrodeposition of ZnO via (i) Zn deposition and posterior oxidation and (ii) direct ZnO electrodeposition.

Critical Reviews in Solid State and Materials Sciences Volume 47, Issue 5, Pages 772 – 805, 2022

https://doi.org/10.1080/10408436.2021.1989663

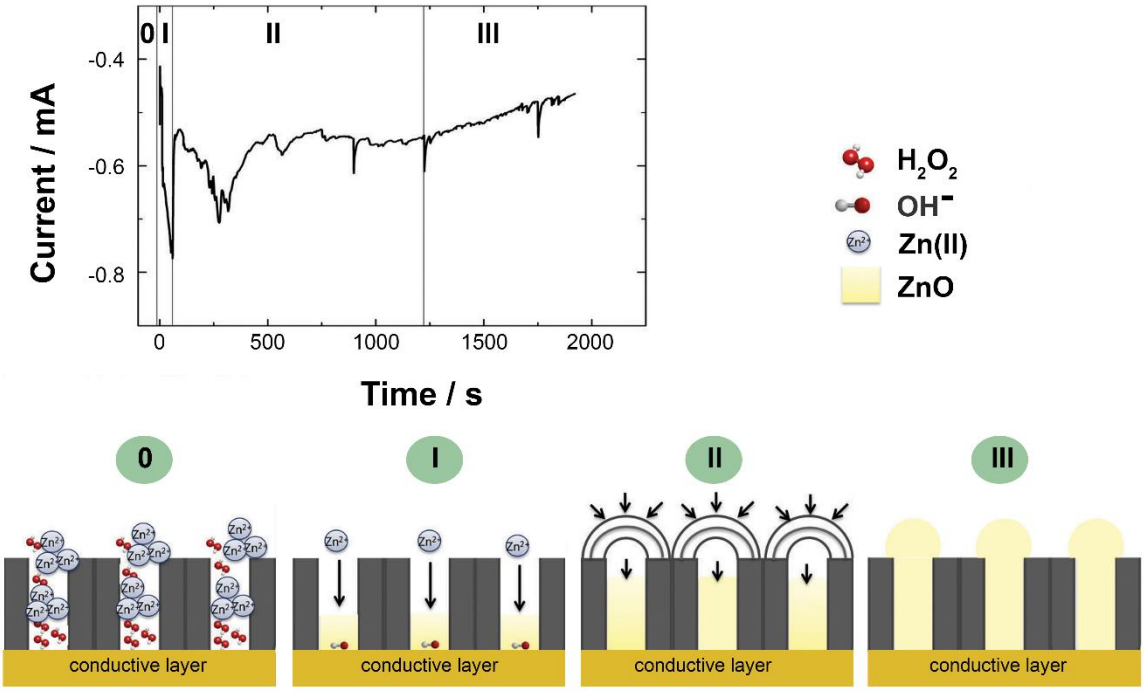

Figure 7: Current–time curve of ZnO nanowires deposited at 70 °C using an aqueous solution of 0.001 M $ZnCl_2$ + 0.04 M H_2O_2 + 0.1 M KCl at -0.8 V versus Ag|AgCl and a schematic representation of the diffusion mechanism of ZnO's deposition. Adapted from [112] with permission.

Critical Reviews in Solid State and Materials Sciences Volume 47, Issue 5, Pages 772 – 805, 2022

https://doi.org/10.1080/10408436.2021.1989663

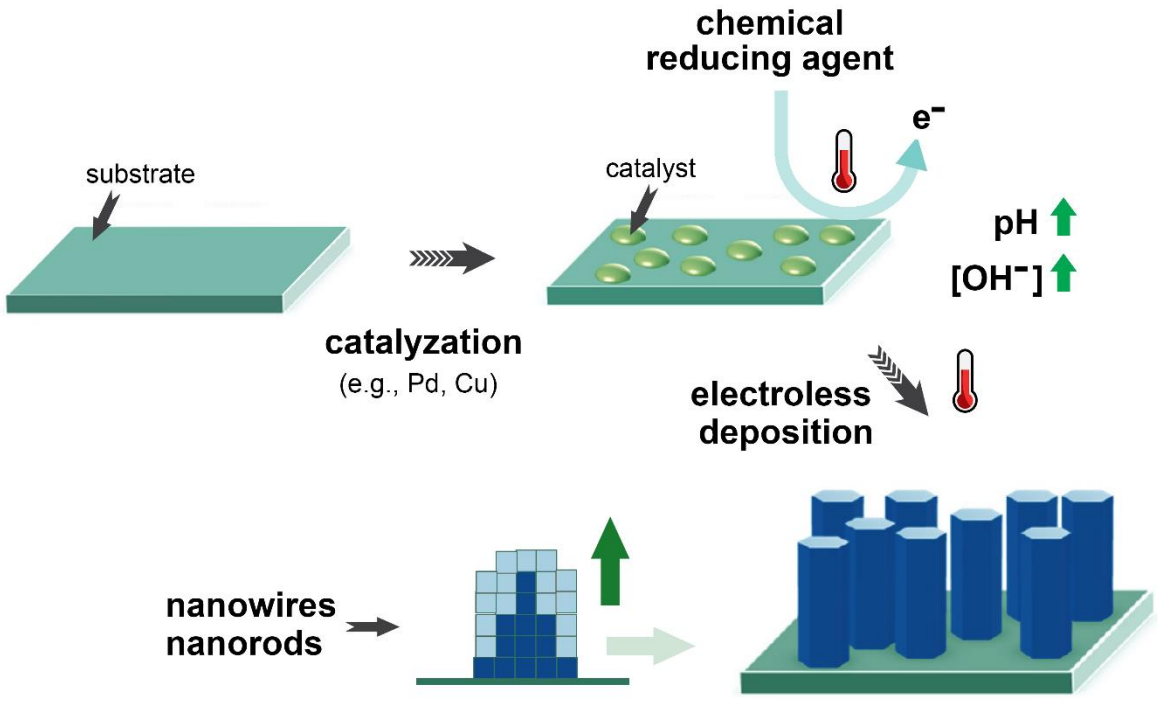

Figure 8: Schematic representation of the electroless deposition of ZnO nanowires or nanorods.

Critical Reviews in Solid State and Materials Sciences Volume 47, Issue 5, Pages 772 – 805, 2022

https://doi.org/10.1080/10408436.2021.1989663

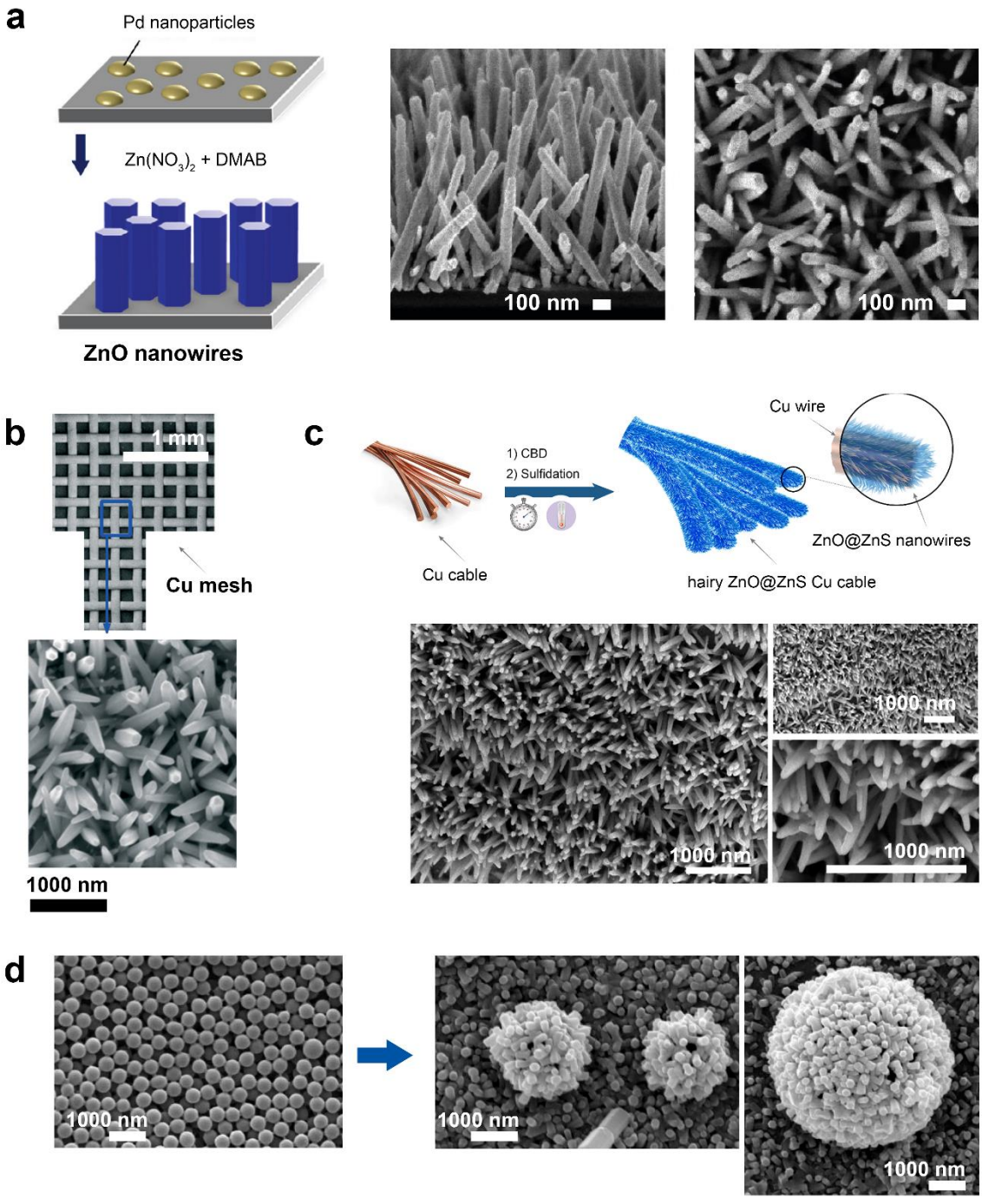

Figure 9: FE-SEM micrographs of ZnO nanowires deposited on (a) Pd-catalyzed glass substrates (adapted with permission from [133]), (b) Cu mesh (adapted with permission from [127]), (c) Cu cables (adapted with permission from [6]), (d) cotton fabrics (adapted with permission

Critical Reviews in Solid State and Materials Sciences Volume 47, Issue 5, Pages 772 – 805, 2022

https://doi.org/10.1080/10408436.2021.1989663

from [136]), and (e) polymeric spheres (adapted with permission from [138]).

Critical Reviews in Solid State and Materials Sciences Volume 47, Issue 5, Pages 772 – 805, 2022

https://doi.org/10.1080/10408436.2021.1989663

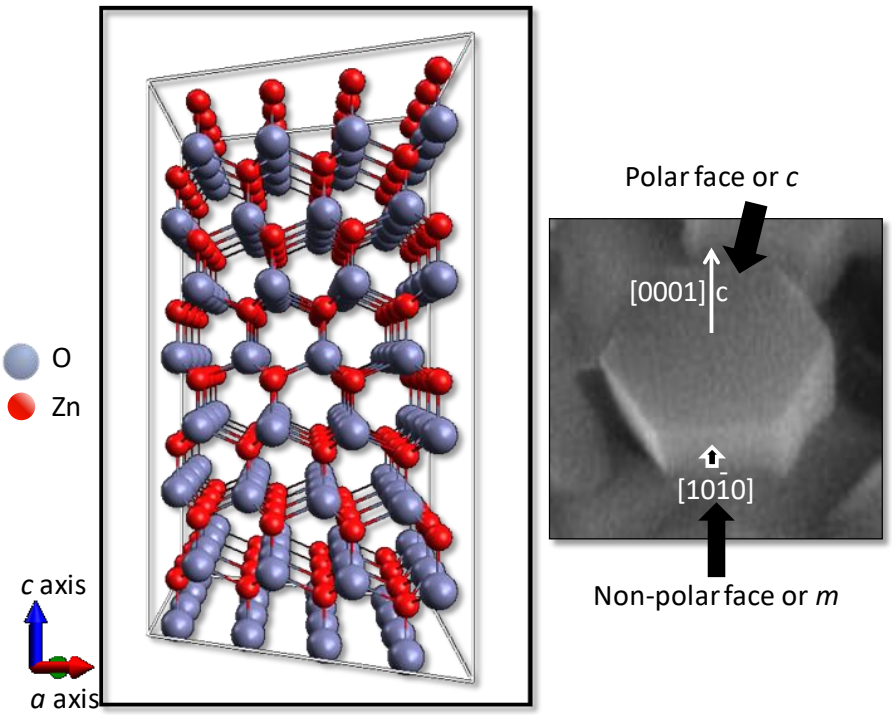

Figure 10: Crystallographic structure of ZnO and the example of one of the polar and non-polar faces of ZnO. Reproduced from [154] with permission.

Critical Reviews in Solid State and Materials Sciences Volume 47, Issue 5, Pages 772 – 805, 2022

https://doi.org/10.1080/10408436.2021.1989663

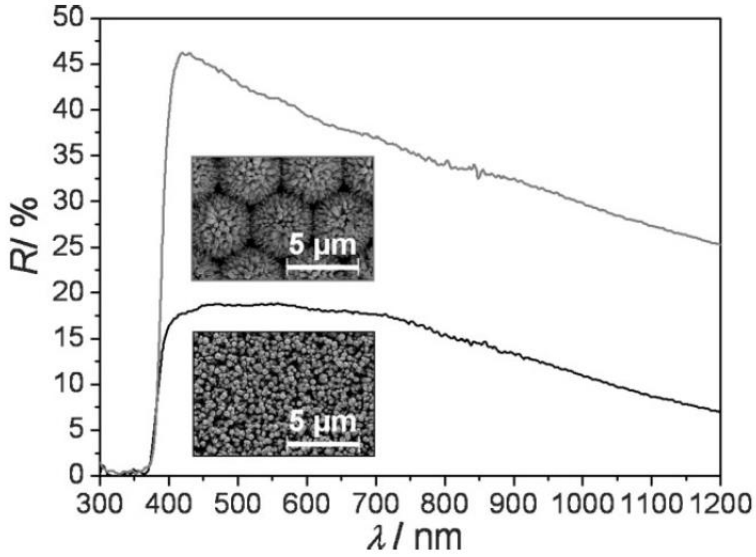

Figure 11. Total reflectance spectra of glass/SnO_2:F/ZnO free-standing nanowires samples and ordered hollow urchin-like structure arrays. Each SEM images corresponds to its spectrum above. Adapted from [75] with permission.

Critical Reviews in Solid State and Materials Sciences Volume 47, Issue 5, Pages 772 – 805, 2022

https://doi.org/10.1080/10408436.2021.1989663

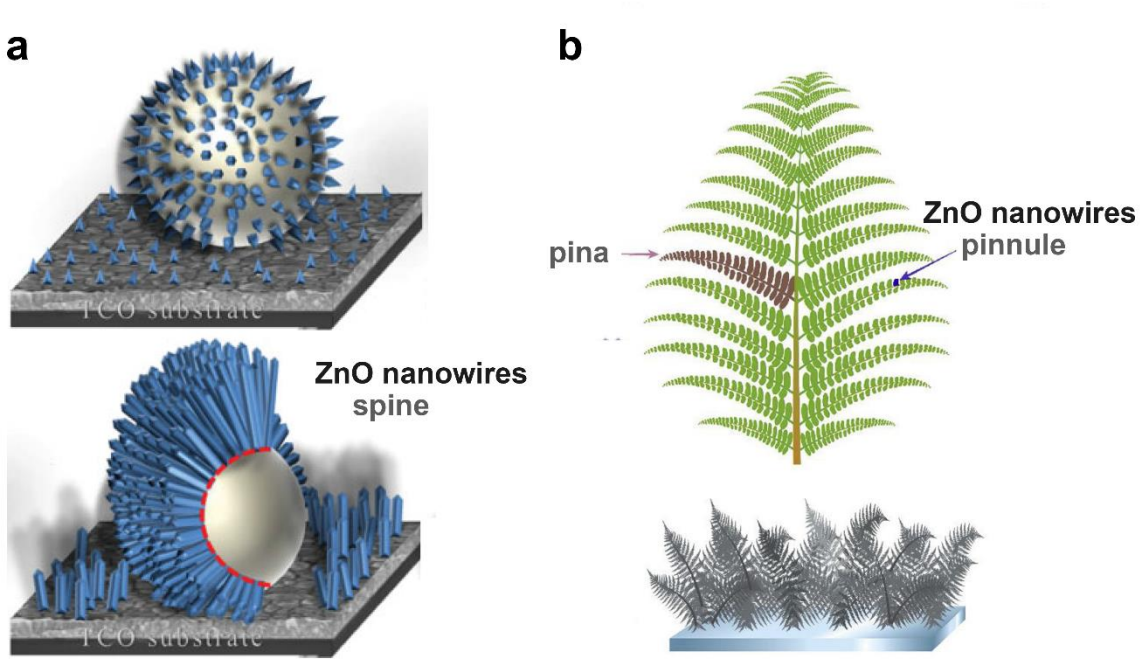

Figure 12: Schematic representation of (a) urchin-like ZnO (adapted from [151] with permission) and (b) ZnO microfern architectures (adapted from [97] with permission).

Critical Reviews in Solid State and Materials Sciences Volume 47, Issue 5, Pages 772 – 805, 2022

https://doi.org/10.1080/10408436.2021.1989663

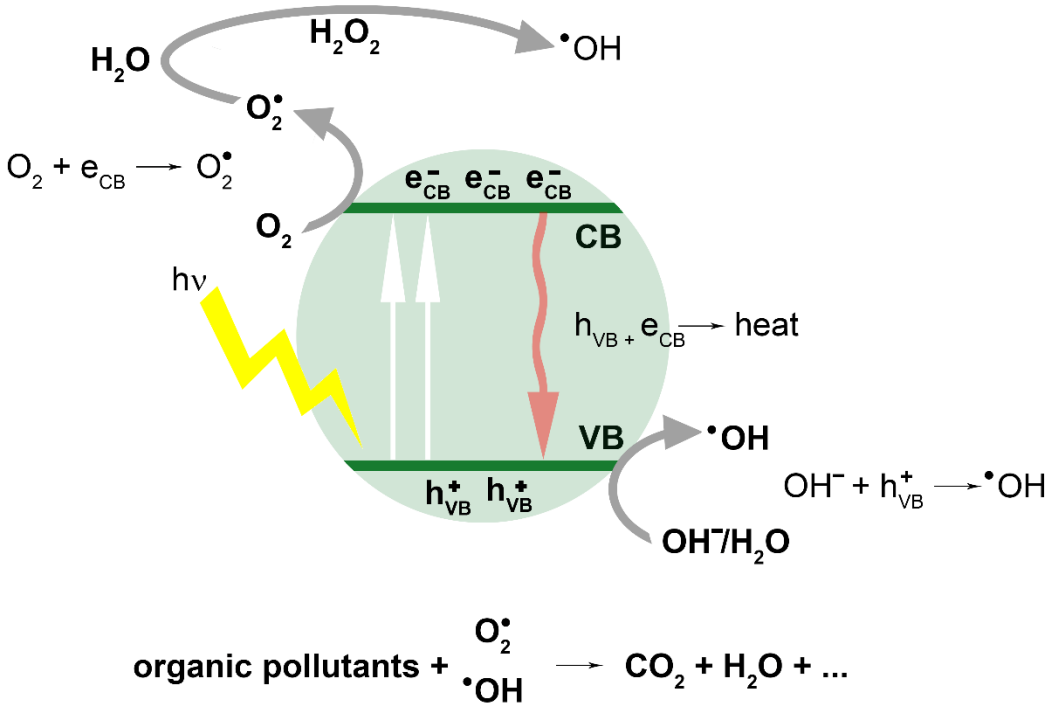

Figure 13: General mechanism of the photocatalysis of ZnO nanowires.